ARISTOTLE UNIVERSITY OF THESSALONIKI

DEPARTMENT OF ELECTRICAL AND COMPUTER ENGINEERING

ÉCOLE POLYTECHNIQUE

DEPARTMENT OF PHYSICS

DEVELOPMENT OF A DYNAMIC STOCHASTIC NEUTRONICS CODE FOR THE ANALYSIS OF CONVENTIONAL AND HYBRID NUCLEAR REACTORS

DOCTORAL DISSERTATION

THALIA A. XENOFONTOS

SUPERVISORS

A. CLOUVAS
Professor

M.-T. JAEKEL
Director of Research

PRESIDENT OF EXAMINATION COMMITTEE

N. CATSAROS
Director of Research

ATHENS, January 2018

ARISTOTLE UNIVERSITY OF THESSALONIKI

DEPARTMENT OF ELECTRICAL AND COMPUTER ENGINEERING

ÉCOLE POLYTECHNIQUE

DEPARTMENT OF PHYSICS

DEVELOPMENT OF A DYNAMIC STOCHASTIC NEUTRONICS CODE FOR THE ANALYSIS OF CONVENTIONAL AND HYBRID NUCLEAR REACTORS

DOCTORAL DISSERTATION

THALIA A. XENOFONTOS

RAPPORTEURS

Pr Gazis E., National Technical University of Athens

Dr Kodeli I., Jozef Stefan Institute

EXAMINATION COMMITTEE

Pr Clouvas A., Aristotle University of Thessaloniki

Dr Jaekel M.T., École Normale Superieure

Dr Varvayanni M., National Center for Scientific Research “Demokritos”

Dr Catsaros N., National Center for Scientific Research “Demokritos”

Pr Gazis E., National Technical University of Athens

Pr Meis C., National Institute for Nuclear Science and Technology (INSTN - CEA)

Dr Kodeli I., Jozef Stefan Institute

Στον πατέρα μου που οι συνθήκες δεν μου επέτρεψαν να γνωρίσω και σε αυτούς που με βοήθησαν να διακρίνω και να συνεισφέρω στην φωτεινή εξέλιξη της ανθρωπότητας.

Table of Contents

ABSTRACT

The necessity for precise simulations of a nuclear reactor especially in case of complex core and fuel configurations has imposed the increasing use of Monte Carlo neutronics codes. Besides, a demand of additional stochastic codes' inherent capabilities has emerged regarding mainly the simulation of the temporal variations in the core isotopic composition as well as the incorporation of the T-H feedback. In addition to the above, the design of innovative nuclear reactor concepts such as the Accelerator Driven Systems, imposed extra requirements of simulation capabilities. More specifically, the combination of an accelerator and a nuclear reactor in the ADS requires the simulation of both subsystems for an integrated system analysis. Therefore a need arises for more advanced simulation tools, able to cover the broad neutrons energy spectrum involved in these systems. In the frame of this thesis, ANET, a new stochastic code was further developed aiming to satisfy the following issues: a) the reliability in simulating certain reactor parameters important to safety, i.e. the reactor criticality as well as the neutron flux and fission rates, b) the internal "on-the-fly" core inventory evolution and fuel depletion calculation and c) the improvement of the ADSs simulation, thus improving the management of highly active nuclear waste. The ANET reliability in analyzing typical configurations was tested using various installations and international benchmarks along with parallel simulations by different codes. The results obtained by the ANET code verify its ability to successfully simulate important parameters of critical and subcritical systems. Also, the application of the enhanced ANET for dynamic reactor core analysis is very promising since it indicates the code capability to inherently provide a reasonable prediction for the core inventory evolution. Lastly, the inherent ANET capability of analyzing ADSs was demonstrated by the satisfactory code performance in the analysis of a prototype accelerator driven system fulfilling thus the requirements of an advanced stochastic neutronics code with scope of application both conventional and innovative nuclear fission reactors.

ACKNOWLEDGMENTS

I would like to thank my thesis supervisors Prof. Alexandros Clouvas and Marc-Thierry Jaekel for giving me the chance to perform this research under the supervision of the School of Electrical and Computer Engineering of the Aristotle University of Thessaloniki and Physics Department of Ecole Polytechnique respectively and for guiding and correcting this thesis.

I would like to express my gratitude to my thesis co-advisor Dr Melina Varvayanni, and to Dr Nicolas Catsaros, Research Directors at the National Centre for Scientific Research Demokritos. Without their scientific guidance and their moral support, this thesis would not have been possible. The discussions we had throughout the thesis inspired me and gave me the strength to continue.

Furthermore, I would like to express my sincere appreciation and gratitude to Dr Jacques Maillard and Dr Jorge Silva, the help of which was crucial for the realization of this thesis. They both supported me through difficult times and helped immensely.

In addition, I really thank Dr Panagiota Savva from the National Centre for Scientific Research Demokritos / Computational Nuclear Technology Group for all the help she provided me during the thesis and especially at the last phase when she overcame herself many times to stand by me.

I am most grateful to Pr Evangelos Gazis for being my teacher but most of all for the moral support during my degree in the National Technical University of Athens and my Master in Paris-Sud and for introducing me to the Computational Nuclear Technology Group of National Centre for Scientific Research Demokritos.

Many thanks must go to the members of the computational nuclear technology group of the National Centre for Scientific Research Demokritos Reactor Laboratory, i.e. Dr Antonios Mylonakis and Dr Nefeli Chrysanthopoulou for the scientific interaction we had during this period and for making research pleasant and fun.

Finally, I really thank my family for their support, both moral and financial during the thesis.

1 INTRODUCTION

The necessity for precise simulations of a nuclear reactor especially in case of complex core and fuel configurations has imposed the increasing use of Monte Carlo (MC) neutronics codes. Besides, a demand of additional stochastic codes' inherent capabilities has emerged regarding mainly the simulation of the temporal variations in the core isotopic composition as well as the incorporation of the T-H feedback. In addition to the above, the design of innovative nuclear reactor concepts, such as the Accelerator Driven System (ADSs), imposed extra requirements of simulation capabilities. More specifically, the combination of an accelerator and a nuclear reactor in the ADS requires the simulation of both subsystems for an integrated system analysis. Therefore a need arises for more advanced simulation tools, able to cover the broad neutron energy spectrum involved in these systems.

Among the most widespread MC neutronics codes are MCNP (*Briesmeister, 2000)*, KENO *(Sumner et al., 2007)*, TRIPOLI *(Petit et al., 2008)* and Serpent *(Leppänen, 2009)*. Steady state neutronics calculations are inherently performed by these codes, while time dependent results can be provided through their coupling with an external module making use of the neutron diffusion theory apart from Serpent which includes inherent burnup capabilities *(Aufiero et al., 2013)*. Burnup assessment by MCNP and KENO is usually performed via coupling with ORIGEN *(Parks, 1992)*, REBUS *(Toppel, 1983)*, and MCB *(Cetnar, 2002)* typical examples are given in *(Zheng et al., 2014)*, *(Bowman et al., 2005)*, *(Hanan et al., 1998)* and *(Zhong et al., 2009)*. Capability of TRIPOLI burnup calculations has been reported in *(Gomit et al., 2003)* by integrating the code in the CRISTAL V1 package, the latter containing (among others) the CESAR computer code capable of performing depletion calculations (*Samson et al., 1998).* Regarding the ADS analysis, the common procedure is to separate the spallation target from the sub-critical core through the utilization of two different codes, i.e. a High Energy Physics (HEP) code for the accelerator (e.g. FLUKA *(Ren et al, 2013)* or MCNPX *(Louis et al., 2012)*) and a neutronics code for the nuclear reactor. Efforts to analyze ADSs using a single code are very few and can be found in *(Kadi et al., 2001)* and *(Bungau et al., 2009).* Apart from the aforementioned, well documented MC neutronics codes, one should also cite those being under development in various Institutes such as the OpenMC *(Romano et*

al., 2013), the MCU *(Gomin et al., 1999)* and the BUCAL1 *(El Bakkari et al., 2009)*, the latter including also burnup calculation capabilities.

Within this thesis the new MC neutronics code ANET (**A**dvanced **N**eutronics with **E**volution and **T**hermal hydraulic feedback), is developed, in a cooperation framework between NCSR Demokritos (Greece) and CNRS/IDRIS[1] and UPMC[2] (France), intending to meet as effectively as possible the above described modelling requirements. ANET is based on the open-source version of the HEP code GEANT3.21 *(Brun et al., 1993)* and is targeting to the creation of an enhanced computational tool in the field of reactor analysis, capable of simulating both GEN II/III reactors and ADSs. ANET is structured with inherent capability of (a) performing burnup calculations and (b) simulating the spallation process in the ADS analysis. The basis for ANET code was established following a fundamental GEANT3.21 modification, i.e. its applicability extension for neutron energies below 20 MeV that is in the region of the neutron energy spectrum involved in nuclear reactors' analysis. The preliminary ANET version (see Chapter 3) was further developed and improved in the framework of this thesis, so as to create a multi-purpose tool with enhanced capabilities. In this context the main goals of this thesis comprise:

a) the reliability in simulating reactor parameters important to safety, i.e. the reactor criticality as well as the neutron flux and fission rates,
b) the internal "on-the-fly" core inventory evolution and fuel depletion calculation
c) the improvement of the ADSs simulation, thus improving the management of highly active nuclear waste.

The improved ANET code utilizes the three standard Monte Carlo estimators for the neutron multiplication factor (k_{eff}) calculation, i.e. the collision estimator, the absorption estimator and the track-length estimator. Regarding the simulation of neutron flux and reaction rates, the collision and the track-length estimators are implemented in ANET following the standard Monte Carlo procedure. For the burnup calculations ANET applies a pure Monte Carlo approach, adopting the typical

[1] Centre National de la Recherche Scientifique / Institut de Développement et des Ressources en Informatique Scientifique

[2] Université Pierre et Marie Curie (Paris-VI)

procedure followed in stochastic codes. The latter (either burnup is provided inherently or through coupling with a deterministic module) includes two computational steps, i.e. calculation of the neutron density distribution and assessment of the nuclide concentrations changes, assuming that these parameters can be estimated sequentially in a cyclic manner by alternating the two computational steps, each time using results from the previous steps. In the above procedure the steady state neutron flux (and therefore the reaction rates) for given materials composition are computed during the first step, while during the second step the changes in the nuclide composition are calculated assuming constant reaction rates. In ANET the above methodology is applied with the difference that reactions rates are computed and utilized directly. In the code version developed in framework of this thesis approximately 150 nuclides are included and can be treated for the transmutation reactions and the radioactive decays. With respect to the ANET development for inherent ADS analysis, the INCL/ABLA code is incorporated so that the spallation process can be inherently simulated.

The ANET reliability in analyzing typical configurations was tested using measurement data and parallel simulations by different codes. Various installations and international benchmarks were considered suitable for the verification and validation of all the previously mentioned features incorporated in the new code ANET. In the framework of the code benchmarking and validation, the Portuguese Research Reactor (RPI) after its conversion to low enrichment in U-235 and the OECD/NEA VENUS-2 MOX international benchmark were considered appropriate for the present study, the former providing criticality and neutron flux data and the latter reaction rates. Concerning criticality benchmarking, the subcritical, Training Nuclear Reactor of the Aristotle University of Thessaloniki (TNR-AUTh) was also analyzed. In addition, the capability to simulate time dependent phenomena with time scales relevant to the core inventory evolution is successfully tested using the international OECD/NEA, Burnup Credit Calculational Criticality Benchmark Phase I-B Results. At the same time, the KUCA (Kyoto University Critical Assembly) which is a critical assembly of a solid-moderated and reflected type core combined with the a fixed-field alternating gradient type accelerator ejecting 100 MeV pulsed protons onto a heavy metal target of Pb-Bi, was utilized for the reliability test of ANET's performance in computing the neutron multiplication factor of an ADS.

The results obtained by the enhanced ANET code, compared with experimental data from the simulated nuclear infrastructures and with computations performed by well-established stochastic or deterministic neutronics codes, verify ANET's ability to successfully simulate important parameters of critical and subcritical systems. Also, the application of the enhanced ANET for dynamic reactor core analysis is very promising since it indicates the code capability to inherently provide a reasonable prediction for the core inventory evolution. Lastly, the inherent ANET capability of analyzing ADSs was demonstrated by the satisfactory code performance in the KUCA analysis fulfilling thus the requirements of an advanced stochastic neutronics code with scope of application conventional as well as innovative nuclear fission reactors.

2 THE FISSION NUCLEAR REACTORS

Based on the produced thermal power and use, fission nuclear reactors fall into two broad categories, namely Power and Experimental Reactors. It also exist fission nuclear reactors commissioned for special purposes such as the embarqued reactors for military (aircraft carriers and submarines) or civil use (ice breakers) and innovative reactor designs, currently in the conception/demonstration phase, such as the Acceleration Driven Systems.

All fission nuclear reactors are further distinguished depending on the kinetic energy E_n of the incident neutrons provoking the fissions, namely Thermal Reactors ($E_n < 0.5$eV) and Fast Reactors (100keV < E_n < ~15MeV).

2.1 Nuclear Reactors Components

All nuclear reactors, regardless of their thermal power output and use, have the same main components *(Lamarsh and Baratta,, 2001).*

The central part of a reactor is the *core*. In a thermal reactor the core contains the fuel, the moderator, the coolant and the control rods while in a fast breeder reactor moderator does not exist. The fuel includes one or two fissile isotopes (^{233}U, ^{235}U, ^{239}Pu, ^{241}Pu) in various chemical forms. The majority of nuclear reactors use Uranium, mainly in the form of UO_2, where the enrichment in ^{235}U is only a few percent, so that most of the fuel is actually ^{238}U.

The *moderator*, which is only present in thermal reactors, is used to moderate the fast neutrons produced by fission reactions to thermal energies. The most often used materials are light water (H_2O), heavy water (D_2O) and graphite (C). Beryllium (Be) and beryllium oxide (BeO) have been occasionally used but they are very costly.

The *coolant* is used to remove the heat from the core and other parts of the reactor where heat may be produced. Light water, heavy water and various gases such as CO_2 and Helium are the most commonly used coolants for thermal reactors. On the contrary, as far as fast reactors are concerned, light water and heavy water cannot be used as coolants, since they would tend to slow down the fission neutrons. Hence, gases can be used to cool fast reactors while most fast reactors are cooled by liquid sodium, since Na has excellent heat transfer properties and low cross section for elastic scattering.

The core of breeder reactors is surrounded by a layer of fertile material called the *blanket*. This region is designed specifically for conversion or breeding. Neutrons that escape from the core are intercepted in the blanket and participate into various conversion reactions. Moreover, a substantial amount of power may also be produced in the blanket resulting from fissions induced by fast neutron, so blanket also must be cooled along with the core.

Controls rods are rods made of materials with high absorption cross sections for neutrons. They are movable pieces used to control the number of fissions in the reactor core. Any movement of the rods affects the multiplication factor k_{eff} of the system. Withdrawal of the rods increases k_{eff}, whereas insertion decreases k_{eff}. The most widely used materials in the control rods and in control elements in general, are alloys or chemical compounds of Boron (B), Gadolinium (Gd), Hafnium (Hf) and Cadmium (Cd). The rods may be cylindrical in shape, sheets, blades or crossed blades, which are called *cruciform rods*.

The region adjacent to the core - or to the blanket if the latter is present - is called the *reflector*. Its purpose is to reflect back to the core after one or more collisions in the reflector a portion of the neutrons which has escaped from it. In this way, neutron economy and a more uniform power density in the core volume are achieved. The reflector material must have the same properties with the moderator, i.e. small neutron absorption cross section and high neutron scattering cross section. Therefore, the material for the reflector and the moderator is almost always the same.

The various reactor components just described are all located within the *reactor vessel*, which, if the components are under pressure, is also called the *pressure vessel*. To reduce the thermal stresses in the reactor vessel caused by the absorption of γ-rays emanating from the core, it is necessary in some reactors to place a *thermal shield*, a thick layer of γ-rays absorbing material (usually iron or steel) between the reflector and the inner wall of the vessel. The thermal shield absorbs considerable energy, so it must be cooled along with the core and the blanket.

The reactor vessel and all other components of the nuclear steam supply system are surrounded by *radiation shielding* in varying amounts for the protection of plant personnel during normal operation of the reactor. To protect the general public from

the consequences of a reactor accident the entire reactor installation is enclosed in a *containment structure*.

2.2 Power Nuclear Reactors

As Power Reactors are characterized the nuclear reactors that produce great thermal power, i.e. up to 4000 MW_{th} and are mainly used for the generation of electricity (over 16% of the world's electricity is produced from nuclear energy). Versions of nuclear power reactors with lower thermal power are used for the propulsion of ships, aircrafts, rockets and satellites while direct use of the produced heat in the reactor is made for the heating of cities and various industrial processes.

Nuclear reactor technology has been under continuous development since the first commercial exploitation of civil nuclear power in the 1950s. This technological development is presented as a number of broad categories, or 'Generations', each representing a significant technical advance, either in terms of performance, cost and safety, compared with the previous generation. At present, three generations of nuclear power systems, i.e. Generations I, II and III are in operation worldwide. Nuclear reactors of Generation III+ are believed to be within the current state-of-the-art, hence fundamental research on nuclear reactors is focused on nuclear alternatives - commonly called Generation IV - and other innovative designs such as ADS that still require considerable effort. In *Figure 2.1* the evolution in Generations and their main representatives are shown throughout the decades. An analysis of the basic features of all four generations is given hereafter. In each case, the reactors are divided in two main categories, i.e. thermal and fast breeder reactors.

Further to their division into Thermal and Fast, Power Reactors are distinguished into Gas-, Light Water- (pressurized or boiling) Heavy Water- and Liquid Metal-cooled reactors, following the material used to remove the heat produced by the fission of the nuclear fuel.

In the frame of this work, special attention is also given to a particular concept of innovative reactor system, the ADS. Initially conceived and analyzed in 1990s *(Bowman et al., 1992; Rubbia et al., 1995; Bacha et al., 1995)*, ADSs have recently been receiving increased attention due to their potential to improve the flexibility and safety characteristics of transmutation systems. In ADS fissions are stimulated by a neutron source, which is obtained by spallation of target nuclei, producing a high

number of neutrons under proton collisions. The neutronic code developed in the frame of this work incorporates the capability of simulating also the production of neutrons resulting from a target spallation due to collisions with accelerated protons. An experimental prototype ADS has been analyzed using the developed code and an innovative ADS concept is proposed, that may work with a closed fuel cycle, i.e. generating enough fissile material to compensate for fuel depletion.

ADS is designed to safely transmute the high level nuclear waste into stable elements (or elements whose radioactivity is relatively short lived), while producing useful power. Although nuclear reactors' safety is a large subject considering several initiating events, ADS is considered inherently safe because it remains sub-critical throughout its life and the nuclear reaction ceases when the outside source stops feeding neutrons. ADSs have not yet been integrated into future nuclear reactors, mainly due to concerns about the window separating the protons from the spallation target, which is expected to be exposed to stress under extreme conditions.

An extensive note describing the main Nuclear Power Reactors is given in *Appendix I* while the ADS concept is exposed in *Appendix II*.

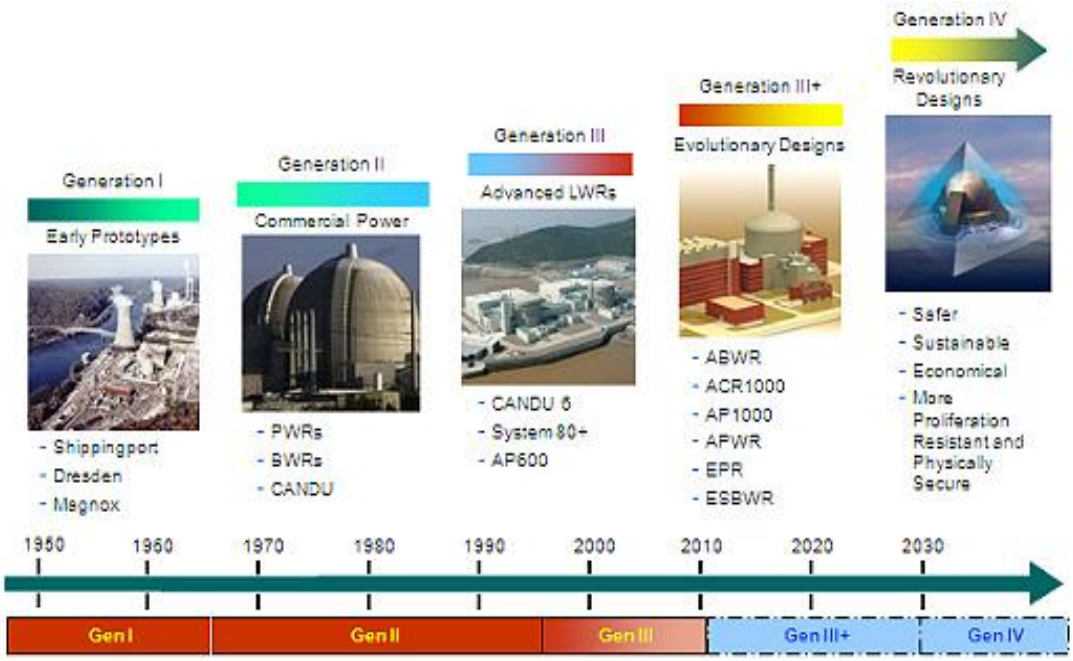

Figure 2.1: Generations of Nuclear Power Reactors

(http://ec.europa.eu/research/energy/euratom/index_en.cfm?pg=fission&section=generation).

3 METHODOLOGIES FOR NEUTRONIC ANALYSIS OF REACTOR CORES

The analysis of a reactor core of either a conventional nuclear reactor or an innovative nuclear system, includes a) steady-state calculations which are based on solving the neutron transport equation and result in the computation of many parameters such as the neutron multiplication factor of the system, the neutron flux and the reaction rates that occur in the core and b) time-dependent burnup calculations that aim to solve the fuel depletion equation in order to predict the temporal changes of the core's material composition and subsequent changes of the neutronic parameters .

3.1 Neutron Transport and Criticality Equation

The determination of the distribution of neutrons in a nuclear reactor is of high importance since it designates the rate at which various nuclear reactions occur within the reactor core. Both the neutron motion in the core and the neutron interactions with the nuclei of the core material must be accounted for it. The neutron transport equation describes the collective behavior of neutrons in a reactor core, hence is a balance equation of the various gain and loss mechanisms for the neutrons inside an arbitrary volume within the system.

The angular neutron density N(**r**, **Ω**, E, t) is defined as the expected number of neutrons in a volume dV about a point **r**, moving in direction **Ω** in solid angle d**Ω,** with energies in the interval [E, E + dE] at the time instant t and its balance is considered in the neutron transport equation. The most common formulation of the time-dependent transport equation is in terms of the angular neutron flux φ(**r**, **Ω**, E), which is defined as

$$\varphi(\mathbf{r}, \mathbf{\Omega}, E, t) = \upsilon \cdot N(\mathbf{r}, \mathbf{\Omega}, E, t) \tag{3.1}$$

where υ is the neutron velocity.

The scalar flux is obtained by integrating the angular flux over all directions:

$$\Phi(\mathbf{r}, E) = \int_{4\pi} \varphi(\mathbf{r}, \mathbf{\Omega}, E)\, d\Omega \tag{3.2}$$

The integro-differential form of the neutron transport equation can be written as:

$$\frac{1}{\upsilon}\frac{\partial\varphi(\mathbf{r}, \mathbf{\Omega}, E, t)}{\partial t} + \Omega \cdot \nabla_r \varphi(\mathbf{r}, \mathbf{\Omega}, E, t) + \Sigma_t \varphi(\mathbf{r}, \mathbf{\Omega}, E, t) =$$

$$\int_{4\pi} d\mathbf{\Omega'} \int_0^{\infty} \Sigma_s(\mathbf{r}, \mathbf{\Omega'} \rightarrow \mathbf{\Omega}, E' \rightarrow E)\, \varphi(\mathbf{r}, \mathbf{\Omega'}, E', t)\, dE' \quad (3.3)$$

$$+ \chi(E) \int_{4\pi} d\mathbf{\Omega'} \int_0^{\infty} \nu(E') \Sigma_f(\mathbf{r}, \mathbf{\Omega'}, E',) \varphi(\mathbf{r}, \mathbf{\Omega'}, E', t)\, dE'$$

$$+ S(\mathbf{r}, \mathbf{\Omega}, E, t)$$

where

Σ_t, Σ_s, Σ_f	total, scattering and fission macroscopic cross-sections
χ	fission energy distribution function
v	mean number of neutrons produced per fission
S	external neutron source

The first term describes the rate of change of angular flux, the second term is the neutron leakage contribution over the entire surface of the volume dV, the third term corresponds to the collision rate over the volume dV, the fourth term characterizes neutrons scattering from other energies or directions into dEd$\mathbf{\Omega}$, the fifth term provides the production of neutrons by fission and the last term describes the external neutron source for reactor startup.

Usually, the time-independent form of *Eq. 3.3* is solved under the assumption that, by properly adjusting the neutrons emitted by fission, one can arrive to equal neutron production and loss by absorption and leakage rates. Therefore, *Eq. 3.3* can be written as eigenvalue problem called the criticality equation. The largest eigenvalue k which is called the effective neutron multiplication factor and is denoted as k_{eff}, provides a non-negative solution for the neutron flux. If k_{eff} =1, then the system is called critical while if $k_{eff} < 1$ the system is called subcritical and the flux will decrease eventually. Finally, the case $k_{eff} > 1$ corresponds to a constantly increasing flux and the system now is called supercritical *(Duderstadt and Hamilton, 1976)*.

3.2 Methodologies for the Solution of the Neutron Transport Equation

The mathematical complexity of the neutron transport equation imposes a limit on achieving an analytical solution in the vast majority of realistic cases. This problem is treated by using numerical techniques. Two fundamentally different computational methods are followed, i.e., the deterministic approach and the

stochastic approach. The work performed in this thesis is based on the latter approach hence a more detailed description is given for it.

3.2.1 Deterministic Approach

The solution of the neutron transport equation is a function of several independent variables, i.e. energy, space, angle and time. The deterministic methods replace the continuous variables by a set of discrete values in order to obtain an algebraic system of equations with the scalar fluxes as unknowns. The energy is usually discretized by the multi-energy-group approximation while space discretization is achieved by several methods, i.e. the finite difference method, the finite element method, the nodal method and others. Regarding the discretization of the angle variable, several strategies like the discrete ordinates method, the spherical harmonics method, the collision probability method and the transmission probability method can be applied. Finally, if the problem is time-dependent, the direct discrete method is also used for the time variables. Very often the discretization is quite coarse leading to significant truncation errors. The numerical calculation process of the deterministic method is simpler and has a faster convergence rate compared to the stochastic one which is analyzed right below while capability of time-dependent calculations is inherent. Nonetheless, the deterministic approach has poor adaptability to complex geometries and its computational time increases significantly with the dimension of the problem. A review of the deterministic methods is given in (*Lewis and Miller*, 1993).

3.2.2 Stochastic (Monte Carlo) Approach

The Monte Carlo method does not actually solve the neutron transport equation. The underlying idea of the stochastic approach originates from the probability theory which states that if the solution to a problem is the mathematical expectation of a random variable, then the arithmetical mean of several specific observations of the random variable which is obtained through numerical experiments, corresponds to the solution to that problem. In the Monte Carlo approach, a large number of individual neutron histories is simulated and aspects of their average behavior are recorded so as to compute the estimate of a variable, i.e. the effective multiplication factor, the neutron flux, the reaction rate etc., which is the solution to the problem.

A general overview of the Monte Carlo simulation for the solution of the neutron transport problem involves:

- source sampling from a probability distribution
- tracking of the neutrons' locations, energies and directions and computation of the distance travelled by the neutron until its next collision with a nucleus via a probability distribution
- sample the reaction that will take place from a probability distribution
- record contributions for the quantity of interest and finally compute results.

In more detail, the progress of the Monte Carlo simulation process is determined by the nature of the problem, i.e. subcritical systems or critical and supercritical systems. The main difference with the previous systems' treatment is the way the initial position and energy of the neutrons are selected (*Lewis and Miller*, 1993).

In the first case, the neutron population is preserved by an external source and the relevant simulation is carried out in a *fixed source mode*. Each neutron is randomly generated from a predefined initial distribution and is followed until it disappears, by absorption or leakage. Secondary neutrons, if generated, are handled similarly after the parent neutron. A new neutron is sampled from the source distribution and simulated accordingly, only when all the secondary neutrons have been simulated. The run is finished when a pre-defined number of neutron histories has been simulated.

Critical and supercritical systems are simulated using the *criticality source mode*. In this case, the neutron population balance is sustained by the chain fission reactions and the course of the simulation comprises source cycles. For the first cycle the position and the energy of the neutrons are guessed while for the subsequent cycles they are sampled from the neutron distribution of the previous cycle. The source convergence is problem dependent, nonetheless is always achieved after a number of cycles which must be discarded.

The Monte-Carlo estimates are not associated with truncation error. However, they are related with statistical error, which according to the Central Limit Theorem is proportional to $1/\sqrt{n}$, where n is the number of events that contribute to the estimate and depends linearly on the total number of neutron histories. Therefore, in order to have a reliable estimate of the quantity of interest especially over small volumes and

energy ranges, a large number of neutrons has to be simulated to reach a given accuracy. Due to this behavior, Monte Carlo is far less efficient in simulating local than global values of an estimate. In addition, the computational cost is directly proportional to the number of histories; therefore, in order to reduce the statistical uncertainty by 50% one has to quadruple the running time. This may result to very long computational times.

The main advantage of the stochastic approach is that it can treat complex geometries and physical experiments in a very detailed way. The improvement of computer performance resulted in the predominance of the Monte Carlo codes as a neutronics simulation tool.

3.3 Fuel Depletion Equation

In an operating nuclear reactor, the composition of the nuclear fuel material changes constantly due to neutron-induced fission and transmutation reactions and to spontaneous radioactive decay. The rates of the former reactions are determined by the neutron density distribution in the system. In addition, the neutronic properties of the nuclear fuel depend strongly on the isotopic composition of the fissile material and the poisons' concentrations during the reactor's operation. The depletion equations or Bateman equations *(Bateman, 1910)* which describe the material composition changes during the operation of a nuclear reactor are:

$$\frac{dN_i}{dt} = \sum_j \gamma_{ji}\sigma_{f,i}N_j\phi + \sum_k \sigma_{c,k\to i}N_k\phi + \sum_l \lambda_{l\to i}N_l - \left(\sigma_{f,i}N_i\phi + \sigma_{\alpha,i}N_i\phi + \lambda_i N_i\right) \quad (3.4)$$

where

dN_i/dt	the change rate in concentration of isotope *i*
$\sum_j \gamma_{ji}\sigma_{f,i}N_j\phi$	the production rate per unit volume of isotope *i* from fission of fissionable nuclides
$\sum_k \sigma_{c,k\to i}N_k\phi$	the production rate per unit volume of isotope *i* from neutron transmutation of all isotopes including (n, γ)
$\sum_l \lambda_{l\to i}N_l$	the production rate per unit volume of isotope *i* from decay of all isotopes including β^-, β^+, α, γ decay etc
$\sigma_{f,i}N_i\phi$	the removal rate per unit volume of isotope *i* by fission
$\sigma_{\alpha,i}N_i\phi$	the removal rate per unit volume of isotope *i* by neutron absorption (excluding fission)

$\lambda_i N_i$ the removal rate per unit volume of isotope *i* by decay.

3.4 Methodologies for the Solution of the Depletion Equation

There are several methods which can be applied for the solution of the depletion equation. Some of them can handle the full system of nuclides actually existing in the core of an operational nuclear reactor, while others require the removal of the unimportant and short-lived nuclides from the system to make it smaller and less stiff. In the following paragraphs the most important methodologies for burnup calculations that stochastic codes use are presented.

3.4.1 Transmutation Trajectory Analysis (TTA)

One of the main methods to solve analytically the Bateman equations is the Transmutation Trajectory Analysis method. The basic idea is that the complex transmutation chains governing the reactor operation can be resolved into a set of linear chains which contain all possible trajectories as shown in *Figure 3.1* where $b_{i,k}$ is the branching ratio defined to specify the relative fraction for the different type *k* decays for the nuclide *i*. One can start every linear chain from a specific nuclide assuming it has an initial concentration $N_i(0) \neq 0$ and construct all the potential trajectories. Assuming that a chain starts from nuclide 1, then according to *(Cetnar, 2006)* the atomic density of the *k*th nuclide at time *t* is given by

$$N_k(t) = \frac{N_1(0)}{\lambda_k} \sum_{i=1}^{k} \lambda_\iota \prod_{\substack{j=1 \\ j \neq i}}^{k} \left(\frac{\lambda_j}{\lambda_j - \lambda_i} \right) exp(-\lambda_i t) \tag{3.5}$$

Decomposing the transmutation chains results into numerous linear chains that practically cannot be treated. Also, cyclic chains by default cannot be linearized. Hence, termination of chains can be achieved by applying specific criteria, i.e. passage and chain termination criteria. TTA was first applied in a code dedicated to accelerator driven systems *(Cetnar, 1999).*

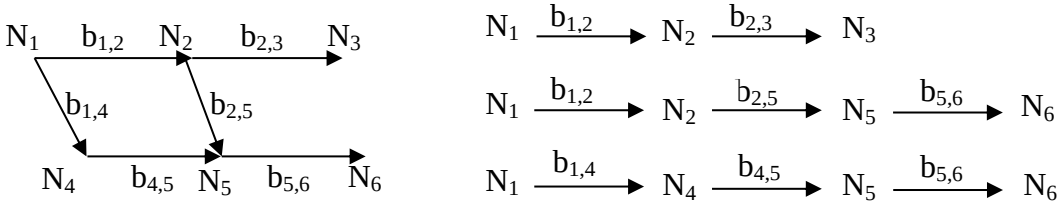

Figure 3.1: Example for decomposing decay and transmutation reactions to linear chains.

3.4.2 Matrix Exponential Methods

The depletion equation can be formulated in compact vector form as

$$\frac{d\boldsymbol{N}}{dt} = \boldsymbol{A}\boldsymbol{N}(t) \tag{3.6}$$

where $\boldsymbol{N}(t) \in \Re^{n}$ is the nuclide concentration vector and $\boldsymbol{A} \in \Re^{n \times n}$ is called the *transition* or *burnup matrix* and contains the decay and transmutation coefficients of the nuclides in the irradiated material. The formal solution of the matrix form is

$$\boldsymbol{N}(t) = e^{\boldsymbol{A}t}\boldsymbol{N}(0) \tag{3.7}$$

where the exponential of the matrix $\boldsymbol{A}t$ is defined by the power series expression

$$e^{\boldsymbol{A}t} = \sum_{k=0}^{\infty} \frac{1}{k!}(\boldsymbol{A}t)^{k} \tag{3.8}$$

and $\boldsymbol{A}^{0}$ = I is the identity matrix.

The various matrix exponential methods apply different numerical approximations for computing the matrix exponential (*Mole et al.*, 2003) but only a few of them are suitable for burnup calculations, especially when the full system of nuclides is solved.

ORIGEN

ORIGEN *(Croff, 1980), (Croff, 1983)* is the most widely spread algorithm concerning Monte Carlo depletion calculations. The methodology applied in ORIGEN is constituted by three solution methods, the centerpiece of which is the matrix exponential technique for solving differential equations.

In the first step, the short-lived nuclides, i.e. $T_{1/2}^{eff} \leq 0.1t$ where t is the time-step, that have also short-lived precursors are dealt with. For each nuclide the relevant chains containing only short-lived nuclides are established and solved. These nuclides will reach equilibrium within the time-step, hence their concentrations will be calculated and stored at the end of the time step while their contributions to the long-lived nuclides are added to their initial concentration.

Thereinafter, a reduced transition matrix which includes only the long-lived members of the full transition matrix is generated and a corresponding equation to *Equation (3.6)* is created. The resulting significantly reduced system is evaluated using the series representation of the exponential function and incorporating enough terms so that the answer achieves a specified degree of accuracy.

The final phase of the composite solution method involves the calculation of the contributions from long-lived nuclides to short-lived nuclides using again the decay and transmutation chains. Here, the produced chains are in secular equilibrium at the end of the step and the requested contributions are calculated by using a Gauss-Seidel algorithm. At this point, the final concentrations of short-lived nuclides can be derived by superposing the results of steps one and three.

Chebyshev Rational Approximation Method (CRAM)

CRAM is a new matrix exponential method developed by *(Pusa et al., 2010)* and it is based on the observation that the eigenvalues of the depletion matrix $\boldsymbol{A}$ are clustered around the negative real axis. This can be exploited by making a Chebyshev rational approximation of the exponential function for the interval (-∞, 0]. The resulting rational function is then decomposed into a pole-residue form and when the denominator and numerator orders of the Chebyshev approximation are selected equal and even, the poles form conjugate pairs and the imaginary parts cancel out for a real valued variable. Thus, an order (k, k) approximation becomes

$$e^z \approx \frac{P_k(x)}{Q_k(x)} = \alpha_0 + \sum_{i=1}^{k} \frac{\alpha_i}{z+\theta_i} = \alpha_0 + 2Re\left[\sum_{i=1}^{\frac{k}{2}} \frac{\alpha_i}{z+\theta_i}\right] \qquad (3.9)$$

where P_k and Q_k are polynomials of order k, whose coefficients have been selected to minimize absolute deviation from exponential function on the negative real axis, α_0 is the limiting value of the approximation at infinity, and α_i and θ_i are the residues and poles. When this approximation is applied to *Equation (3.7)*, it becomes

$$\boldsymbol{N}(t) \approx \alpha_0 \boldsymbol{N}(0) + 2Re\left[\sum_{i=1}^{\frac{k}{2}} a_i (At - \theta_i I)^{-1}\right] \boldsymbol{N}(0) \qquad (3.10)$$

The coefficients α_i and θ_i depend only on the order of the approximation, so they can be pre-calculated. As a result, evaluating the expression requires only solving $k/2$ linear systems of the form

$$\left(At - \theta_j I\right)\boldsymbol{N}_j = \alpha_j \boldsymbol{N}_0 \tag{3.11}$$

Due to the special structure of the depletion matrix, this can be done accurately and efficiently by using symbolic LU decomposition *(Rose et al., 1976)* and Gaussian elimination *(Pusa et al., 2012)*.

3.5 Well Established and Under Development Monte Carlo Codes

MCNP *(Briesmeister, 2000)*, TRIPOLI-4 *(Petit et al., 2008)*, MCNPX *(MCNPX Manual, 2002)*, Serpent *(Leppänen, 2009)* and FLUKA *(Aarnio et al., 2010)* are among the well-established Monte Carlo neutronics codes. Apart from the aforementioned, one should also cite those being under development in various Institutes such as the OpenMC *(Romano et al., 2013)*, MCU *(Gomin et al., 1999)* and BUCAL1 *(El Bakkari et al., 2009)*. For the scope of this thesis, only some of the codes that are used widely in the nuclear technology community are further analyzed in this text.

MCNP

MCNP is a general-purpose Monte Carlo N–Particle code that can be used for neutron, photon, electron, or coupled neutron/photon/electron transport. The neutron energy regime is from 10-11 MeV to 20 MeV for all isotopes and up to 150 MeV for some isotopes, the photon energy regime is from 1 keV to 100 GeV, and the electron energy regime is from 1 KeV to 1 GeV. The capability to calculate k*eff* eigenvalues for fissile systems is also a standard feature.

The code treats an arbitrary three-dimensional configuration of materials in geometric cells bounded by first- and second-degree surfaces and fourth-degree elliptical tori. Pointwise cross-section data are used. For neutrons, all reactions given in a particular cross-section evaluation (such as ENDF/B-VI) are accounted for. Thermal neutrons are described by both the free gas and S(α,β) models. For photons, the code accounts for incoherent and coherent scattering, the possibility of fluorescent emission after photoelectric absorption, and absorption in electron-positron pair

production. Electron/positron transport processes account for angular deflection through multiple Coulomb scattering, collisional energy loss with optional straggling, and the production of secondary particles including K x-rays, knock-on and Auger electrons, bremsstrahlung, and annihilation gamma rays from positron annihilation at rest. Electron transport does not include the effects of external or self-induced electromagnetic fields. Photonuclear physics is available for a limited number of isotopes.

Important standard features that make MCNP very versatile and easy to use include a powerful general source, criticality source and surface source, both geometry and output tally plotters, a rich collection of variance reduction techniques, a flexible tally structure, and an extensive collection of cross-section data.

TRIPOLI-4

TRIPOLI-4 is a general purpose radiation transport code. It uses the Monte Carlo method to simulate neutron and photon behaviour in three-dimensional geometries. The main areas of applications include but are not restricted to: radiation protection and shielding, nuclear criticality safety, fission and fusion reactor design, nuclear instrumentation. Any pointwise cross-section data in ENDF/B format may be used: JEFF2, ENDF/B-VI, JEFF3, ENDF/B-VII, JENDL3.3 etc. As for thermal neutrons, both free gas and S(alpha, beta) models are available. Easy-to-use powerful variance-reduction tools help the user to solve deep penetration problems. TRIPOLI-4 features a versatile and robust parallel operation mode, for heterogeneous network of workstations, or massively parallel machines. TRIPOLI-4 is supported by a range of graphics and algorithmic productivity tools which means that checking for geometry and input deck errors is easy. As for the qualification, TRIPOLI-4 benefits from an extensive range of benchmarks and comparisons with real measurements, and is therefore qualified for R&D, teaching as well as industrial use.

MCNPX

The MCNPX code is a coupling of two codes: LAHET *(Prael et al., 1989)* and MCNP. MCNPX only needs one input file for both codes and avoids the transfer of large data files. It allows the treatment of transport problems in a large range of energies, from thermal energy (25 meV) to a few GeV. For energies lower than 20

MeV, quite complete sets of cross-sections are available for the major part of the stable nuclei. International cross-sections libraries such as ENDF, JEFF (OECD/NEA, 2009), JENDL, are available and are regularly updated. To treat the transport, MCNP uses data deduced of these libraries after processing them using NJOY/ACER. For energies larger than 20 MeV, there are less cross-section data. Presently the LA150 and NRG-2003 libraries, which cover around 50 isotopes (most common in ADS) up to 150-200 MeV, are included in the MCNPX code package and the preparation of complete data files up to 150 MeV is in progress in several projects.

After running a MCNPX-job, several evaluations can be performed with an auxiliary code, HTAPE3X, to obtain specific information (neutron spectrum, energy deposition, residual nuclei, etc.)

FLUKA

FLUKA is a general purpose tool for calculations of particle transport and interactions with matter, covering an extended range of applications spanning from proton and electron accelerator shielding to target design, calorimetry, activation, dosimetry, detector design, ADS, cosmic rays, neutrino physics, radiotherapy etc. It can simulate with high accuracy the interaction and propagation in matter of about 60 different particles, including photons and electrons from 1 keV to thousands of TeV, neutrinos, muons of any energy, hadrons of energies up to 20 TeV and all the corresponding antiparticles, neutrons down to thermal energies and heavy ions. The code can also transport polarized photons (e.g., synchrotron radiation) and optical photons. Time evolution and tracking of emitted radiation from unstable residual nuclei can be performed on line.

The PEANUT (PreEquilibrium Approach to NUclear Thermalization) *(Ferrari et al., 1994)* is used for the simulation of hadron-nuclear interactions from GeV region down to 20 MeV, through more steps (Generalized IntraNuclear Cascade, Preequilibrium stage, FLUKA evaporation model). The cross-section libraries used in FLUKA are imported from ENDF/B-VI.

Serpent

Serpent is a multi-purpose three-dimensional continuous-energy Monte Carlo particle transport code, developed at VTT Technical Research Centre of Finland, Ltd.

The development started in 2004, and the code has been publicly distributed by the OECD/NEA Data Bank and RSICC since 2009. Serpent started out as a simplified reactor physics code, but the capabilities of the current development version, Serpent 2, extend well beyond reactor modeling. The applications can be roughly divided into three categories: a) traditional reactor physics applications, including spatial homogenization, criticality calculations, fuel cycle studies, research reactor modeling, validation of deterministic transport codes, etc., b) multi-physics simulations, i.e. coupled calculations with thermal hydraulics, CFD and fuel performance codes and c) neutron and photon transport simulations for radiation dose rate calculations, shielding, fusion research and medical physics.

OpenMC

OpenMC is a Monte Carlo particle transport simulation code focused on neutron criticality calculations and was originally developed by members of the Computational Reactor Physics Group at the Massachusetts Institute of Technology starting in 2011 while now various universities, laboratories, and other organizations contribute to the development of OpenMC. It is capable of simulating 3D models based on constructive solid geometry with second-order surfaces. OpenMC supports either continuous-energy or multi-group transport. The continuous-energy particle interaction data is based on ACE format cross sections, also used in the MCNP and Serpent Monte Carlo codes.

While well-established Monte Carlo neutronics codes such as MCNP5, KENO, and TRIPOLI-4.8 can inherently perform steady state neutronics calculations, time dependent results can be provided through their coupling with an external module making use of the neutron diffusion theory. Fuel burnup assessment by MCNP and KENO is usually performed via coupling with ORIGEN *(Parks, 1992)*, REBUS *(Toppel, 1983)*, and MCB *(Cetnar, 2002)*. Capability of TRIPOLI fuel burnup calculations has been reported in *(Gomit et al., 2003)* where the code is integrated in the CRISTAL V1 package, the latter containing (among others) the CESAR computer code capable of performing depletion calculations (*Samson et al., 1998)*. It is worth mentioning that Serpent is one of the most rapidly evolving stochastic codes that includes inherent stochastic burnup calculation capabilities *(Aufiero et al., 2013)* and in the frame of its development a new methodology, CRAM

(see Chapter 3.4.2), has been proposed which provides very satisfactory results *(Pusa et al., 2012)* whereas the TTA method has been implemented *(Isotalo et al., 2013)*. In addition, Serpent can be combined with other codes only as a neutronic solver if chosen.

Apart from the aforementioned, one should also cite codes being under development in various Institutes such as BUCAL1, OpenMC, MCU and RMC *(Wang et al., 2015)*. Moreover, RMC has incorporated the deterministic code ORIGEN2 as a subroutine, rather than using an interface *(She at al., 2013)* while BUCAL1 has proposed a solution technique for depletion calculations based on the fourth order Runge Kutta *(El Bakkari et al., 2009)*. In *Tables 3.1* and *3.2* the various capabilities concerning the fuel burnup and the ADS analysis of several well-established and under-development codes respectively, are presented. ANET capabilities have been added in *Table 3.2* so as to underline the novelty of this work.

Table 3.1: Capabilities concerning the fuel burnup and the ADS analysis of several well-established codes.

Code	**Inherent burnup capability**	**Burnup capability with external coupling**	**ADS treatment**
MCNP		✓	
TRIPOLI-4		✓	
KENO-ORIGEN		✓	
MCNPX		✓	✓

Table 3.2: Capabilities concerning the fuel burnup and the ADS analysis of several under-development codes.

Code	**Inherent burnup capability**	**Burnup capability with external coupling**	**ADS treatment**
Serpent	✓		
OpenMC		✓	
MCU		✓	
RMC	✓		
BUCAL1	✓		
ANET	✓		✓

3.6 State of the Art in the ADSs Simulation

The main problems encountered when analyzing an ADS can be summarized in (a) the simulation of the spallation mechanisms and the neutron source, necessarily of complex configuration and (b) the simulation of a complex reactor core due to the presence of a composite fuel, i.e. traditional nuclear material (U, Pu) and minor actinides generated as waste during the operation of conventional reactors.

3.6.1 Fuel Depletion Mechanisms

The exact knowledge of the neutronics characteristics and the fuel depletion mechanisms is of major importance for the conservation of the sub-criticality and the energy balance during ADS operation. It is also necessary to accurately simulate high energy nuclear reactions, a capability that is not offered by traditional neutronics codes. Hence, regarding the ADS analysis a High Energy Physics (HEP) code for the accelerator (e.g. FLUKA or MCNPX) and a neutronics code for the nuclear reactor core are commonly used. As an example, the ATRAS code system *(Sasa et al., 2001)* conceived to analyze ADSs, is composed from three codes, one simulating the spallation target (source of neutrons), a second one computing the diffusion of neutrons in the core and a third one computing fuel depletion. The use of multiple codes necessitates complex code interfaces which are common sources of problems.

3.6.2 Spallation Process

Several studies using the aforementioned codes have been made, in order to validate their performance in simulating the spallation process. In *(Křížek et al., 2006)*, MCNPX 2.4.0 simulation was performed and the calculated yields of various nuclear reactions were compared to experimental data from a setup exposed to 1.5 GeV proton beam from the Nuclotron accelerator. A good qualitative agreement was found between each other. The simulations followed quite well the trends of the measured data. Nevertheless, the quantitative agreement was not perfect. For high energy threshold reactions, MCNPX predicted a more rapid decrease in isotope production with growing radial coordinate. The bigger the reaction threshold was, the more steeply increased the ratios of the experimental over simulated B-values. In the framework of the European Spallation Source (ESS) project, INCL4.6 and Abla07 were implemented in a beta version of MCNPX2.7 *(Leprince et al. 2014)* and this

spallation model was benchmark on excitation functions (p+W) on a thin target by means of the produced isotope and the projectile energy. These results were supplemented by another benchmark done involving a thick tungsten target and giving isotope production along the beam axis as well as radially. The INCL4.6-Abla07 benchmark on thin and thick target provided a good agreement (average ratio ~2) with available data even if it was less good than expected with nuclei produced mainly by low energy projectile.

MCNPX 2.4 simulations were used by *(Feghhi et al., 2013)* for the comparison with benchmark results to verify the code's potential for calculating various parameters of an accelerator driven system target. Using the computation method, neutron interaction processes such as loss, capture and (n,xn) into a spallation target have been studied for W, Ta, Pb, Bi, and LBE spallation targets in different target dimensions. With relative errors less than 10%, the numerical simulation provided by the MCNPX code agrees qualitatively with other simulation results previously carried out, qualifying it for spallation calculations.

(Majerle et al., 2008) studied the neutron field and the transmutation of 129I and used MCNPX v.2.4.0 to simulate the experimental setup. The results of the simulations were compared to the experimental values, and the influence of the setup parts to the neutron field was explored. Most calculated values were in good agreement with the experimental data with discrepancies up to 20%. Generally, for most similar experiments analyzed by the authors, the MCNPX simulations underestimate the production rates near the end of the target.

The shape and the intensity of neutron field produced in the reactions of relativistic protons in a thick lead target surrounded by moderator by the activation analysis method were studied by *(Krása et al., 2005)*. They found out that the energetic spectrum becomes harder at the end of the target. They reached good qualitative agreement between experimental data and simulations (LAHET+MCNP and MCNPX codes) for high-energy neutron production. The simulations underestimate production of isotopes in foils placed beyond the blanket and at the end of the target. This could indicate a difference between the development of the secondary particle shower and the fission in uranium blanket in the real experiment and in the model used in the simulations.

The spallation model INCL4/ABLA implementation in the LAHET code was studied by *(David et al., 2003)* through the use of accurate neutron spectra on thick targets measured at the SATURNE National Laboratory, Saclay (France).The angle emission, cross section and energy of the neutrons emitted from a thick target was calculated. The INCL4/ABLA spallation model, which gave good results for thin targets, was found to perform well for thick targets as well. Slight discrepancies from the data were, however, observed.

Several experiments were performed at the Phasotron and Nuclotron accelerators in JINR Dubna in which spallation reactions and neutron transport were studied. The experimental results were checked against the predictions of the Monte-Carlo code MCNPX (*Oden et al., 2007)*. The discrepancies at 1.5 GeV and 2 GeV on the "Energy plus Transmutation" setup were observed. Therefore the experimental results were also checked with FLUKA. FLUKA and MCNPX codes predicted similar results for the experimental tests and both Monte Carlo codes underestimated the reaction rates in the radial detectors at larger distances from the target axis for experiment with proton energy 1.5 GeV.

The total neutron yields from spallation processes inside Pb targets were computed by *(Bungau et al., 2009)*, and comparisons were made between the GEANT4 and MCNPX predictions. The two code predictions were found to be in a reasonably good agreement, however in almost all cases GEANT4 gave results that were higher than the MCNPX predictions, especially for the low energy neutrons which, according to the MCNPX results, are more likely to be absorbed inside the target.

(Piénkowski et al., 2006) performed realistic simulations of neutron detection using the FLUKA simulation code. Experimental data from NESSI collaboration were used for thin and thick spallation targets. The calculations were done using the Berlin Neutron Ball (BNB) 4¼ detector emulator. It was found that the FLUKA code reproduces qualitatively the experimental data; however, the data were not well reproduced quantitatively, especially for thin spallation targets.

Obviously the necessity for precise simulations of a nuclear reactor especially in case of complex core and fuel configurations triggered the increasing use of Monte Carlo (MC) neutronics codes with the requirement of multi-task capabilities.

4 THE ANET CODE

ANET (Advanced Neutronics with Evolution and Thermal hydraulic feedback) is an under development Monte Carlo code based on the open-source version of the high energy physics code GEANT3.21 of CERN in collaboration of NCSR "Demokritos", Greece, with CNRS/IDRIS and Université Pierre et Marie Curie, France. Its development is motivated by the need of a new code capable of inherently simulating GEN II/III reactors and innovative nuclear reactor designs, such as the Accelerator Driven Systems. The latter, combining two subsystems, i.e. an accelerator and a nuclear reactor, require the combination of two different codes in order to be simulated, i.e. a High Energy Physics (HEP) code for the first component and a neutronics code for the second. So far, the most common way to simulate an ADS is by separating the spallation target from the sub-critical core. Typical codes used for the spallation reaction simulation include FLUKA *(Ren et al., 2013), (Mantha et al., 2007)* and MCNPX *(Feghhi et al. 2013), (Louis et al., 2012), (Barros et al. 2012)* while several neutronic codes are utilized for the neutronic / thermo-hydraulic subcritical core analysis, e.g. *(Meloni et al., 2008).* Only in a few cases *(Bungau et al., 2009), (Kadi et al., 2001),* an effort has been made to analyze ADSs using a single code able to cover the broad energy neutrons spectrum involved in these systems. ANET is being developed as a continuation of these efforts, since it can simulate neutrons of energy above and below the threshold of 20 MeV, by FLUKA or INCL/ABLA and ANET procedures respectively. In GEANT 3.21, FLUKA is used so as to treat only the hadronic interaction part.

Before the beginning of this thesis work, calculations with a prototype version of the ANET code were carried out to demonstrate the code capability to accurately simulate elastic collision, capture and fission. In these preliminary applications criticality was derived indirectly through dividing the neutrons produced from two successive generations of fissions, while an assumption of a fixed, pre-defined neutron yield for a tungsten spallation source (without including inherent spallation process) was adopted *(Catsaros et al., 2009), (Catsaros et al., 2012), (Catsaros et al., 2013).*

ANET takes into account all particles' creation and collisions, hadronic showers and nuclear cascades. It contains three main loops, i.e. on events (macroscopic time), on particle tracking and on step (microscopic time). The history of a single particle,

e.g. a neutron, from birth to death is considered as an event. Step is the minimum evaluation of the following two quantities, i.e. the flight distance in a material, which is inversely proportional to the total macroscopic cross section of the current material and the distance to surface boundary taking into account the direction of the particle. The program input includes geometry as well as initial chemical and isotopic composition of the reactor core, temperature distribution, source of neutrons or particle beam (e.g. deuteron or proton) and nuclear data (cross sections, fission parameters). ANET provides the number of absorption and fission events at different locations within the core as well as the neutron energy spectrum. In addition, it allows for specific calculation of the step length, simulation of specific interactions, definition of the particles initiating each event, definition and storage of particle(s) created during the step and definition of the process that must follow each event. Moreover, a new high energy physics code developed in CEA, France named INCL/ABLA *(Ferrari et al., 2007)* has been incorporated into ANET, as an alternative for the treatment of the hadrons and leptons reactions involved in the spallation procedure required in the ADS. In the frame of ANET, several GEANT3 standard procedures have been appropriately modified while others have been added, so as to include the capability of simulating low energy particles' transport and interactions. During the particle tracking, the energy of the particle is checked and is accordingly treated either by FLUKA or INCL/ABLA (energy above 20 MeV) or standard ANET procedures (energy below 20 MEV). As a result, particles of a wide range of energies can be simulated inherently in ANET. Concerning neutrons interactions, at this stage ANET includes elastic collision, capture and fission. For the elastic collision, the energy dependent angular distribution is used, taking also into account the effect of temperature. Cross sections are pre-tabulated point by point, using available nuclear data libraries for each nuclide-energy pair. Currently, only JEFF libraries are available for ANET. Integration of new procedures that account for the computation of the neutron multiplication factor, neutron fluence rates and core power density distribution has been performed, based on the Monte Carlo approach. In addition, several new subroutines concerning the dynamic assessment of the changes in the fuel isotopic composition during reactor's operation have been incorporated in the first version of ANET. Core inventory evolution including fuel burnup, transmutation of long-lived actinides, production / consumption of poisons and U-233 production by neutron capture on Th-232 can thus be followed for specific

time-steps during operation. Furthermore, ANET is designed to be finally coupled with thermal-hydraulic calculations.

4.1 Criticality Calculations

In reactor theory, k_{eff} is thought of as the ratio between the number of neutrons in successive generations, with the fission process regarded as the birth event that separates generations of neutrons. The calculation of k_{eff} consists of estimating the mean number of fission neutrons produced per incoming fission neutron in one generation. A neutron generation is considered as the life of a neutron form birth in fission to death by escape, capture or absorption leading to fission. On the contrary, the processes (n, 2n) and (n, 3n) are treated as internal and do not act as termination. In a Monte Carlo simulation the computational equivalent of a generation is a k_{eff} cycle, i.e. a cycle is a computed estimate of an actual fission generation. The fission neutrons of each cycle are terminated and stored properly so as to provide the fission source for the next cycle. The effect of the delayed neutrons is taken into account by the use of the total $\bar{\nu}$, i.e. the average number of prompt or total neutrons produced per fission by the collision nuclide at the incident neutron energy, when data is available. The current version of ANET utilizes the three standard Monte Carlo estimators for the multiplication factor calculation, i.e. the collision estimator, the absorption estimator and the tracklength estimator. Specific subroutines especially dedicated to the computation of the k_{eff} estimators and their statistical error have been developed for ANET. The theoretical background for the k_{eff} estimators (*Lewis and Miller*, 1993) utilized in stochastic codes is presented below:

4.1.1 Collision Estimator

The collision estimator for k_{eff} for any active cycle writes:

$$k_{eff}^{C} = \frac{1}{W} \sum_{i \in C} w_i \frac{\sum_k f_k \bar{\nu}_k \sigma_{f_k}}{\sum_k f_k \sigma_{T_k}} \tag{4.1}$$

where i is summed over all collisions in a cycle where fission is possible.

k is summed over all nuclides of the material involved in the ith collision.

σ_{T_k} is the total microscopic cross section.

σ_{f_k} is the microscopic fission cross section.

$\bar{\nu}_k$ is the average number of prompt or total neutrons produced per fission by the collision nuclide at the incident energy.

f_k is the atomic fraction for nuclide k.

W is the nominal source size for cycle.

w_i is the weight of particle entering collision.

The number of neutrons entering the ith collision is represented by w_i, hence $w_i \frac{\sum_k f_k \bar{\nu}_k \sigma_{f_k}}{\sum_k f_k \sigma_{T_k}}$ is the expected number of neutrons to be produced from all fission processes in the collision.

4.1.2 Absorption Estimator

The k_{eff} absorption estimator for any active cycle is calculated when a neutron interacts with a fissionable nuclide. In ANET the estimator for absorption is computed and it is given by:

$$k_{eff}^{A} = \frac{1}{W} \sum_{i \in A} w_i \bar{\nu}_k \frac{\sigma_{f_k}}{\sigma_{C_k} + \sigma_{f_k}} \tag{4.2}$$

where i is summed over each analog absorption event in the kth nuclide and σ_{C_k} is the microscopic capture (n,0n) cross section. It should be noted that the analog absorption k_{eff} estimate is very similar to the collision estimator of the multiplication factor except that only the kth absorbing nuclide, as sampled in the collision, is used rather than averaging over all nuclides.

The absorption estimate differs from the collision estimator in that the collision estimate is based upon the expected value at each collision, whereas the absorption estimate is based upon the events actually sampled at a collision. Thus all collisions will contribute to the collision estimate of k_{eff} by the probability of fission in the

material. On the contrary, contributions to the absorption estimator will only occur if an actual fission event occurs for the sampled nuclide in the case of analog absorption.

4.1.3 Track Length Estimator

The track length estimator of k_{eff} is accumulated every time the neutron traverses a distance ℓ in a fissionable material cell and it is computed by the formula:

$$k_{eff}^{T} = \frac{1}{W} \sum_{i \in T} w_i \rho \ell_i \sum_k f_k \bar{\nu}_k \sigma_{f_k} \tag{4.3}$$

where i is summed over all neutron trajectories within a fissionable material.

ρ is the atomic density in the cell.

ℓ is the trajectory track length from the last event.

It is noteworthy to mention that $\rho \ell_i \sum_k f_k \bar{\nu}_k \sigma_{f_k}$ is the expected number of fission neutrons produced along trajectory ℓ, therefore k_{eff}^{T} is a third estimate of the mean number of fission neutrons produced in a cycle per nominal fission source neutron.

4.2 Flux Calculations

Following the standard Monte Carlo procedure for the computation of neutron flux utilized in stochastic codes (*Lewis and Miller*, 1993), e.g. MCNP, TRIPOLI and OpenMC, the relevant subroutines for both the collision and the track-length estimators are implemented in ANET. The formulae used for the collision and the track-length estimator are presented in *Equations (4.4)* and *(4.5)* respectively.

$$\phi^{C} = \frac{1}{W} \sum_{i \in C} \frac{w_i}{\Sigma_t(E_i)} \tag{4.4}$$

$$\phi^{T} = \frac{1}{W} \sum_{i \in T} w_i \ell_i \tag{4.5}$$

where W is the total starting weight of the particles.

w_i is the pre-collision weight of the particles.

C is the set of all events resulting in a collision with a nucleus.

$\Sigma_t(E_i)$ is the total macroscopic cross section of the target material at the incoming energy E_i of the particle.

T is the set of all the particle's trajectories within the desired volume.

ℓ_i is the length of the *i*-th trajectory.

Particular subroutines that test the position and energy of the neutron and afterwards apply the previous formulae for the fluence rates calculation in a specific volume and for the desired energy range have been implemented in ANET. The ANET user must provide to the code the number of the positions and the relevant volumes in which the fluence rates will be computed whereas more than one positions can be treated simultaneously in a run. In addition, the energy boundaries of the energy groups for the fluence rate computation must also be defined by the user. The results are presented in $\frac{n}{cm^2 \cdot s}$.

4.3 Reaction Rates Calculations

The Monte Carlo approach for the simulation of the reaction rates utilized in the neutronics stochastic codes comprises the collision and the track-length estimators (*Lewis and Miller*, 1993). The formulae for the two estimators are given in *Equations* (*4.6)* and (*4.7)* respectively.

$$R_x^C = \frac{1}{W} \sum_{i \in C} \frac{w_i \Sigma_x(E_i)}{\Sigma_t(E_i)} \tag{4.7}$$

$$R_x^T = \frac{1}{W} \sum_{i \in T} w_i \ell_i \Sigma_x(E_i) \tag{4.7}$$

where $\Sigma_x(E_i)$ is the macroscopic cross section of the target material for the reaction x (where x stands for *absorption*, *elastic scattering*, *fission*) at the incoming energy E_i of the particle. For the reaction rates calculation the user must provide to the code the number of the positions and the relevant volumes, the energy boundaries of the energy groups and specify which reactions should be followed by the code. Moreover, the results are presented in $\frac{reactions}{cm^3 \cdot s}$, hence are not volume integrated.

4.4 Dynamic Assessment of Core Isotopic Composition

The purpose of this work is to simulate the long-term behaviour of a nuclear reactor by modelling the changes in the composition of fuel and other materials under irradiation along with the resulting changes in the neutronic properties of the system.

The Monte Carlo approach for calculating the fuel composition evolution includes two computational steps: the calculation of the neutron density distribution and the assessment of the changes in the nuclide concentrations. The basis of this approach is the assumption that the neutron density distribution and the changes in the nuclide concentrations can be solved sequentially in a cyclic manner by alternating the two computational steps and using results from the previous steps. During the first step, stochastic codes compute the steady state neutron flux for given materials composition therefore the reaction rates are easily derived. During the second step, the changes in the nuclide composition are calculated assuming constant reaction rates during a time-step.

The above described methodology for burnup calculations is applied in ANET, with the difference that reactions rates are computed and utilized directly. The real life time-step and the relevant computational time-step are assigned to two variables defined in the input file of ANET. It is in the user's discretion to decide the correspondence between the real life time-step and the number of cycles (computational time-step) that will be used by the code so as to calculate the reaction rates and subsequently the material evolution. The number of cycles that will be chosen for the computation of the reaction rates is a compromise between computational cost and minimization of reaction rates' statistical error.

In *Chapter 3*, the depletion equations were introduced explicitly but for the reader's convenience are given again.

$$\frac{dN_i}{dt} = \sum_j \gamma_{ji}\sigma_{f,i}N_j\phi + \sum_k \sigma_{c,k\to i}N_k\phi + \sum_l \lambda_{l\to i}N_l - \left(\sigma_{f,i}N_i\phi + \sigma_{\alpha,i}N_i\phi + \lambda_i N_i\right) \quad (4.8)$$

The applied solution technique in the current version of the ANET code is the fifth-order Runge-Kutta method. The system of differential equations of the isotopes' densities *(4.8)* can be thus transformed into a system of linear *Equations (4.9)* and *(4.10)*. The solution of the aforementioned Eqs can be performed without great effort in a time interval [t_{in}, t_f] where the number of considered steps, otherwise sub-

intervals, is *n*. The variables i = 1, 2, … , m and k = 0, 1, 2, … , n-1 run for the number of followed isotopes' densities and the number of sub-intervals the initial interval [t_{in}, t_f] is divided respectively. Parameter t_k is the real time at the beginning of step while *h* is the chosen time-step. The particular values of the various constants, $\alpha_1 - \alpha_6$, $b_{21} - b_{65}$ and $c_1 - c_6$ that are widely applied are those found by Cash and Carp *(Cash and Carp, 1990)* and are given in *Table 4.1* below.

$$
\begin{aligned}
N_{1,k+1} &= N_{1,k} + c_1K_{1,a} + c_2K_{1,b} + c_3K_{1,c} + c_4K_{1,d} + c_5K_{1,e} + c_6K_{1,f} \\
N_{2,k+1} &= N_{2,k} + c_1K_{2,a} + c_2K_{2,b} + c_3K_{2,c} + c_4K_{2,d} + c_5K_{2,e} + c_6K_{2,f} \qquad (4.9) \\
&\ldots \\
N_{i,k+1} &= N_{i,k} + c_1K_{i,a} + c_2K_{i,b} + c_3K_{i,c} + c_4K_{i,d} + c_5K_{i,e} + c_6K_{i,f}
\end{aligned}
$$

where

$$
\begin{aligned}
K_{i,a} &= hf_i\left(t_k, N_{1,k}, N_{2,k}, \ldots, N_{m,k}\right) \\
K_{i,b} &= hf_i\left(t_k + \alpha_2 h, N_{1,k} + b_{21}K_{1,a}, N_{2,k} + b_{21}K_{2,a}, \ldots, N_{m,k} + b_{21}K_{m,a}\right) \\
K_{i,c} &= hf_i(t_k + a_3h, N_{1,k} + b_{31}K_{1,a} + b_{32}K_{1,b}, N_{2,k} + b_{31}K_{2,a} + b_{32}K_{2,b}, \ldots, \\
&\quad N_{m,k} + b_{31}K_{m,a} + b_{32}K_{m,b}) \\
K_{i,d} &= hf_i(t_k + a_4h, N_{1,k} + b_{41}K_{1,a} + b_{42}K_{1,b} + b_{43}K_{1,c}, \\
&\quad N_{2,k} + b_{41}K_{2,a} + b_{42}K_{2,b} + b_{43}K_{2,c}, \ldots, \qquad (4.10) \\
&\quad N_{m,k} + b_{41}K_{m,a} + b_{42}K_{m,b} + b_{43}K_{m,c}) \\
K_{i,e} &= hf_i(t_k + a_5h, N_{1,k} + b_{51}K_{1,a} + b_{52}K_{1,b} + b_{53}K_{1,c} + b_{54}K_{1,d}, \\
&\quad N_{2,k} + b_{51}K_{2,a} + b_{52}K_{2,b} + b_{53}K_{2,c} + b_{54}K_{2,d}, \ldots, \\
&\quad N_{i,k} + b_{51}K_{i,a} + b_{52}K_{i,b} + b_{53}K_{i,c} + b_{54}K_{i,d}) \\
K_{i,f} &= hf_i(t_k + a_6h, N_{1,k} + b_{61}K_{1,a} + b_{62}K_{1,b} + b_{63}K_{1,c} + b_{64}K_{1,d} + b_{65}K_{1,e}, \\
&\quad N_{2,k} + b_{61}K_{2,a} + b_{62}K_{2,b} + b_{63}K_{2,c} + b_{64}K_{2,d} + b_{65}K_{2,e}, \ldots, \\
&\quad N_{i,k} + b_{61}K_{i,a} + b_{62}K_{i,b} + b_{63}K_{i,c} + b_{64}K_{i,d} + b_{65}K_{i,e})
\end{aligned}
$$

Table 4.1: Cash and Carp constants for the fifth order Runge-Kutta method.

Cash-Karp Parameters for Embedded Runge-Kutta Method							
i	α_i	b_{ij}					c_i
1							$\frac{2528}{27648}$
2	$\frac{1}{5}$	$\frac{1}{5}$					0
3	$\frac{3}{10}$	$\frac{3}{40}$	$\frac{9}{40}$				$\frac{18575}{48384}$
4	$\frac{3}{5}$	$-\frac{9}{10}$	$\frac{6}{5}$				$\frac{13525}{55296}$
5	1	$-\frac{11}{54}$	$\frac{5}{2}$	$-\frac{70}{27}$	$\frac{35}{27}$		$\frac{277}{14336}$
6	$\frac{7}{8}$	$\frac{1631}{55296}$	$\frac{175}{512}$	$\frac{575}{13824}$	$\frac{44275}{110592}$	$\frac{253}{4096}$	$\frac{1}{4}$
j	1	2	3	4	5		

Detailed nuclide chains containing the most important fission products and transuranic elements with the relevant half-lives for decay and thermal absorption cross sections have been constructed and are presented in Appendix III. In the current version of the code approximately 150 nuclides, presented in *Tables 4.2 - 4.6* are included and can be treated for the transmutation reactions and the radioactive decays. Data concerning the decay constant of the various nuclides are stored in a particular file, called *decay.dat*, while nuclides with radioactive decay half-life greater than 10^3 years are considered steady. Special care has been granted for the isotopes with unavailable cross sections. The cumulative and independent fission yields for selected fission products are stored in a fission data file for each one of the fissile nuclides, i.e. ^{233}U, ^{235}U, ^{239}Pu and ^{241}Pu as well as for the nuclei with an energy threshold for fission of the order of 1 MeV, i.e. ^{232}Th, ^{238}U, ^{240}Pu and ^{242}Pu and finally for the nuclides ^{234}U, ^{236}U, ^{241}Am, ^{243}Am, ^{243}Cm and ^{245}Cm. The current version of ANET utilizes the JEFF-3.1 incident neutron data as far as the cumulative yields are concerned.

Table 4.2: Fission products treated in the ANET code.

Nuclide (direct fission product)	$t_{1/2}$	**Daughter Nuclide (β^- decay)**	$t_{1/2}$
${}^{85}_{36}Kr$	10.8yr	${}^{85}_{37}Rb$	stable
${}^{86}_{37}Rb$	18.6d	${}^{86}_{38}Sr$	stable
${}^{87}_{37}Rb$	~stable		
${}^{87}_{38}Sr$	stable		
${}^{88}_{38}Sr$	stable		
${}^{89}_{38}Sr$	50.5d	${}^{89}_{39}Y$	stable
${}^{90}_{38}Sr$	28.9yr	${}^{90}_{39}Y$	64.0h
${}^{91}_{38}Sr$	9.5h	${}^{91}_{39}Y$	58.5d
${}^{90}_{39}Y$	64.0h	${}^{90}_{40}Zr$	stable
${}^{91}_{39}Y$	58.5d	${}^{91}_{40}Zr$	stable
${}^{92}_{40}Zr$	stable		
${}^{93}_{40}Zr$	stable		
${}^{94}_{40}Zr$	stable		
${}^{95}_{40}Zr$	64.0d	${}^{95}_{41}Nb$	35.0d
${}^{95}_{41}Nb$	35.0d	${}^{95}_{42}Mo$	stable

Table 4.3: Fission products treated in the ANET code.

Nuclide (direct fission product)	$t_{1/2}$	**Daughter Nuclide (β^- decay)**	$t_{1/2}$
$^{96}_{42}Mo$	stable		
$^{97}_{42}Mo$	stable		
$^{98}_{42}Mo$	stable		
$^{99}_{42}Mo$	66.0h	$^{99}_{43}Tc$	~stable
$^{100}_{43}Tc$	15.5s	$^{100}_{44}Ru$	stable
$^{101}_{44}Ru$	stable		
$^{102}_{44}Ru$	stable		
$^{103}_{44}Ru$	39.2d	$^{103}_{45}Rh$	stable
$^{104}_{44}Ru$	stable		
$^{105}_{44}Ru$	4.4h	$^{105}_{45}Rh$	35.4h
$^{104}_{45}Rh$	42.3s	$^{104}_{46}Pd$	stable
$^{105}_{45}Rh$	35.4h	$^{105}_{46}Pd$	stable
$^{106}_{45}Rh$	30.1s	$^{106}_{46}Pd$	stable
$^{107}_{45}Rh$	21.7min	$^{107}_{46}Pd$	stable
$^{110}_{47}Ag$	24.6s	$^{110}_{48}Cd$	stable

Table 4.4: Fission products treated in the ANET code.

Nuclide (direct fission product)	$t_{1/2}$	**Daughter Nuclide (β^- decay)**	$t_{1/2}$
$^{111}_{48}Cd$	stable		
$^{112}_{48}Cd$	stable		
$^{113}_{48}Cd$	~stable		
$^{114}_{48}Cd$	~stable		
$^{115}_{48}Cd$	53.5h	$^{115}_{49}In$	~stable
$^{130}_{53}I$	12.4h	$^{130}_{54}Xe$	stable
$^{131}_{53}I$	8.0d	$^{131}_{54}Xe$	stable
$^{132}_{53}I$	2.3h	$^{132}_{54}Xe$	stable
$^{133}_{53}I$	20.8h	$^{133}_{54}Xe$	5.2d
$^{134}_{53}I$	52.5min	$^{134}_{54}Xe$	~stable
$^{135}_{53}I$	6.6h	$^{135}_{54}Xe$	9.1h
$^{128}_{54}Xe$	stable		
$^{129}_{54}Xe$	stable		
$^{136}_{54}Xe$	~stable		
$^{133}_{55}Cs$	stable		

Table 4.5: Fission products treated in the ANET code.

Nuclide (direct fission product)	$t_{1/2}$	**Daughter Nuclide (β^- decay)**	$t_{1/2}$
$^{134}_{55}Cs$	2.1yr	$^{134}_{56}Ba$	stable
$^{135}_{54}Xe$	9.1h	$^{135}_{55}Cs$	~stable
$^{136}_{55}Cs$	13.0d	$^{136}_{56}Ba$	stable
$^{137}_{55}Cs$	30.1yr	$^{137}_{56}Ba$	stable
$^{135}_{56}Ba$	stable		
$^{138}_{56}Ba$	stable		
$^{139}_{56}Ba$	83.1min	$^{139}_{57}La$	stable
$^{140}_{56}Ba$	12.8d	$^{140}_{57}La$	1.7d
$^{141}_{56}Ba$	18.3min	$^{141}_{57}La$	3.9h
$^{141}_{57}La$	3.9h	$^{141}_{58}Ce$	32.5d
$^{141}_{59}\mathrm{Pr}$	stable		
$^{142}_{59}\mathrm{Pr}$	19.2h	$^{142}_{60}Nd$	stable
$^{143}_{59}\mathrm{Pr}$	13.6d	$^{143}_{60}Nd$	stable
$^{144}_{60}Nd$	~stable		
$^{145}_{60}Nd$	stable		

Table 4.6: Fission products treated in the ANET code.

Nuclide (direct fission product)	$t_{1/2}$	**Daughter Nuclide (β^- decay)**	$t_{1/2}$
$^{146}_{60}Nd$	stable		
$^{147}_{60}Nd$	11.0d	$^{147}_{61}Pm$	2.6yr
$^{148}_{60}Nd$	stable		
$^{147}_{61}Pm$	2.6yr	$^{147}_{62}Sm$	~stable
$^{148}_{61}Pm$	5.4d	$^{148}_{62}Sm$	~stable
$^{149}_{61}Pm$	53.1h	$^{149}_{62}Sm$	stable
$^{150}_{62}Sm$	stable		
$^{151}_{62}Sm$	90.0yr	$^{151}_{63}Eu$	~stable
$^{152}_{62}Sm$	stable		
$^{153}_{62}Sm$	46.3h	$^{153}_{63}Eu$	stable
$^{152}_{63}Eu$	13.5yr	$^{152}_{64}Gd$	~stable
$^{154}_{63}Eu$	8.6yr	$^{154}_{64}Gd$	stable
$^{155}_{63}Eu$	4.8yr	$^{155}_{64}Gd$	stable
$^{156}_{63}Eu$	15.2d	$^{156}_{64}Gd$	stable
$^{157}_{63}Eu$	15.2yr	$^{157}_{64}Gd$	stable
$^{158}_{64}Gd$	stable		

The evolving materials must be declared by the user in the subroutine where the initial composition of the materials is defined. The nuclides for each evolving material that will be followed in the code and treated for transmutation reactions, radioactive decay and fission should be carefully chosen and are problem dependent while they must be designated in a specific file. It should be mentioned that only the nuclides included in this file will be treated in the evolution calculations. At the initialization of the code during the reading of the geometry and the material composition, the additional nuclides that will be followed are added to the initial composition of each evolving material. During the tracking procedure for the neutron, the code checks if the neutron is located in an evolving material and only then assesses the reaction rates with constant material composition for the number of cycles that corresponds to the time-step. Consequently, when the cycle that corresponds to the completion of the computational time-step is reached, the material composition is updated by using the above mentioned formulae. The updated material composition is utilized for the reaction rate computation in the following cycles and this iterative procedure is repeated until the termination of the program which corresponds to the selected lifetime of the reactor's operation. A simplified flow diagram of the ANET code is given in *Figure 4.1*.

Figure 4.1: Simplified flow diagram of the ANET code.

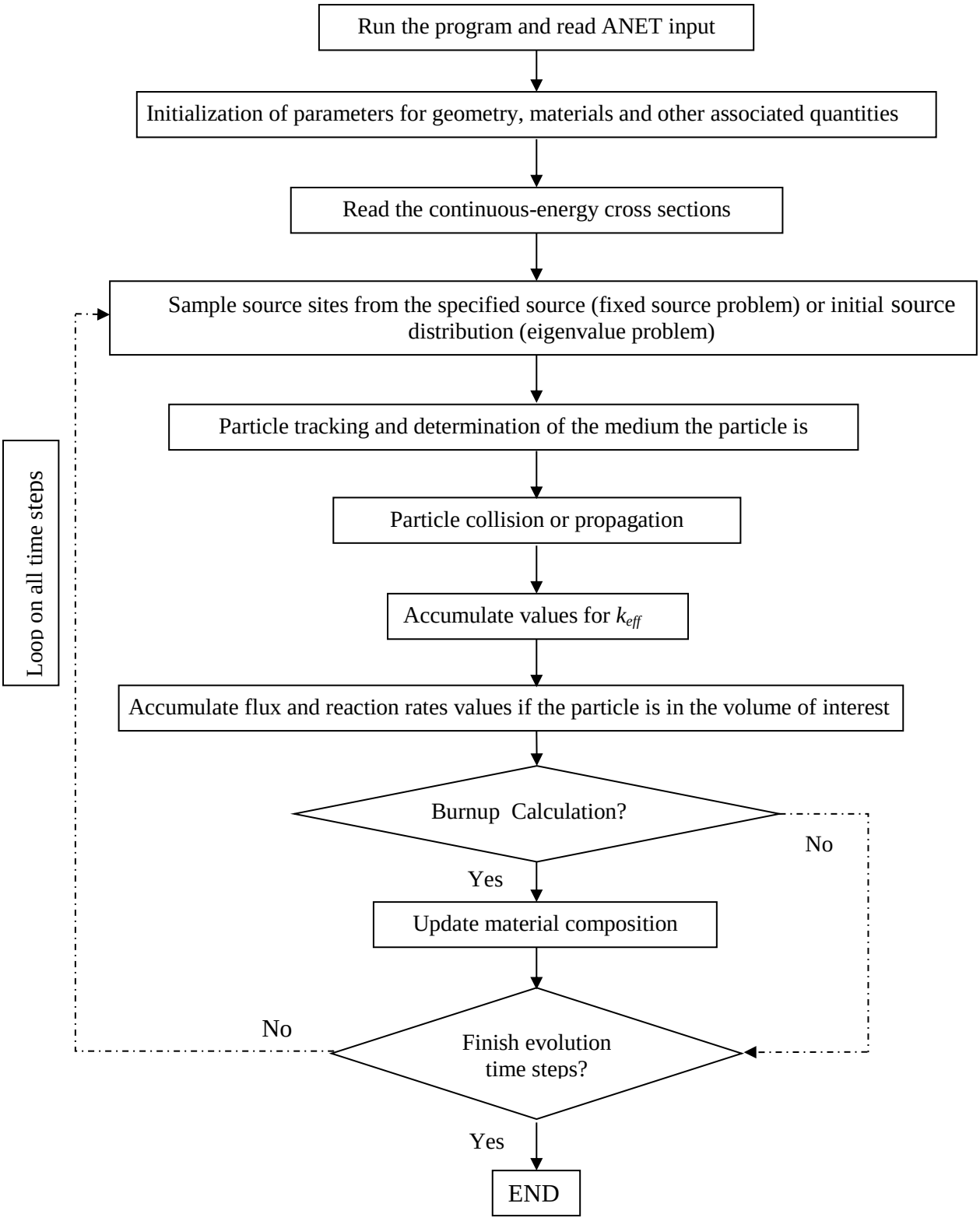

5 SETUPS OF THE SIMULATED INSTALLATIONS

Successive testing applications performed throughout the ANET development have been utilized to validate and verify the new code capabilities concerning the simulation of certain reactor parameters important to safety, i.e. reactor criticality, neutron fluence and fission rates. The Portuguese Research Reactor (RPI) after its conversion to low enrichment in U-235 and the OECD/NEA VENUS-2 MOX international benchmark were considered appropriate for the present study, the former providing criticality and neutron flux data and the latter providing reaction rates. Concerning criticality benchmarking, the subcritical, Training Nuclear Reactor of the Aristotle University of Thessaloniki (TNR-AUTh) was also analyzed. Moreover, the OECD/NEA, Burnup Credit Calculation Benchmark was chosen for the preliminary tests on ANET's capability of performing depletion calculations.

5.1 The Training Nuclear Reactor Model 9000 of the Aristotle University of Thessaloniki (TNR-AUTh)

The Student Training Nuclear Reactor hosted by the Physics Department of the Aristotle University of Thessaloniki (TNR-AUTh) *(Nuclear Chicago Corporation, 1959)* is a subcritical assembly. The cylindrical reactor tank contains the fuel tubes and two supporting grids. Light water is used as moderator and reflector and 270 fuel tubes are arranged in a hexagonal lattice. The fuel tube at the lattice center is excluded in order to allow for the insertion of the neutron source which is a 6cm height cylinder with 1.5cm radius. A vertical cross section of the reactor with geometrical details is shown in *Figure 5.1*. The dimensions of all parts of the assembly are shown in *Figures 5.2 - 5.4*. In particular, in *Figure 5.2* the fuel tube is described, in *Figure 5.3* the dimensions of the fuel slug are given and in *Figure 5.4* the hexagonal lattice unit is shown. The full hexagonal lattice arrangement is shown in *Figure 5.5*. The fuel composition is natural uranium metal 99.29% ^{238}U and 0.71% ^{235}U. The materials specification of TNR-AUTh are included in *Table 5.1*. The neutron source used is a 5Ci ^{241}Am-^{9}Be with $1.1 \cdot 10^{7}$ $n \cdot s^{-1}$ intensity. The source is of X.14 type and consists of a compacted mixture of Americium oxide with Beryllium metal, doubly encapsulated in welded stainless steel. The specific neutron spectrum and its distribution into energy groups has been derived from available data concerning a 1Ci ^{241}Am-^{9}Be (α, n) source *(Vijaya et al., 1973)* adjusted to the TNR-AUTh source specifications. The neutron spectrum from the ^{241}Am-^{9}Be (α,n) source

of 5Ci and its distribution into energy groups are shown in *Figure 5.7* and in *Table 5.2* respectively.

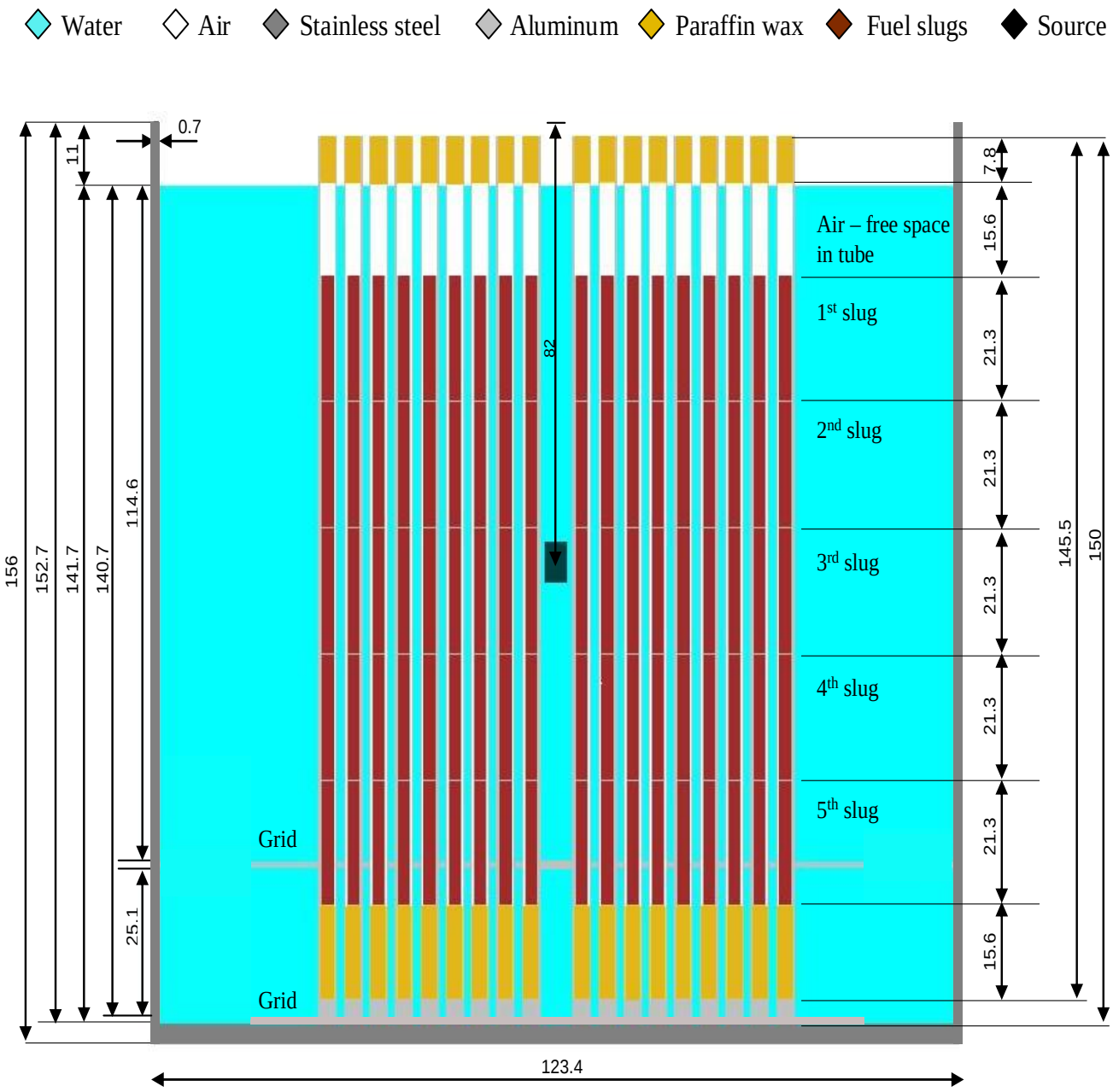

Figure 5.1: Geometrical description of the TNR-AUTh. All dimensions are in cm. The source's position is 82 ± 5 cm below tank's surface.

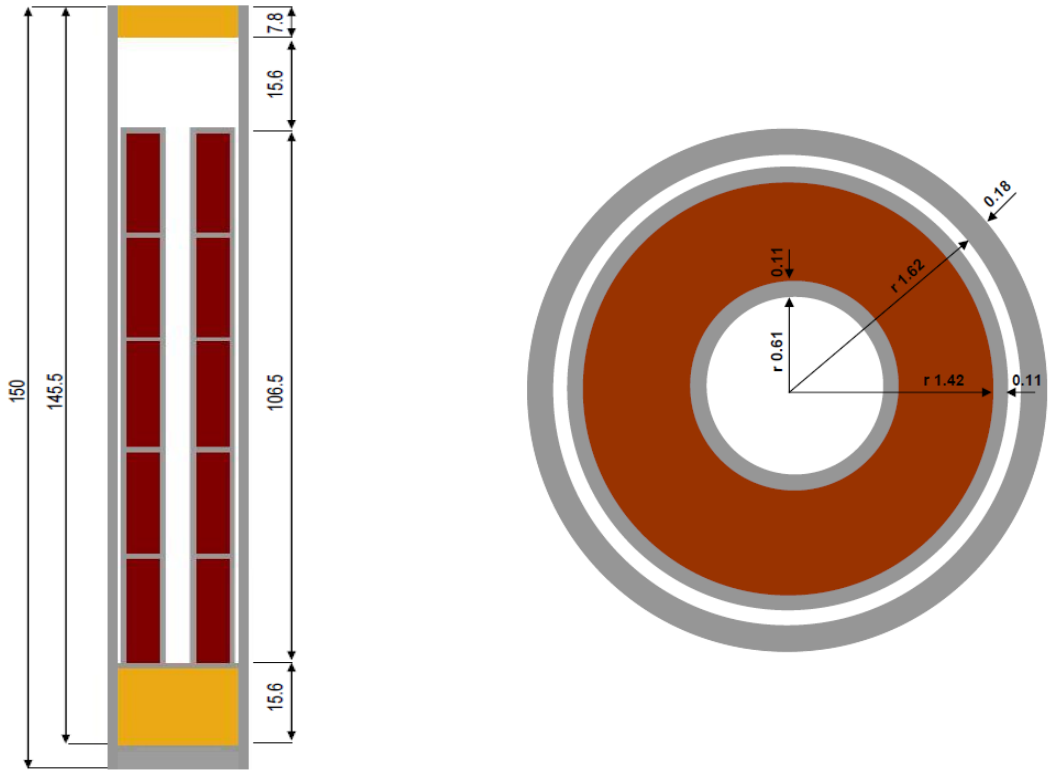

Figure 5.2: Description of the TNR-AUTh fuel tube (dimensions in cm).

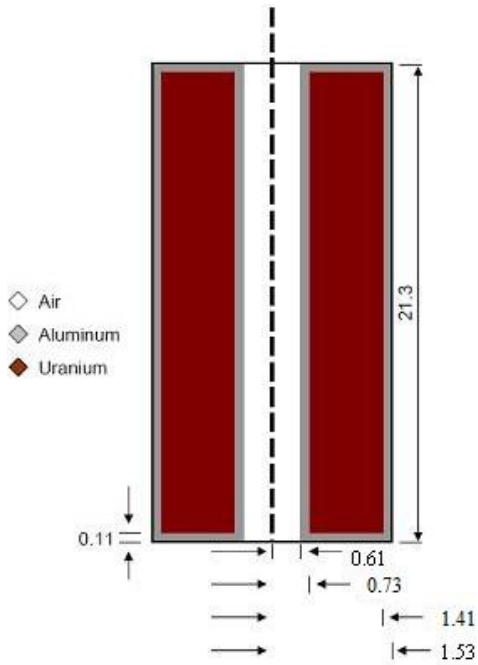

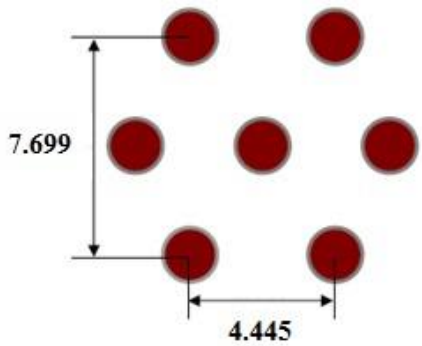

Figure 5.3: Description of the TNR-AUTh fuel slug (dimensions in cm).

Figure 5.4: The unit of the TNR-AUTh hexagonal lattice (dimensions in cm).

Table 5.1: Density and composition of the TNR-AUTh assembly's materials.

Assembly Part	Material	Density ($g \cdot cm^{-3}$)	Composition
Tank	Stainless steel	7.6051	^{55}Mn 2.10% ^{50}Cr 0.009% ^{52}Cr 15.9% ^{53}Cr 1.83% ^{54}Cr 0.007% ^{58}Ni 7.10% ^{60}Ni 2.81% ^{61}Ni 0.129% ^{62}Ni 0.399% ^{64}Ni 0.104% ^{54}Fe 0.045% ^{56}Fe 67.7% ^{57}Fe 1.65% ^{58}Fe 0.217%
Tube	Aluminum	2.70	^{27}Al 100.00%
Grid			
Moderator	Light water	1.00	^{1}H 11.00% ^{16}O 89.00%
Reflector			
Fuel	Natural Uranium metal	18.7	^{238}U 99.29% ^{235}U 0.71%
Paraffin Wax	$C_{25}H_{52}$	0.9	^{12}C 85.23% ^{1}H 14.77%

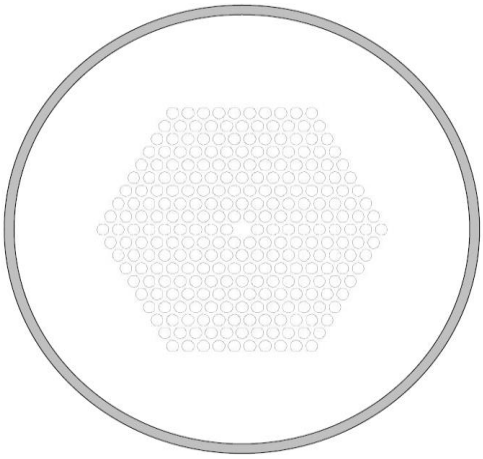

Figure 5.5: Full hexagonal lattice arrangement of the TNR-AUTh.

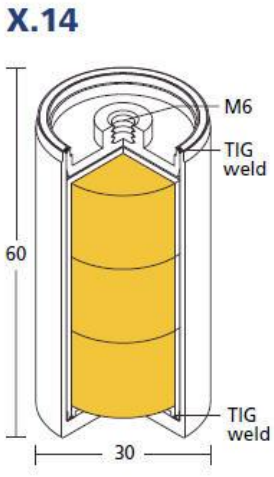

Figure 5.6: X.14-type ^{241}Am-^{9}Be source (dimensions are in mm).

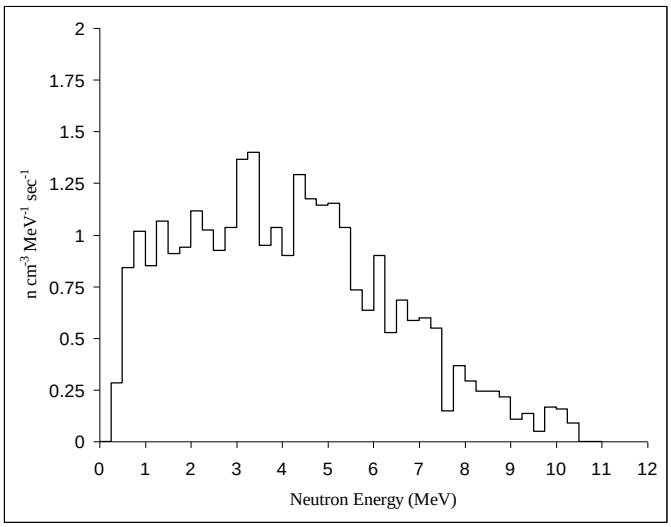

Figure 5.7: Energy spectrum of the neutrons emitted from the ^{241}Am-^{9}Be of 5Ci. (The width of each energy group is 0.25MeV).

Table 5.2: Tabulated neutron spectrum of the ^{241}Am-^{9}Be neutron source.

Energy group (MeV)	Neutron Source Intensity $n \cdot cm^{-3} \cdot MeV^{-1} \cdot s^{-1}$	Energy group (MeV)	Neutron Source Intensity $n \cdot cm^{-3} \cdot MeV^{-1} \cdot s^{-1}$
0.00 - 0.25	0.0000	5.50 - 5.75	0.7334
0.25 - 0.50	0.2836	5.75 - 6.00	0.6356
0.50 - 0.75	0.8409	6.00 - 6.25	0.8996
0.75 - 1.00	1.0170	6.25 - 6.50	0.5280
1.00 - 1.25	0.8507	6.50 - 6.75	0.6845
1.25 - 1.50	1.0658	6.75 - 7.00	0.5867
1.50 - 1.75	0.9094	7.00 - 7.25	0.5965
1.75 - 2.00	0.9387	7.25 - 7.50	0.5476
2.00 - 2.25	1.1147	7.50 - 7.75	0.1467
2.25 - 2.50	1.0218	7.75 - 8.00	0.3667
2.50 - 2.75	0.9241	8.00 - 8.25	0.2934
2.75 - 3.00	1.0365	8.25 - 8.50	0.2445
3.00 - 3.25	1.3641	8.50 - 8.75	0.2445
3.25 - 3.50	1.3983	8.75 - 9.00	0.2151
3.50 - 3.75	0.9485	9.00 - 9.25	0.1076
3.75 - 4.00	1.0365	9.25 - 9.50	0.1369
4.00 - 4.25	0.8996	9.50 - 9.75	0.0489
4.25 - 4.50	1.2908	9.75 - 10.00	0.1662
4.50 - 4.75	1.1734	10.00 - 10.25	0.1565
4.75 - 5.00	1.1441	10.25 - 10.50	0.0880
5.00 - 5.25	1.1539	10.50 - 10.75	0.0000
5.25 - 5.50	1.0365	10.75 - 11.00	0.0000

5.2 The Portuguese Research Reactor (RPI)

The Portuguese Research Reactor is a 1MW pool-type reactor built by American Machinery and Foundry (AMF) Atomics, US, commissioned in 1961. Its design is similar to the one of the Greek Research Reactor (GRR-1), in Athens, the ‘‘Hoger Onderwijsreactor’’ in Delft, The Netherlands and the McMaster Reactor in Canada.

Core conversion to LEU fuel was concluded in 2007 after feasibility and safety studies, made with the assistance of the RERTR program within project POR4012 of the International Atomic Energy Agency (IAEA). The LEU fuel (19.75% nominal U-235 enrichment) was supplied by the US, following Y-12 specifications *(Nelson et al., 2010)*, which are more stringent than the ASTM C1462-00 standard, namely in the allowed amounts of U-234 and U-236. Detailed neutronic core analyses using the Monte Carlo code MCNP-4C were performed for the RPI *(Matos et al., 2006)*.

The analyzed core configuration (*Figure 5.8*) consists of seven standard and five control LEU fuel assemblies of the Materials Testing Reactor (MTR) type *(Rosenthal et al., 2010)* manufactured by CERCA (AREVA group, France). Control and standard fuel assemblies (*Figure 5.9*) contain 10 and 18 fuel flat plates, with approximately 20.9 g of U-235 per plate, respectively. Each fuel plate contains a meat of U_3Si_2 (silicide) powder dispersed in pure Al, clad of AG3NE Al alloy (similar to 6061 Alcoa alloy). Silicide dispersion fuel was fully qualified by the US Nuclear Regulatory Commission in 1988 and has been widely used in research reactors.

For control purposes, four shim-safety rods and one regulation rod are included in the analyzed configuration, located in the central channels of the control assemblies. The shim-safety rods consist of a 1 mm-thick cadmium layer supported and covered by 1.5 mm-thick stainless steel, while the regulating rod is a hollow 2.2 mm-thick stainless steel tube. Rods have oval cross- sectional shapes and 61 cm length. When fully inserted, the centre line of the rods is displaced 14 mm above that of the fuel meat. Further details about the fuel description and assemblies design are given in *Table 5.3* and are also reported in *(Matos et al., 2006)*. The core is reflected by graphite (in the thermal column), by beryllium and by light water. The beryllium reflectors were supplied by the former USSR through the Technical Cooperation program of the IAEA in the 1980s. A set of impurities was considered based on previous experience with Be of the same origin *(Matos*Matos, *2005)*. Four dummy assemblies were introduced in the core periphery in order to improve the thermal hydraulic safety margin. The fuel, dummies and beryllium reflectors are mounted on a grid plate in a 9x6 pattern. The free grid positions, the dummies and cavities at some beryllium reflectors are sample irradiation positions. The dummies have the same external structure as fuel assemblies but instead of fuel plates they contain only an aluminum tube in the central region allowing sample irradiation.

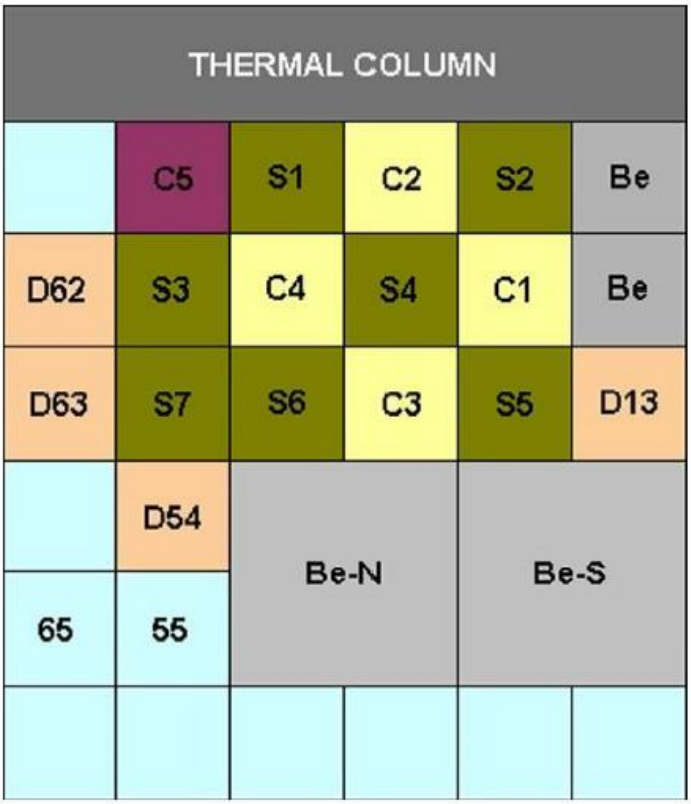

Figure 5.8: The analyzed RPI core configuration

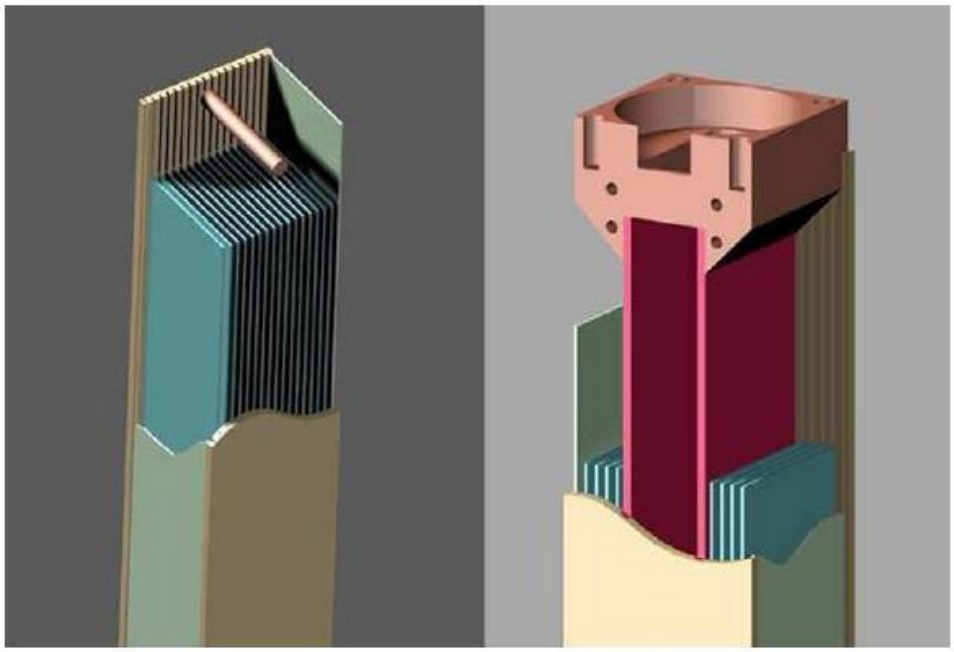

Figure 5.9: Schematic view of the RPI fuel assemblies, standard (left) and control right).

Table 5.3: Summary of RPI core design data.

Fuel type	MTR plate
Meat composition	U_3Si_2-Al
Nominal enrichment in ^{235}U (%)	19.75
Average mass of ^{235}U per plate (g)	20.9
Cladding material	AG3NE alloy
Number of plates per assembly	Standard: 18; Control: 10
Number of assemblies (initial core)	Standard: 7; Control: 5
Meat dimensions (mm)	0.6 x 63.4 x 596.9
Plate dimensions (mm)	1.37 x 71.0 x 625.5
Assembly dimensions (mm)	79.8 x 75.9 x 714.4
Cladding thickness of fuel plate (mm)	0.38
Coolant channel thickness (mm)	3.05
Absorber material in control rod	Cd
Absorber material in regulating rod	Stainless steel 18/10
Cladding material of control rod	Stainless steel 18/10
Number of rods	Control: 4; Regulating: 1
External dimensions of control rod (mm)	56.0 x 21.0 x 642.0
External dimensions of regulating rod (mm)	57.2 x 22.2 x 642.0
Absorber height (mm)	608.0
Absorber thickness (mm)	Control rod: 1; Regulating rod: 2.2
Cladding thickness in control rod (mm)	1.5 mm in each side of the absorber

5.3 The VENUS Facility

The VENUS facility is a zero power critical reactor located at SCK·CEN in Belgium. As shown in *Figure 5.10*, the core consists of 12 “15×15” subassemblies. The central part of the core (four 15×15 assemblies) consists of fuel pins 3.3 wt % enriched in ^{235}U (called 3/0 UO2 pins). There are five Pyrex pins in 1/8 of the core. Of the eight assemblies on the periphery of the core, all of which contain fuel pins 4.0 wt.% enriched in ^{235}U (called 4/0 UO2 pins), eight rows of the most external fuel pins have been replaced by mixed oxide fuel pins (UO2-PuO2) enriched 2.0 wt.% in ^{235}U and 2.7 wt.% in high-grade plutonium (called 2/2.7 MOX pins). The isotopic composition of the three fuel types is given in *Table 5.4*. The average fission rate in the core, which corresponds to the absolute reference irradiation, is 1.87E+08 fissions/cm/s at the midplane. This average fission rate corresponds to a power of 595 Watts.

Table 5.4: Isotopic composition of each fuel type in the VENUS facility (10^{24} atoms/cm^3).

Isotope	3/0 fuel	4/0 fuel	2/2.7 MOX fuel
^{234}U	6.74213E−06	7.17988E−06	3.31550E−06
^{235}U	7.65322E−04	9.27556E−04	4.13082E−04
^{236}U	3.68820E−06	5.28177E−06	2.67097E−06
^{238}U	2.20912E−02	2.18426E−02	1.99605E−02
^{239}Pu			4.47077E−04
^{240}Pu			9.61437E−05
^{241}Pu			1.70372E−05
^{242}Pu			2.44766E−06
^{241}Am			4.18948E−07
O	4.57338E−02	4.55653E−02	4.18853E−02
^{10}B	3.64042E−09		
^{11}B	1.46531E−08		

A complete description of the benchmark specification, including details of the VENUS-2 core, is given in *(Na et al., 2003)*. Included in this specification are all geometry and material data required to develop the detailed three-dimensional computational model of the VENUS-2 reactor core. Apart from the geometry and material data, the isotopic concentrations of each medium were also provided to minimize the discrepancies from the atomic density calculations.

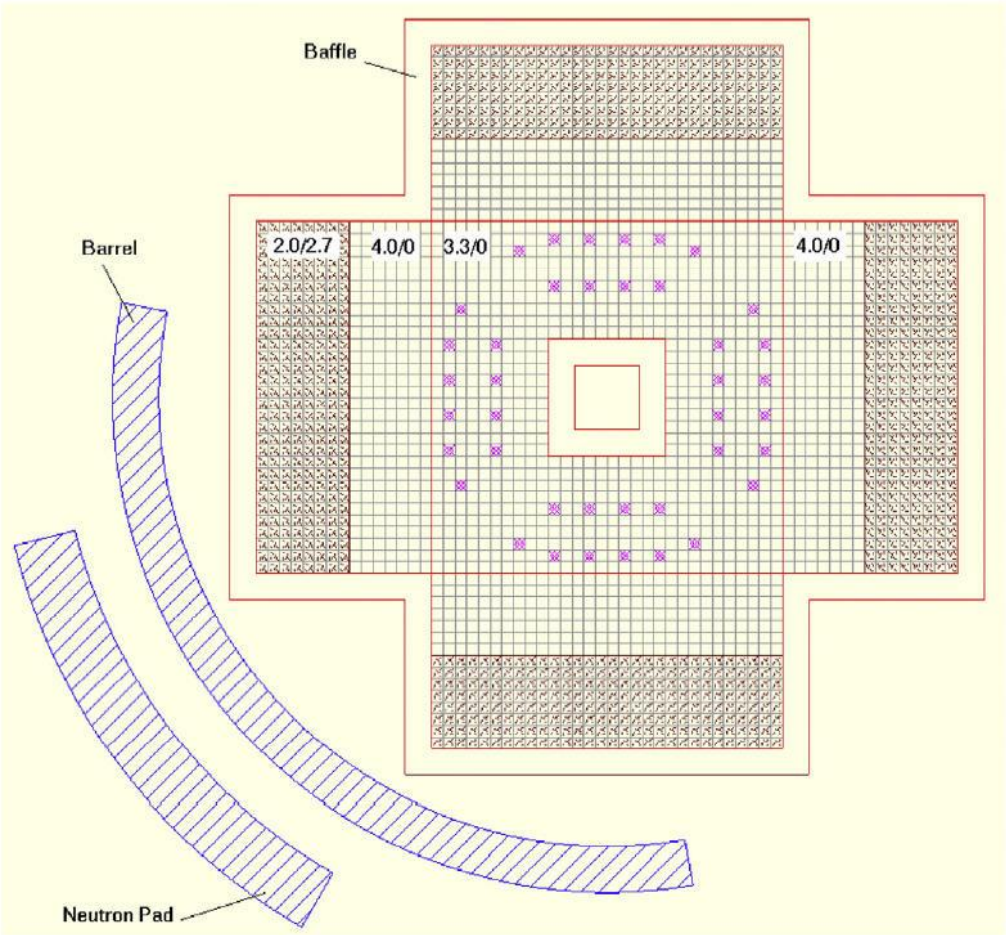

Figure 5.10: VENUS-2 core geometry.

5.4 OECD/NEA Burnup Credit Calculation Benchmark

The purpose of this calculation benchmark *(DeHart et al., 1996)* problem was to compare nuclide concentrations computed by several participants for depletion in a simple pin-cell model. The fuel pin-cell description is given in *Table 5.5*. The fuel sample assay at Materials Characterization Center (MCC) was from a Combustion Engineering 14x14 assembly design. For the purposes of this benchmark, actual pin

dimensions were used but the fuel pin pitch was modified such that the fuel-to-moderator ratio matched that of the actual two dimensional (2-D) assembly. The fuel sample was burned for four complete cycles. This benchmark consists of three cases, corresponding to fuel samples taken from three different axial locations in the reference fuel pin, each with a different total burnup. The goal of this study was to compare the isotopic concentrations calculated by the study participants using various codes and data libraries. *Table 5.6* lists the initial isotopic concentrations to be used for the fuel material for all three cases. In this thesis, case A was considered with 17.24 kW/kgU specific power.

Table 5.5: Physical data for benchmark problem pin-cell calculation.

Parameter	**Data**
Type fuel pellet	UO_2
Fuel density	10.045 g/cm^3
Rod pitch	1.5586 cm
Rod OD	1.118 cm
Rod ID	0.986 cm
Fuel diameter	0.9563 cm
Active fuel length	347.2 cm
Effective fuel temperature	841 K
Clad temperature	620 K
Clad material	Zircaloy-2 (97.91 wt % Zr, 1.59 wt % Sn, 0.5 wt % Fe)
Water temperature	558 K
Water density	0.7569 g/cm^3

Table 5.6: Initial isotopic concentrations of fuel material.

Nuclide	Number density (atoms/b-cm)
^{234}U	6.15165×10^{-6}
^{235}U	6.89220×10^{-4}
^{236}U	3.16265×10^{-6}
^{238}U	2.17104×10^{-2}
^{12}C	9.13357×10^{-6}
^{14}N	1.04072×10^{-5}
^{16}O	4.48178×10^{-2}

5.5 Kyoto University Critical Assembly (KUCA)

The KUCA is located at the Kyoto University Research Reactor Institute (KURRI). At KUCA, by combining a critical assembly of a solid-moderated and reflected type core with the new fixed-field alternating gradient type accelerator installed in 2008, 100 MeV pulsed protons are injected onto the heavy metal target of Pb-Bi and the spallation neutrons are directed into the subcritical system, where highly enriched uranium fuel is loaded together with the polyethylene moderator and reflector *(Pyeon et al., 2017).* At KUCA, cores A and B are polyethylene moderated and reflected cores while core C is a light water-moderated and reflected one. The three cores are operated at a low (order of mW) power level in the normal operating state, the maximum power being 100 W.

For the present work, core A (*Figure 5.11*) and particularly case V (*Figure 5.11b*) configuration was selected. In the A-core, the normal fuel assembly (F: 3/8”P36EU) (*Figure 5.12a*) is composed of 36 fuel plates (unit cells), and lower and upper polyethylene blocks about 478 and 584 mm long, respectively, in an Al sheath 54.3 x 54.3 x 1524 mm^3. The Pb-Bi loaded fuel rod (*Figure 5.13a*) comprises of 60 fuel plates, 30 of them containing Pb-Bi plate, and polyethylene blocks at both end about 484 and 593 mm long starting from bottom in the aforementioned Al sheath. For the normal fuel assemblies, a unit cell in the fuel region is composed of an

enriched uranium fuel plate 1/16” and a polyethylene plate 3/8” (1/8” x 3) thick and a polyethylene plate 1/8” thick whilst for the Pb-Bi loaded ones, two unit cells exist containing both a highly-enriched uranium (HEU) fuel plate 1/8” (1/16” x 2) and 1/8” polyethylene or Pb-Bi plate. A more detailed description of the Pb-Bi plate covering in the HEU fuel assembly is given in *Figure 5.13b*. For the selected core configuration, all the control and safety rods are withdrawn. The main characteristics of the proton beam are 1 nA intensity, 20 Hz pulsed frequency, 100 ns pulsed width and 40 mm diameter spot size at the target. The target is attached to an Al sheath 62 mm below the mid-height of the assembly as shown in (*Figure 5.14*). The atom densities of the materials that compose the core elements are presented in *Tables 5.7-5.12*. A more detailed description of the experiments that are conducted in the Kyoto University facility along with the relevant results can be found in *(Pyeon et al., 2017)*.

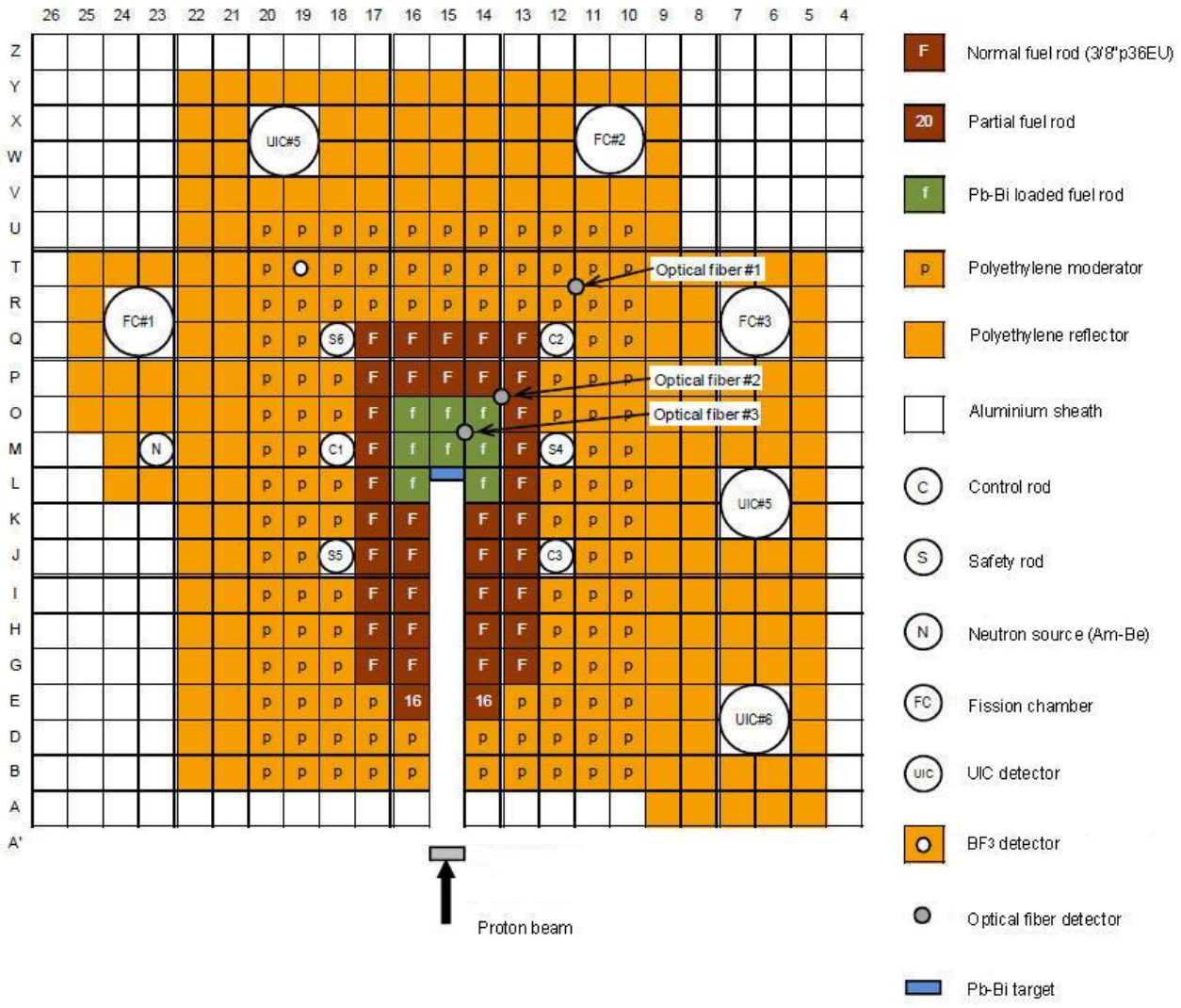

Figure 5.11a: Top view of the KUCA A-core with 100 Mev protons.

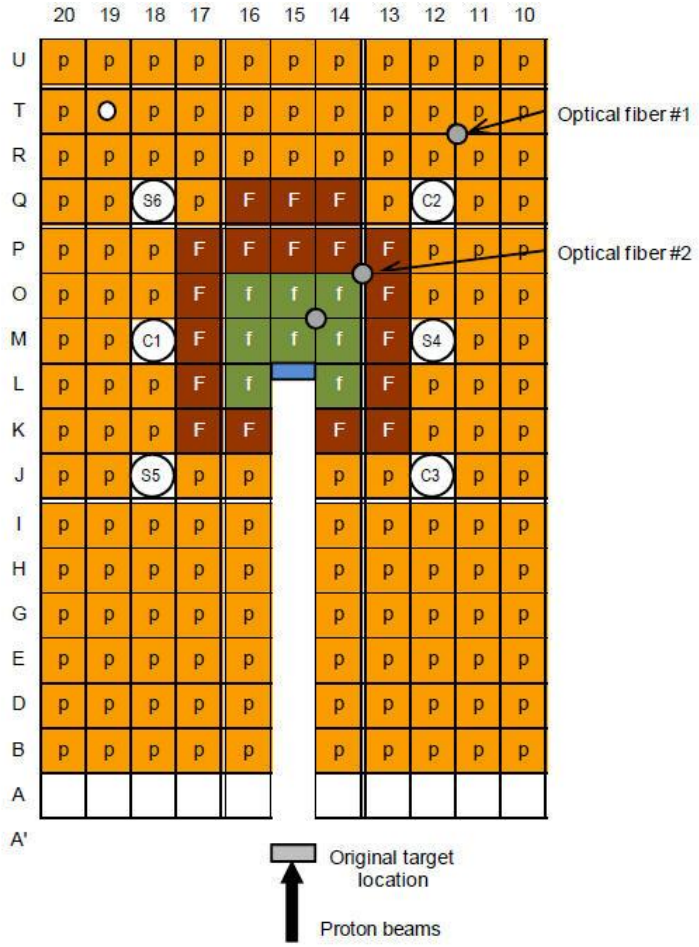

Figure 5.11b: Core configuration case V of KUCA.

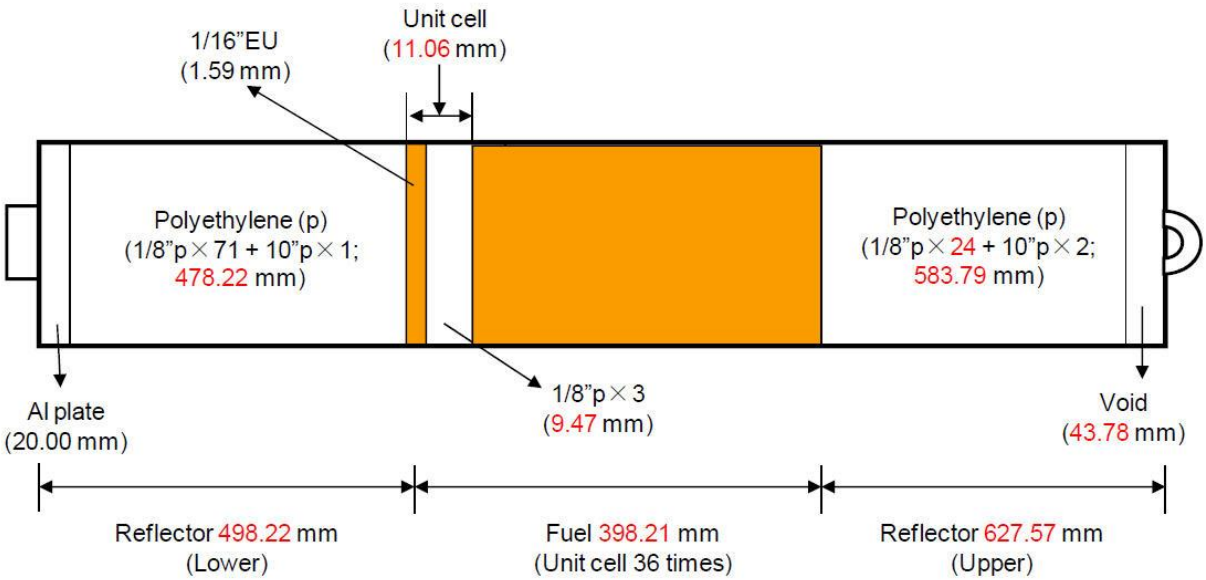

Figure 5.12: Schematic drawings of fuel assembly 3/8"p36EU ("F" in *Figure 5.11*) of KUCA.

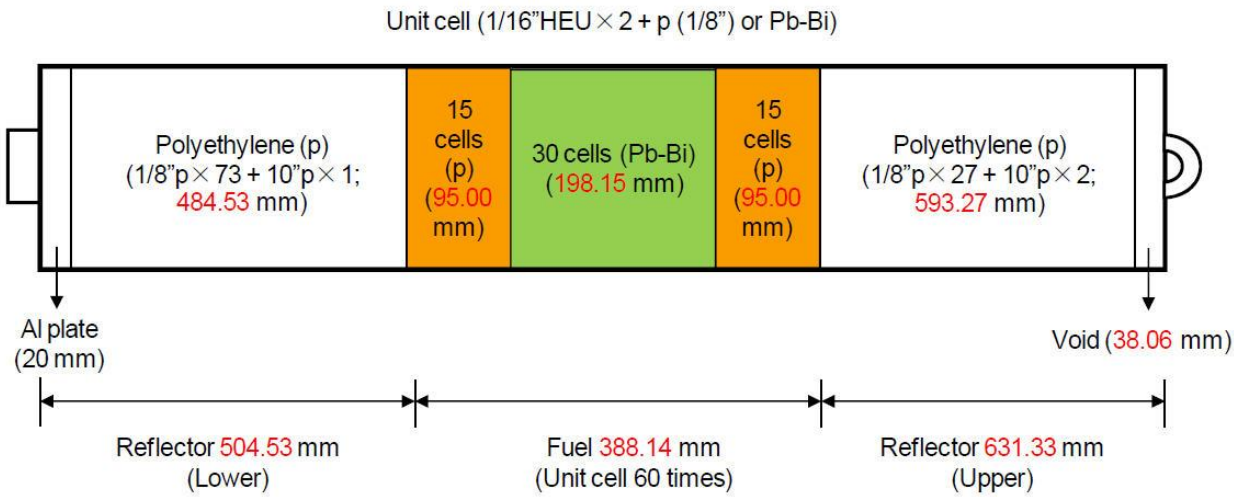

Figure 5.13 Schematic drawings of fuel assembly 1/8"p15EUEU <1/8"PbBi30EUEU > 1/8"p15EUEU ("f" in *Figure 5.11*) of KUCA.

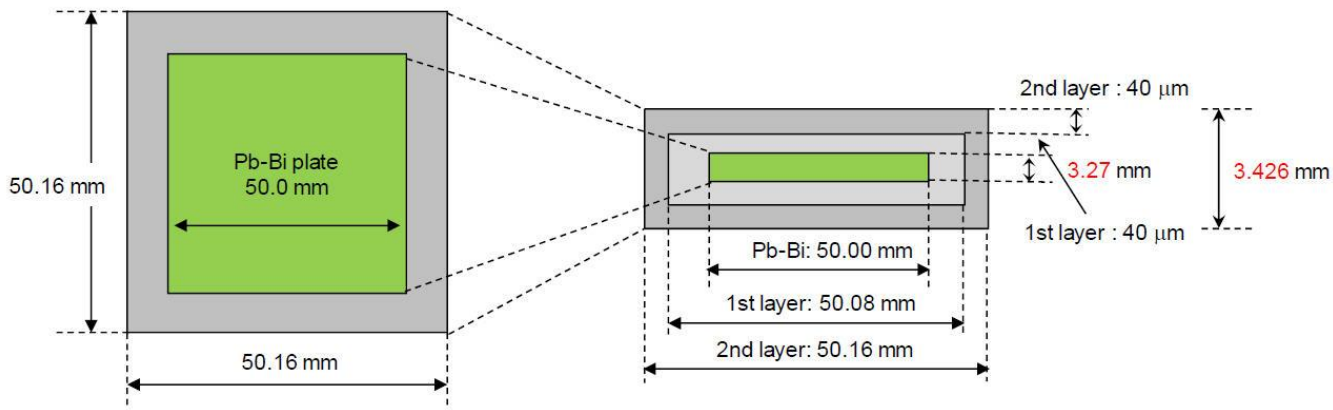

Figure 5.13b: Description of Pb-Bi plate covering over coating materials in "f" assembly of KUCA.

Table 5.7: Atomic densities of 1/16" thick HEU fuel plate (U-Al alloy).

Nuclide	Number density (atoms/b-cm)
^{234}U	1.13659E-05
^{235}U	1.50682E-03
^{236}U	4.82971E-06
^{238}U	9.25879E-05
Al	5.56436E-02

Table 5.8: Atomic density of polyethylene reflector.

Nuclide	Number density (atoms/b-cm)
H	8.00083E-02
C	4.00042E-02

Table 5.9: Atomic density of polyethylene moderator "p".

Nuclide	Number density (atoms/b-cm)	Number density (atoms/b-cm)
	1/8" thick plate	10" Polyethylene square rod
H	7.77938E-02	7.97990E-02
C	3.95860E-02	4.08960E-02

Table 5.10: Atomic density of aluminum sheath for the core element.

Nuclide	Number density (atoms/b-cm)
Al	6.00385E-02

Table 5.11: Atomic density of Pb-Bi.

Nuclide	Abundance	Number density (atoms/b-cm)
^{204}Pb	1.4	1.87461E-04
^{206}Pb	24.1	3.25860E-03
^{207}Pb	22.1	3.00266E-03
^{208}Pb	52.4	7.15378E-03
^{209}Bi	100	1.67670E-02

Table 5.12: Atomic density of coating materials over Pb-Bi plate.

Nuclide	Isotope	Number density (atoms/b-cm) (1st layer)	Number density (atoms/b-cm) (2nd layer)
H	^{1}H	2.83301E-03	3.78991E-03
	^{2}H	4.25015E-07	5.64072E-07
C	C	2.27058E-03	4.03671E-03
O	^{16}O	2.06885E-03	4.58782E-04
	^{17}O	7.88039E-07	1.74753E-07
	^{18}O	4.14757E-06	9.19753E-07
Ti	^{46}Ti	2.50941E-05	5.36896E-05
	^{47}Ti	2.28983E-05	4.89918E-05
	^{48}Ti	2.31493E-04	4.95287E-04
	^{49}Ti	1.72522E-05	3.69116E-05
	^{50}Ti	1.69385E-05	3.62405E-05
Si	^{28}Si	-	1.86243E-05
	^{29}Si	-	9.43026E-07
	^{30}Si	-	6.25992E-07
S	^{32}S	4.16818E-04	-
	^{33}S	3.28997E-06	-
	^{34}S	1.84677E-05	-
	^{35}S	8.77326E-08	-
Ba	^{132}Ba	4.43050E-07	-
	^{134}Ba	1.06025E-05	-
	^{135}Ba	2.89167E-05	-
	^{136}Ba	3.44526E-05	-
	^{137}Ba	4.92619E-05	
	^{138}Ba	3.14521E-04	-

6 ANET VALIDATION & VERIFICATION STUDIES AND RESULTS

The well-established neutronics stochastic codes TRIPOLI-4.8 and MCNP5 are employed for the verification of ANET's capability to satisfactorily determine the effective multiplication factor k_{eff}, the neutron fluence rates throughout the neutron energy spectrum as well as the fission rates. ANET results are tested against corresponding measurements as regards the two latter parameters.

For the present applications TRIPOLI uses the CEAV5.1.1 library, which is mainly based on JEFF3.1.1. As reported in *(OECD/NEA, JEFF3.1.2)*, the modifications included in the release of JEFF3.1.2 library concern mostly evaluations of Hf isotopes and gamma production data from neutron capture has been added to fission products. As a result, one can conclude that no major differences arise in the two library versions especially for this work. It should be mentioned that the CEAV5.1.1 library is the library officially distributed with the TRIPOLI-4.8 version. In the present study MCNP and ANET are applied using the JEFF3.1.2 neutron cross section library.

6.1 Criticality Assessment

Simulations concerning the effective multiplication factor, k_{eff}, have been realized by ANET for all the configurations described in Chapter 5 and are compared with corresponding computations performed by TRIPOLI-4.8 and MCNP5. All simulation results are compared in *Tables 6.1, 6.2* and *6.3*.

The TNR-AUTh Case

In the TNR-AUTh case it can be seen that the ANET result has a good agreement with the ones obtained by the two independent simulations, since k_{eff} differences remain below 237 pcm. Regarding statistics, in MCNP 1000 cycles of 100000 neutrons/cycle (80 cycles skipped) were used while in ANET and in TRIPOLI 10000 cycles of 10000 neutrons/cycle (100 cycles skipped) were performed.

The RPI Case

The RPI core configuration selected to be simulated by ANET is the newly commissioned one, after conversion to LEU. Since this specific configuration contains totally fresh fuel, i.e. free of uncertainties due to possible approximations in estimating fuel burnup and fission products concentration, it offers a valuable data

base for testing, evaluation and intercomparison of neutronic codes. Calculations of k_{eff} are performed by the three codes, considering the regulating and the control rods plunged at the level for which the reactor was made critical.

As regards the results, ANET shows a satisfactory agreement with the different codes, with discrepancies equivalent to, or lower than, those found in typical benchmarks *(DICE, 2001)*. The comparison with the observation can also be considered as satisfactory. Divergence from criticality which appears in all simulations can mainly be attributed to uncertainties in geometrical features; for example the gap between the graphite and the core, which is given between 5mm and 10mm, in the simulations has been ascribed the average value of 7.5 mm. It is noteworthy that sensitivity runs performed with MCNP for maximum gap width showed a k_{eff} modification of about 280 pcm. In MCNP 3000 cycles of 30000 neutrons were followed (80 cycles were skipped). For ANET and TRIPOLI the statistics used was 15000 cycles of 30000 neutrons/cycle (200 cycles were skipped).

The VENUS-2 Case

The VENUS-2 core was modelled in a three-dimensional geometry according to the benchmark specifications and by applying the same assumptions on all codes. In MCNP 3000 cycles of 100000 neutrons/cycle (100 cycles skipped) were utilized whereas 20000 cycles of 30000 neutrons/cycle (200 cycles were skipped) were treated in both ANET and TRIPOLI. The k_{eff} results show an excellent agreement with the benchmark average and the other codes' results since the discrepancies are 18 pcm, 107 pcm and 156 pcm respectively.

Table 6.1. ANET k_{eff} results for TNR-AUTh compared with three different code results.

k_{eff}	
ANET	0.80104 ± 2.9e-04
TRIPOLI-4.8	0.80341 ± 2.5e-04
MCNP5	0.80133 ± 1.7e-04

Table 6.2. ANET k_{eff} results for RPI compared with three different codes and observation.

k_{eff}	
OBSERVATION	1.00000
ANET	1.00231 ± 5.4e-04
TRIPOLI-4.8	1.00776 ± 1.0e-04
MCNP5	1.00786 ± 2.8e-04

Table 6.3. ANET k_{eff} results for VENUS-2 compared with three different codes and observation.

k_{eff}	
Monte Carlo Benchmark Average	1.00232 ± 34.1e-04
ANET	1.00250 ± 5.3e-04
TRIPOLI-4.8	1.00357 ± 5.8e-04
MCNP5	1.00094 ± 4.0e-04

6.2 Flux Assessment

6.2.1 Measurements

Neutron fluence rate measurements for three energy groups, i.e. thermal (neutron energy $E < 0.5$ eV), lower epithermal (0.5 eV $< E <$ 10 keV) and fast (1 MeV $< E <$ 20 MeV), were performed within a large part of the RPI core. The method of foil activation was utilized for the characterization of the energy groups. More particularly, gold foils were used for the thermal and epithermal region of the neutron spectrum, while the distinction between these energy regions was based on the cadmium-ratio method. Fluence rates of fast neutrons were determined by the use of indium, nickel and aluminum foils, wrapped in cadmium so as to decrease target irradiation by thermal neutrons.

Criticality throughout all the measurements was achieved by the withdrawal of the safety and regulation rods, by 56% and 40% respectively. In the present work, two sets of neutron fluence rates measurements are exploited. The determination of relative fluence rate profiles along the fuel height was realized in positions E3 (standard fuel assembly), E4 (dummy assembly) and in the beryllium reflector Be-N identified in *Figure 5.8*. In addition, fluence rate measurements were performed immediately below the fuel mid-height in nine core positions, i.e. in positions E2, B3, D3 and E3 (standard fuel assemblies), F2, F3, E4 and A3 (dummy assemblies) and finally in beryllium reflector Be-N, also shown in *Figure 5.8*. Detailed information about the conduction of the measurements can be found in *(Fernandes et al., 2010)*.

As stated in *(Fernandes et al., 2010)*, propagation of uncertainties in the measurement responses and data constants, results into uncertainties for fluence rates measurements at full length of the neutron spectrum. In particular, for thermal and epithermal fluence rates uncertainties of 12% and 10% are respectively observed at the fuel assemblies, whereas for fast neutrons uncertainties of 5% are mentioned in all irradiation positions.

6.2.2 Simulations

The core configuration and geometrical assumptions applied in the simulations by all codes were identical. Both local fluence rates and vertical fluence rate profiles are computed in all the positions mentioned in *Section 6.2.1*. Fluence rates are calculated in segments of 15 cm length located immediately below fuel mid-height. The detection volumes are water cylinders of 15 cm height and 10 mm diameter in all positions, apart from the case of the standard assembly where the diameter is 3 mm. The average fluence rates in a 15 cm segment below fuel mid-height for thermal, epithermal and fast neutrons assessed by ANET are compared with corresponding ones by TRIPOLI-4.8 and MCNP5, along with the corresponding measurements, in *Tables 6.4, 6.5* and *6.6* respectively. The discrepancy from measurement (DfM in tables) given from $(\Phi_c-\Phi_m)/\Phi_m$, where Φ_c and Φ_m stand for computed and measured fluence rates, is also shown in *Tables 6.4 - 6.6*. Detailed vertical fluence rate profiles are obtained using adjacent volumes of 3 cm length, along the fuel height. Diameter restrictions are as stated above. ANET results are compared with MCNP5 and TRIPOLI-4.8 computations in *Figures 6.6, 6.7* and *6.8* for positions E3, E4 and Be-N

respectively. For all fluence rates computations MCNP performed runs of 1500 cycles of 200000 neutrons/cycle while ANET and TRIPOLI used 30000 cycles of 30000 neutrons/cycle. It should be noted that in all simulations the statistical error remains below 1%.

The neutron fluence rate values in various core positions and the vertical fluence rate profiles computed by ANET are in satisfactory agreement with the well-established stochastic codes MCNP and TRIPOLI as well as with measurements. More specifically, the discrepancies of ANET from measurements concerning the thermal range remain below 12% in the majority of the core positions. ANET discrepancies in channels E3 and Be-N are slightly increased, reaching 19% and 15% respectively, nevertheless this applies to all codes. ANET epithermal fluence rate simulations exhibit even lower discrepancies, ranging up to 9%, apart from positions E2 (25%) and Be-N (22%) where again all codes' results are less favourable.

Table 6.4: ANET computations for average thermal fluence rates Φ_t (n/cm^{2}s) in comparison with other stochastic codes and corresponding measurements.

Thermal	Standard Assemblies				Dummy Assemblies				Be
	Φ_t (*10^{-12}) DfM (%)				Φ_t (*10^{-13}) DfM (%)				Φ_t (*10^{-13}) DfM (%)
Position	E2	E3	D3	B3	F2	F3	E4	A3	Be-N
Measurements	8.71	8.94	9.81	9.45	2.04	1.72	2.20	2.33	2.79
ANET	8.27 -5	7.27 -19	10.40 6	9.17 -3	2.22 9	1.91 11	2.31 5	2.58 11	3.22 15
TRIPOLI	7.41 -15	6.77 -24	9.55 -3	8.51 -10	2.03 0	1.78 3	2.19 0	2.44 5	2.95 6
MCNP	8.35 -4	7.45 -17	10.82 10	9.77 3	2.20 8	1.92 12	2.39 9	2.75 18	3.28 18

Table 6.5: ANET computations for average epithermal fluence rates Φ_t (n/cm^{2}s) in comparison with other stochastic codes and corresponding measurements.

Epithermal	Standard Assemblies				Dummy Assemblies				Be
	Φ_e (*10^{-13}) DfM (%)				Φ_e (*10^{-12}) DfM (%)				Φ_e (*10^{-12}) DfM (%)
Position	E2	E3	D3	B3	F2	F3	E4	A3	Be-N
Measurements	1.14	1.04	1.59	1.39	4.80	3.97	5.35	5.96	8.44
ANET	1.41 25	1.09 6	1.66 4	1.38 0	4.95 3	4.20 6	4.88 -9	5.74 -4	6.50 -22
TRIPOLI	1.26 11	1.01 -3	1.53 -4	1.30 -6	4.52 -6	3.89 -2	4.68 -3	5.47 -8	6.69 -21
MCNP	1.41 24	1.11 7	1.73 9	1.48 6	4.89 2	4.17 5	5.08 -5	6.14 3	7.48 -11

Table 6.6: ANET computations for average fast fluence rates Φ_t (n/cm^{2}s) in comparison with other stochastic codes and corresponding measurements.

Fast	Standard Assemblies				Dummy Assemblies				Be
	Φ_f (*10^{-13}) DfM (%)				Φ_f (*10^{-12}) DfM (%)				Φ_f (*10^{-12}) DfM (%)
Position	E2	E3	D3	B3	F2	F3	E4	A3	Be-N
Measurements	1.39	1.23	1.66	1.36	2.68	2.65	2.78	2.56	1.94
ANET	1.41 1	1.12 -9	1.59 -4	1.34 -1	2.68 0	2.28 -14	2.48 -11	2.71 6	2.43 25
TRIPOLI	1.26 -9	1.04 -15	1.44 -13	1.22 -10	2.44 -9	2.10 -21	2.25 -19	2.44 -5	2.09 8
MCNP	1.41 1	1.13 -8	1.63 -2	1.40 3	2.63 -2	2.26 -15	2.44 -12	2.74 7	2.34 21

Similarly, ANET fast neutron fluence rate results show less than 10% deviation from measurements for the bulk of the positions. Nonetheless, in positions F3, E4 and Be-N, the three codes' computations display higher deviation from measurements, ranging up to 25% for ANET. It is noteworthy however, that uncertainties of 12% and

10% for thermal and epithermal fluence rates in fuel assemblies and 5% for fast fluence rates are mentioned in the measurement responses in Section 6.2.1. In almost all cases, ANET seems to be in better accordance with MCNP results which can be attributed to the common use of the JEFF3.1.2 library whereas in positions with higher ANET deviation, similar behaviour is observed for all codes.

The vertical flux profiles obtained by ANET, TRIPOLI and MCNP are depicted in *Figures 6.6, 6.7* and *6.8*. It should be noted that in all simulations the statistical error remains below 1%. In the standard assembly, ANET's maximum discrepancy from both codes is 4%, 5% and 6% for the thermal, epithermal and fast neutron flux profiles respectively. Similar deviations arise from ANET's calculations for the flux profiles in the dummy assemblies, namely 6%, 4% and 5% for the thermal, epithermal and fast energy range. The most pronounced differences are shown in the Be-N reflector and in particular for the epithermal, 13% and fast, 9% flux profile, probably due to the angular treatment at the edges of the reactor core. In all cases, the relevant maximum discrepancies between TRIPOLI and MCNP are 4%. The obtained results show that ANET can perform these simulations at least as satisfactorily as other well documented stochastic codes since similar differences among various codes' computations can be found in *(Savva et al., 2014)*. Nonetheless, ANET is a code under development and the effort for incorporations of improvements will continue.

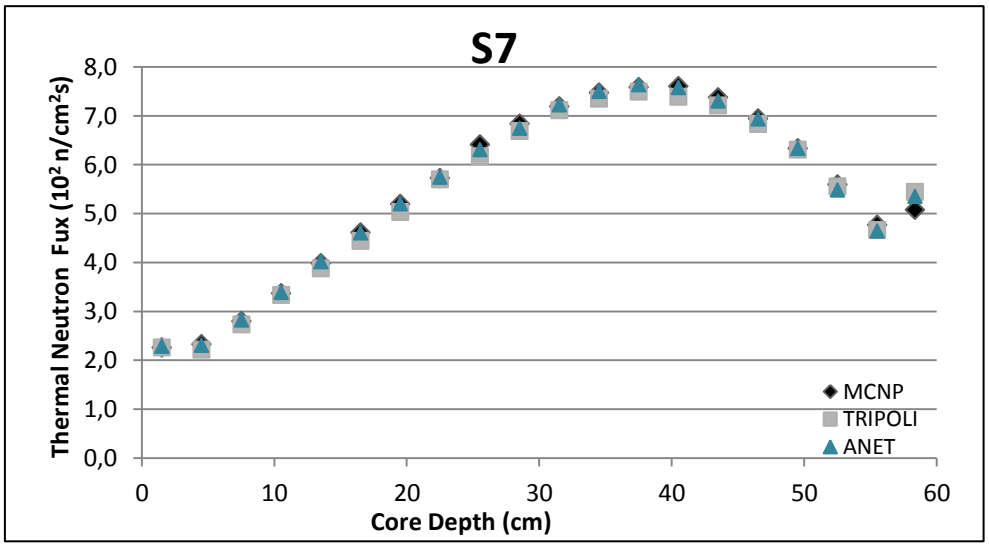

Figure 6.6a: Thermal neutron flux profile in fuel assembly F-S7 by ANET vs two independent stochastic results.

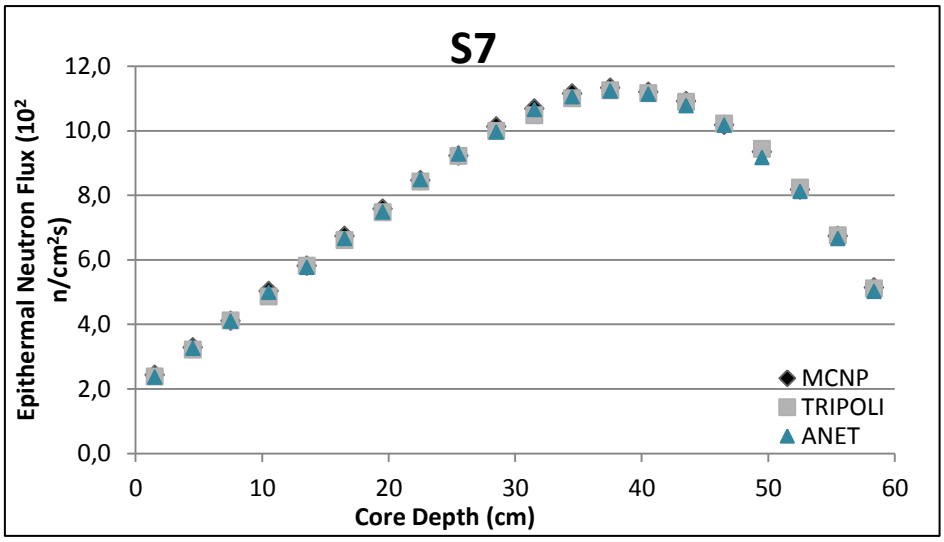

Figure 6.6b: Epithermal neutron flux profile in fuel assembly F-S7 by ANET vs two independent stochastic results.

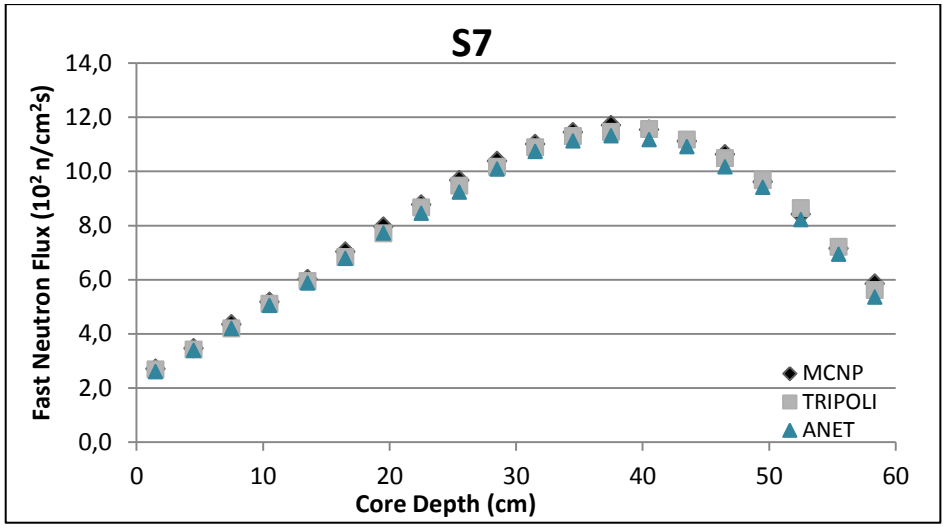

Figure 6.6c: Fast neutron flux profile in fuel assembly F-S7 by ANET vs two independent stochastic results.

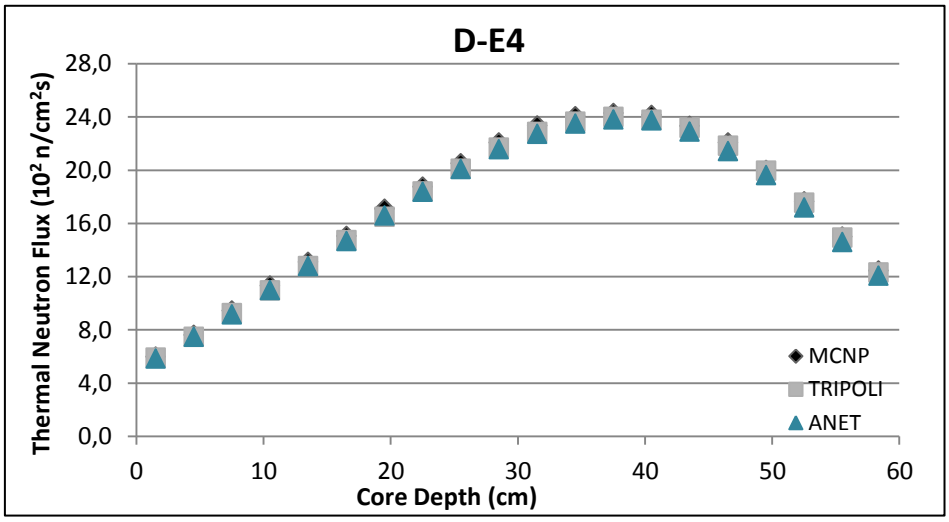

Figure 6.7a: Thermal neutron flux profile in dummy assembly D-E4 by ANET vs two independent stochastic results.

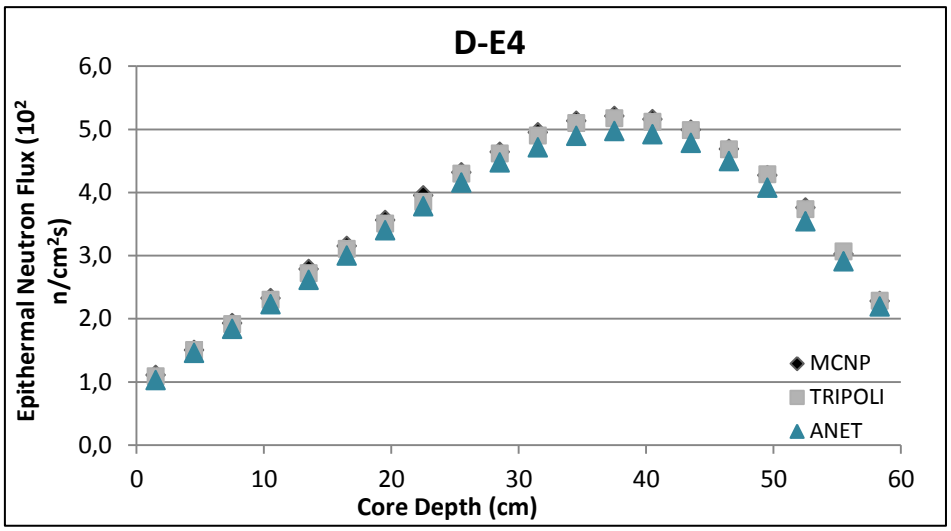

Figure 6.7b: Epihermal neutron flux profile in dummy assembly D-E4 by ANET vs two independent stochastic results.

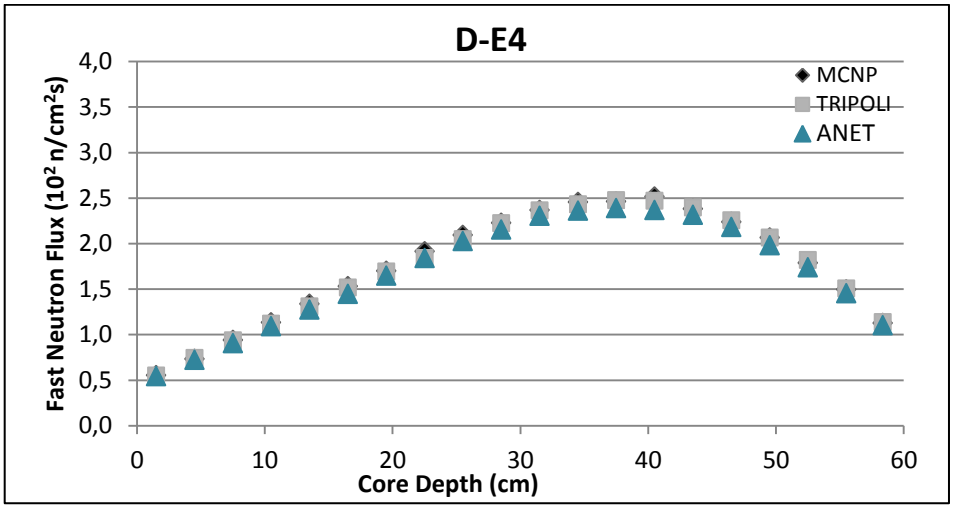

Figure 6.7c: Fast neutron flux profile in dummy assembly D-E4 by ANET vs two independent stochastic results.

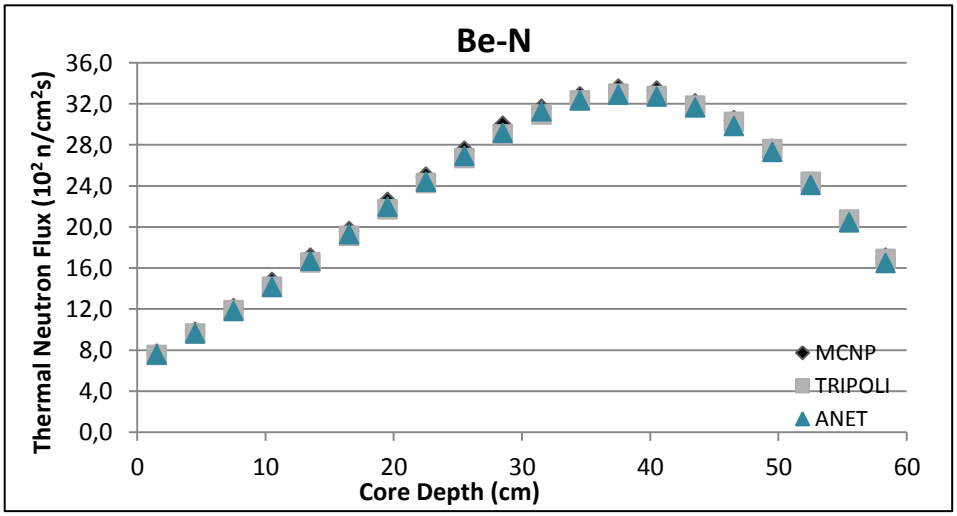

Figure 6.8a: Thermal neutron flux profile in reflector Be-N by ANET vs two independent stochastic results.

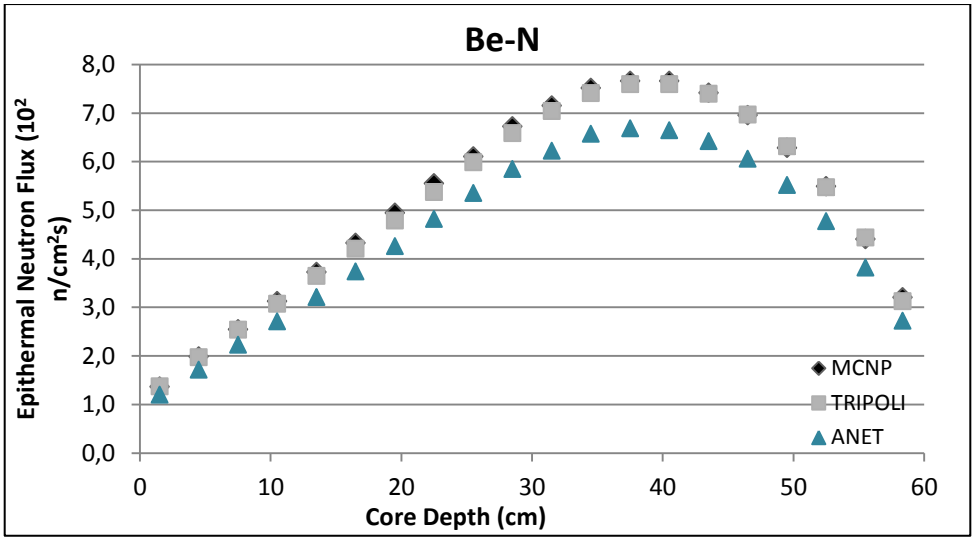

Figure 6.8b: Epithermal neutron flux profile in reflector Be-N by ANET vs two independent stochastic results.

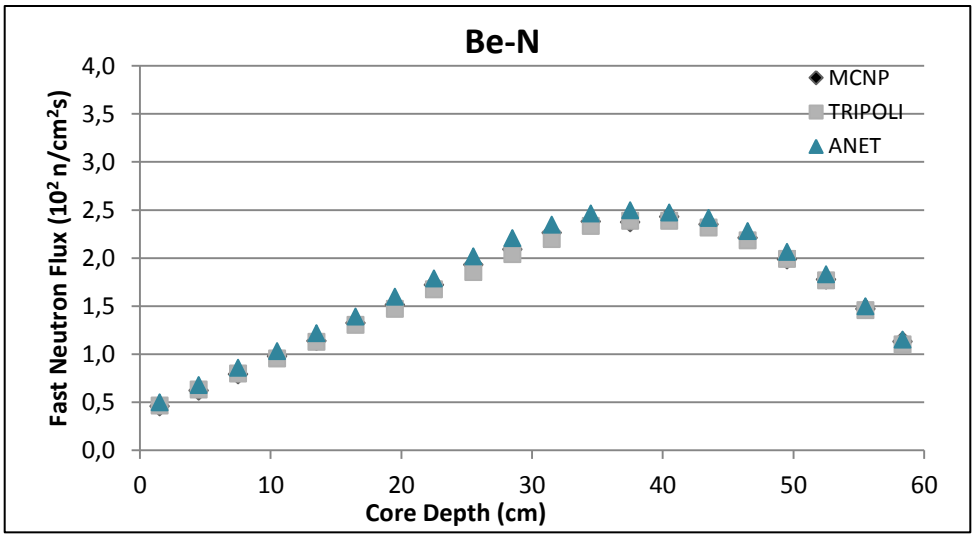

Figure 6.8b: Fast neutron flux profile in reflector Be-N by ANET vs two independent stochastic results.

6.3 Fission Rate Distribution Assessment

6.3.1 Measurements

In the framework of the 3-D version of the VENUS-2 benchmark, measurements concerning the fission rate distributions of six fuel pins, i.e. two 3/0 UO_2, two 4/0 UO_2 and two 2/2.7 MOX pins, for incident neutron energies throughout the whole spectrum were conducted. The average fission rate in the core, which corresponds to the absolute reference irradiation, is 1.87E+08 fissions$\cdot$cm$^{-3}\cdot$s^{-1} at the mid-plane. This average corresponds to a power of 595 Watts. The fission rates were

measured axially by γ-scanning after an irradiation of 8 hours at 90% of the VENUS maximum power. The positions of the measurements were 21 different vertical planes along 50 cm of the fuel pin length (from 105 cm to 155 cm), starting from 110 cm and at every 2 cm upwards to 150 cm. Experimental data were collected by the gamma activity of the fission product ^{140}La (fission yields ~6.3% for ^{235}U and ~5.5% for ^{239}Pu, energy 1.6 MeV, effective half-life ~12.8d). The reported uncertainty of the measured data is ±1.0% in UO_2 and ±1.5% in MOX pins *(Na et al., 2003)*. The fuel pins' positions of the measurements in the VENUS-2 core are depicted in *Figure 6.1*. The axial measurements were performed in fuel pin numbers 30 and 74 (3/0 UO_2), 115 and 131 (4/0 UO_2), 240 and 325 (MOX).

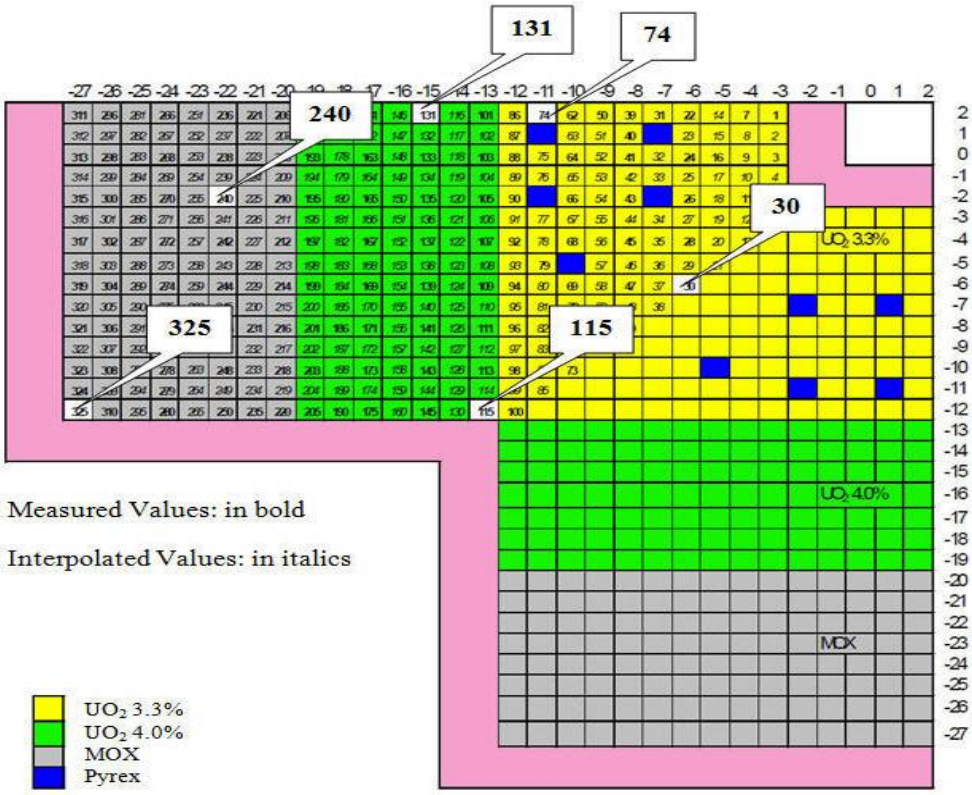

Figure 6.1: Measured and interpolated pin power positions in VENUS-2. The axially measured fuel pins are indicated.

6.3.2 Simulations

TRIPOLI-4.8 and MCNP5 are again appointed for the computation of the normalized axial fission rate distribution of six fuel pins while the results are compared between each other as well as with the corresponding measurements. Three-dimensional geometry for the core configuration and equivalent geometrical assumptions were applied in all computations. Fission rates are calculated in 21

different axial levels for all proposed positions and suggested isotopes, i.e. ^{235}U and ^{238}U for the 3/0 and 4/0 pins and ^{234}U, ^{235}U, ^{236}U, ^{238}U, ^{239}Pu, ^{240}Pu, ^{241}Pu, ^{242}Pu and ^{242}Am for the MOX pins, following the measurements protocol. The results obtained by ANET, TRIPOLI-4.8 and MCNP5 along with the discrepancies from measurements given from [*C*/*E*]-1 (%), where *C* and *E* stand for "Computed" and "Experimental" fission rates are shown in *Tables 6.7 - 6.12*. In respect of the results, no units are applied since they comprise normalized axial fission rate. The presented values correspond to the total fission rates normalized to the sum of fission rates in the 21 vertical planes per position, for the whole neutron energy spectrum, taking into account the relative isotopic composition of each fuel type.

Concerning the axial fission rate distribution in various core positions, the ANET computations presented in *Tables 6.7 - 6.12* are in satisfactory agreement with TRIPOLI and MCNP as well as with measurements with discrepancies equivalent to those found in the official OECD benchmark *(VENUS-2 2004)*. More precisely, the discrepancies of ANET from measurements for 3/0 UO_2 fuel pins remain below 4.9% and 6.5% in rods 30 and 74 respectively. For 4/0 UO_2 fuel pins 115 and 131 ANET deviations are slightly increased reaching 6.5% and 8.1% respectively while for MOX fuel pins 240 and 325 the discrepancies remain at the same level ranging from 7.3% to 6.0%. Nonetheless, TRIPOLI displays similar discrepancies which range from 3.1% to 7.6% whereas for MCNP they vary from 3.0% to 6.8%. Moreover, it should be noted that all codes exhibit the highest deviations from measurements at both extremities of the fuel pin length which is also mentioned as a common remark made by all the participants in the OECD benchmark *(VENUS-2 2004)*, due to the pronounced reflector effect near the axial upper and lower reflectors. Finally, it is noteworthy that all codes display similar behaviour concerning the uncertainties, which increase in all positions moving from the central to the outer parts of the core. In the above simulations, ANET and TRIPOLI used 30000 cycles of 30000 neutrons/cycle (300 cycles skipped) and MCNP 3000 cycles of 100000 neutrons/cycle (100 cycles skipped) and the statistical error remains below 2%.

Table 6.7: Normalized axial fission rate distribution of 3/0 UO_2 fuel rod 30 in VENUS-2.

Axial position (cm)	Calculated fission rates			Experimental fission rates	[C/E-1] (%)		
	ANET	TRIPOLI-4.8	MCNP5		ANET	TRIPOLI-4.8	MCNP5
110	0.0340	0.0333	0.0333	0.0324	4.9	2.9	2.8
112	0.0381	0.0375	0.0375	0.0364	4.6	3.1	3.0
114	0.0411	0.0410	0.0412	0.0405	1.4	1.3	1.7
116	0.0439	0.0451	0.0445	0.0440	-0.3	2.4	1.1
118	0.0472	0.0482	0.0475	0.0477	-1.0	1.0	-0.3
120	0.0501	0.0511	0.0498	0.0505	-0.8	1.1	-1.4
122	0.0521	0.0517	0.0525	0.0524	-0.5	-1.4	0.2
124	0.0540	0.0541	0.0540	0.0546	-1.1	-0.9	-1.0
126	0.0564	0.0557	0.0553	0.0554	1.7	0.5	-0.1
128	0.0558	0.0556	0.0553	0.0567	-1.5	-2.0	-2.5
130	0.0560	0.0569	0.0573	0.0562	-0.4	1.2	1.9
132	0.0554	0.0558	0.0564	0.0569	-2.6	-1.9	-0.9
134	0.0551	0.0557	0.0551	0.0559	-1.5	-0.4	-1.4
136	0.0533	0.0542	0.0542	0.0545	-2.2	-0.5	-0.5
138	0.0517	0.0521	0.0524	0.0524	-1.2	-0.5	0.0
140	0.0507	0.0493	0.0501	0.0504	0.6	-2.1	-0.5
142	0.0471	0.0473	0.0474	0.0474	-0.7	-0.1	-0.1
144	0.0439	0.0444	0.0444	0.0446	-1.7	-0.5	-0.5
146	0.0410	0.0405	0.0404	0.0407	0.7	-0.4	-0.6
148	0.0387	0.0367	0.0369	0.0369	4.8	-0.4	0.0
150	0.0346	0.0337	0.0345	0.0337	2.5	0.1	2.3

Table 6.8: Normalized axial fission rate distribution of 3/0 UO_2 fuel rod 74 in VENUS-2.

Axial position (cm)	Calculated fission rates			Experimental fission rates	[C/E-1] (%)		
	ANET	TRIPOLI-4.8	MCNP5		ANET	TRIPOLI-4.8	MCNP5
110	0.0339	0.0331	0.0337	0.0322	5.2	2.7	4.7
112	0.0374	0.0371	0.0367	0.0366	2.2	1.4	0.4
114	0.0406	0.0415	0.0420	0.0399	1.8	4.1	5.2
116	0.0442	0.0447	0.0447	0.0441	0.1	1.4	1.4
118	0.0473	0.0471	0.0477	0.0481	-1.6	-2.0	-0.9
120	0.0493	0.0509	0.0493	0.0500	-1.3	1.7	-1.3
122	0.0525	0.0521	0.0513	0.0528	-0.6	-1.3	-2.8
124	0.0547	0.0538	0.0543	0.0550	-0.5	-2.2	-1.2
126	0.0557	0.0557	0.0556	0.0563	-1.1	-1.1	-1.2
128	0.0553	0.0570	0.0559	0.0563	-1.8	1.3	-0.8
130	0.0564	0.0560	0.0562	0.0571	-1.2	-1.9	-1.6
132	0.0558	0.0560	0.0561	0.0565	-1.2	-0.9	-0.7
134	0.0548	0.0548	0.0555	0.0560	-2.2	-2.1	-0.9
136	0.0535	0.0541	0.0538	0.0546	-2.0	-1.0	-1.5
138	0.0525	0.0524	0.0527	0.0526	-0.1	-0.4	0.2
140	0.0512	0.0503	0.0512	0.0503	1.7	0.0	1.8
142	0.0472	0.0484	0.0476	0.0476	-0.8	1.6	0.0
144	0.0441	0.0442	0.0447	0.0442	-0.3	0.0	1.1
146	0.0409	0.0414	0.0405	0.0409	0.1	1.3	-0.9
148	0.0381	0.0371	0.0366	0.0366	4.1	1.4	0.1
150	0.0346	0.0322	0.0337	0.0325	6.5	-0.8	3.8

Table 6.9: Normalized axial fission rate distribution of 4/0 UO_2 fuel rod 115 in VENUS-2.

Axial position (cm)	Calculated fission rates			Experimental fission rates	[C/E-1] (%)		
	ANET	TRIPOLI-4.8	MCNP5		ANET	TRIPOLI-4.8	MCNP5
110	0.0344	0.0339	0.0331	0.0323	6.5	4.9	2.6
112	0.0371	0.0370	0.0361	0.0358	3.6	3.4	0.7
114	0.0401	0.0412	0.0418	0.0402	-0.1	2.6	3.9
116	0.0445	0.0446	0.0433	0.0444	0.3	0.5	-2.4
118	0.0482	0.0478	0.0462	0.0472	2.2	1.2	-2.2
120	0.0505	0.0498	0.0500	0.0503	0.4	-1.0	-0.7
122	0.0510	0.0529	0.0528	0.0527	-3.1	0.4	0.1
124	0.0538	0.0551	0.0544	0.0544	-1.0	1.4	0.0
126	0.0556	0.0548	0.0567	0.0557	-0.2	-1.7	1.8
128	0.0574	0.0557	0.0570	0.0564	1.8	-1.3	1.1
130	0.0572	0.0567	0.0562	0.0564	1.5	0.5	-0.4
132	0.0550	0.0556	0.0570	0.0572	-3.8	-2.7	-0.3
134	0.0552	0.0564	0.0548	0.0561	-1.6	0.6	-2.4
136	0.0528	0.0549	0.0530	0.0555	-4.9	-1.1	-4.4
138	0.0522	0.0519	0.0527	0.0524	-0.3	-1.0	0.6
140	0.0500	0.0496	0.0500	0.0506	-1.3	-1.9	-1.2
142	0.0486	0.0478	0.0468	0.0476	2.2	0.4	-1.8
144	0.0445	0.0443	0.0456	0.0446	-0.2	-0.7	2.3
146	0.0413	0.0413	0.0413	0.0413	0.0	0.0	0.1
148	0.0369	0.0366	0.0374	0.0366	0.9	0.0	2.2
150	0.0335	0.0321	0.0338	0.0321	4.3	0.1	5.4

Table 6.10: Normalized axial fission rate distribution of 4/0 UO_2 fuel rod 131 in VENUS-2.

Axial position (cm)	Calculated fission rates			Experimental fission rates	[C/E-1] (%)		
	ANET	TRIPOLI-4.8	MCNP5		ANET	TRIPOLI-4.8	MCNP5
110	0.0342	0.0332	0.0343	0.0321	6.6	3.5	6.8
112	0.0388	0.0365	0.0374	0.0363	6.8	0.4	2.9
114	0.0414	0.0417	0.0408	0.0404	2.5	3.1	1.1
116	0.0450	0.0441	0.0451	0.0441	2.0	0.0	2.3
118	0.0481	0.0473	0.0472	0.0477	0.7	-0.9	-0.9
120	0.0494	0.0511	0.0502	0.0504	-2.1	1.4	-0.5
122	0.0528	0.0524	0.0526	0.0531	-0.5	-1.2	-0.9
124	0.0532	0.0538	0.0536	0.0542	-1.9	-0.7	-1.1
126	0.0553	0.0544	0.0548	0.0564	-1.9	-3.6	-2.8
128	0.0553	0.0568	0.0558	0.0572	-3.3	-0.7	-2.5
130	0.0566	0.0566	0.0565	0.0568	-0.3	-0.3	-0.5
132	0.0556	0.0558	0.0556	0.0565	-1.7	-1.3	-1.6
134	0.0552	0.0551	0.0562	0.0562	-1.8	-2.0	0.1
136	0.0528	0.0530	0.0539	0.0548	-3.6	-3.3	-1.6
138	0.0524	0.0520	0.0516	0.0537	-2.4	-3.2	-3.8
140	0.0504	0.0506	0.0506	0.0504	0.0	0.4	0.4
142	0.0456	0.0486	0.0482	0.0477	-4.4	2.0	1.1
144	0.0452	0.0455	0.0441	0.0439	2.9	3.6	0.5
146	0.0408	0.0406	0.0408	0.0403	1.2	0.8	1.3
148	0.0374	0.0373	0.0371	0.0365	2.4	2.2	1.7
150	0.0347	0.0337	0.0333	0.0321	8.1	5.1	3.7

Table 6.11: Normalized axial fission rate distribution of 4/2.7 MOX fuel rod 240 in VENUS-2.

Axial position (cm)	Calculated fission rates			Experimental fission rates	[C/E-1] (%)		
	ANET	TRIPOLI-4.8	MCNP5		ANET	TRIPOLI-4.8	MCNP5
110	0.0335	0.0344	0.0331	0.0322	4.1	6.8	2.9
112	0.0357	0.0372	0.0376	0.0366	-2.3	1.7	2.8
114	0.0400	0.0399	0.0404	0.0395	1.3	1.1	2.3
116	0.0455	0.0433	0.0449	0.0424	7.3	2.1	5.9
118	0.0471	0.0470	0.0490	0.0478	-1.4	-1.8	2.5
120	0.0486	0.0495	0.0498	0.0507	-4.1	-2.3	-1.8
122	0.0520	0.0507	0.0518	0.0516	0.7	-1.7	0.4
124	0.0545	0.0559	0.0543	0.0545	0.0	2.5	-0.4
126	0.0544	0.0545	0.0549	0.0559	-2.7	-2.6	-1.8
128	0.0571	0.0574	0.0562	0.0558	2.3	2.9	0.8
130	0.0563	0.0573	0.0557	0.0567	-0.7	1.1	-1.7
132	0.0561	0.0559	0.0558	0.0578	-3.0	-3.3	-3.4
134	0.0557	0.0555	0.0544	0.0564	-1.2	-1.7	-3.6
136	0.0539	0.0532	0.0549	0.0560	-3.8	-5.0	-2.0
138	0.0523	0.0532	0.0523	0.0533	-1.8	-0.2	-1.9
140	0.0518	0.0512	0.0507	0.0508	1.9	0.8	-0.3
142	0.0470	0.0484	0.0473	0.0477	-1.4	1.5	-0.7
144	0.0458	0.0451	0.0445	0.0445	3.0	1.3	0.0
146	0.0419	0.0417	0.0418	0.0412	1.8	1.3	1.5
148	0.0373	0.0366	0.0375	0.0366	1.9	0.1	2.4
150	0.0334	0.0321	0.0330	0.0320	4.4	0.4	3.3

Table 6.12: Normalized axial fission rate distribution of 4/2.7 MOX fuel rod 325 in VENUS-2.

Axial position (cm)	Calculated fission rates			Experimental fission rate	[C/E-1] (%)		
	ANET	TRIPOLI-4.8	MCNP5		ANET	TRIPOLI-4.8	MCNP5
110	0.0350	0.0351	0.0326	0.0333	5.2	5.4	-2.2
112	0.0377	0.0366	0.0370	0.0356	5.8	2.7	4.0
114	0.0415	0.0405	0.0423	0.0399	3.9	1.5	6.0
116	0.0461	0.0438	0.0441	0.0438	5.2	0.0	0.6
118	0.0477	0.0485	0.0473	0.0466	2.5	4.1	1.6
120	0.0477	0.0481	0.0500	0.0500	-4.5	-3.7	-0.1
122	0.0544	0.0491	0.0516	0.0527	3.3	-6.9	-2.0
124	0.0557	0.0517	0.0546	0.0548	1.7	-5.7	-0.4
126	0.0576	0.0563	0.0582	0.0558	3.3	0.8	4.3
128	0.0564	0.0568	0.0560	0.0557	1.3	1.9	0.5
130	0.0559	0.0583	0.0568	0.0574	-2.7	1.5	-1.1
132	0.0551	0.0582	0.0559	0.0567	-2.9	2.7	-1.4
134	0.0559	0.0547	0.0567	0.0559	0.0	-2.1	1.5
136	0.0535	0.0528	0.0533	0.0548	-2.4	-3.6	-2.8
138	0.0515	0.0534	0.0501	0.0529	-2.6	1.0	-5.3
140	0.0485	0.0526	0.0486	0.0506	-4.1	4.0	-4.0
142	0.0456	0.0468	0.0461	0.0481	-5.2	-2.7	-4.2
144	0.0418	0.0435	0.0457	0.0438	-4.6	-0.7	4.4
146	0.0406	0.0415	0.0420	0.0411	-1.1	0.9	2.3
148	0.0367	0.0361	0.0370	0.0375	-2.1	-3.7	-1.3
150	0.0351	0.0356	0.0342	0.0331	6.0	7.6	3.4

6.4 Time Dependent ANET Calculations

At this stage ANET is tested for its capability to simulate time dependent phenomena with time scales relevant to the core inventory evolution. The first verification study of the dynamic ANET is performed for 180 and 340 days operating time using the setup described in *Chapter 5.4*. ANET results are examined in comparison with corresponding calculations by two stochastic codes, i.e. Serpent and MCNP coupled with ORIGEN, for a fuel pin irradiated within a reactor core. Since in the present simulations the fuel pin is not treated for in-core exposure but it is modelled independently as a stand-alone setup, the test against measured values is exploited only to indicate tendencies; it is not claimed that it accurately reproduces the experiment. Representative results are presented in *Tables 6.13* and *6.14*.

The preliminary ANET application for dynamic analysis is encouraging since it indicates the code capability to inherently provide a reasonable prediction for the core inventory evolution. It is worth underlining that uncertainties of the order of 20% and even higher are traditionally expected in core inventory evolution calculations since besides the uncertainty introduced by the algorithms of the simulation code, the nuclear data of the various fission products such as decay, half-life, yield and cross section data constitute additional, major sources of uncertainty *(Cabellos et al., 2010)*. Moreover, the divergence of ANET results could be attributed to the various time-scales of the decay half-lives of the nuclides taken into consideration and the effect of the less capturing nuclides to the behaviour of the system.

In view of the above and also taking into account the differences between experimental and modelling conditions (assumption of a stand-alone setup) as well as between the simulation methods, it may be concluded that the ANET results compare favourably with the simulations performed by well-established codes. Further research on the treatment of the varying decay half-lives while incorporation of the treatment proposed by *(Dat, 1996)* for the less capturing nuclides constitute the subject of further research. Extensive verification and validation effort for ANET's capability to perform burnup calculations is planned for the near future.

Table 6.13: Compared ANET results for irradiated fuel composition (nuclei/b-cm) for 180 days.

Nuclide	ANET	Serpent
U-234	6.1006E-06	5.8942E-06
U-235	6.2135E-04	6.1029E-04
U-236	5.2633E-06	1.6935E-05
U-238	2.1656E-02	2.1669E-02
Np-237	2.0973E-08	3.0823E-07
Pu-238	2.0810E-10	8.9761E-09
Pu-239	3.0234E-05	2.9709E-05
Pu-240	1.7932E-06	1.9283E-06
Pu-241	5.2359E-08	2.7228E-07
Pu-242	1.6450E-09	6.8027E-09
Tc-99	3.3853E-06	4.3533E-06
Ru-101	1.6819E-06	3.8576E-06
Rh-103	7.1682E-07	1.7027E-06
Ag-109	2.9259E-08	8.9007E-08
Cs-133	2.0110E-06	4.5424E-06
Nd-143	2.0110E-06	3.6297E-06
Nd-145	1.2612E-06	2.8196E-06
Sm-149	9.0062E-08	5.2737E-08
Sm-150	8.4970E-07	7.4703E-07
Sm-151	9.8178E-08	1.6998E-07
Sm-152	1.2997E-07	3.5711E-07
Eu-153	1.7489E-07	1.4269E-07

Table 6.14: Compared ANET results for irradiated fuel composition (nuclei/b-cm) for 340 days.

Nuclide	ANET	Serpent
U-234	6.0338E-06	5.6698E-06
U-235	5.7039E-04	5.4735E-04
U-236	6.9106E-06	2.7800E-05
U-238	2.1643E-02	2.1631E-02
Np-237	3.7590E-08	7.4343E-07
Pu-238	6.8884E-10	4.0742E-08
Pu-239	3.5269E-05	4.9208E-05
Pu-240	5.9438E-06	5.6045E-06
Pu-241	4.6361E-07	1.3733E-06
Pu-242	3.0058E-08	6.8954E-08
Tc-99	6.3956E-06	8.2492E-06
Ru-101	3.0703E-06	7.3196E-06
Rh-103	1.6299E-06	3.8937E-06
Ag-109	8.6161E-08	2.5502E-07
Cs-133	3.7507E-06	8.7132E-06
Nd-143	3.1587E-06	7.0169E-06
Nd-145	2.2653E-06	5.2328E-06
Sm-149	9.1122E-08	5.5364E-08
Sm-150	1.6826E-06	1.5045E-06
Sm-151	1.3957E-07	2.1825E-07
Sm-152	2.9180E-07	7.7397E-07
Eu-153	3.5567E-07	3.3042E-07

6.5 Accelerator Driven Systems ANET Simulations

The KUCA core configuration II-5 was chosen to be the first case of realistic ADSs to be simulated by ANET. The core was modelled in a three-dimensional geometry following the benchmark descriptions described in *Chapter 5.5* by ANET and the reference library for this task was JEFF3.1.2. ANET has simulated the 100 MeV proton beam and the Pb-Bi target so as to produce the neutrons generated from spallation. The initial spatial and energetic distribution of the neutrons is the one derived from the spallation process. In ANET, 20000 cycles of 30000 particles were considered, which for the first cycle were protons whereas for the following cycles were neutrons. The results concerning the k_{eff} including the value given by MCNP6.1 simulations performed by the KUCA laboratory are presented in *Table 6.15*. ANET results' discrepancy concerning k_{eff} is 688 pcm and remains equivalent to, or lower than, those found in typical benchmarks *(DICE, 2001)*. Moreover, further sensitivity tests will follow shortly so as to evaluate how the utilization of different neutron libraries affects k_{eff} estimation. Thus, ANET can perform succesfully simulations for the full treatment of ADSs without any external coupling to a High Energy Physics code. It is worth mentioning that at the moment only one code worldwide, i.e. MCNPX, can perform this task.

Table 6.15: ANET k_{eff} results for KUCA compared with MCNP6.1.

k_{eff}	
ANET	0.90667 ± 3.4e-04
MCNP6.1	0.91355 ± 1.3e-04

7 CONCLUSIONS

In the framework of this PhD thesis the new neutronics stochastic code ANET was developed aiming to perform core analysis for GEN II/III reactors and ADSs, including dynamic calculations for the temporal changes of the core isotopic composition. ANET was initially validated and verified with respect to its ability of assessing reactor criticality, as well as neutron flux and reaction rates in GEN II/III reactors. In this context ANET performed criticality calculations in both subcritical and critical nuclear systems of conventional design, as well as simulations of local and axially distributed thermal, epithermal and fast neutron fluence rates in various positions of a MTR core and of axial fission rates in standard and MOX fuel pins in a zero power critical reactor. The ANET results compared with corresponding ones by the well-established Monte Carlo codes TRIPOLI-4.8 and MCNP5 as well as with measurements, demonstrate that the developed code is capable to perform successful simulations of reactor parameters important to safety.

An important task in the framework of the ANET development within this thesis was the incorporation of specific procedures that allow for the dynamic assessment of the reactor core evolution and the fuel-burnup in GEN II/III reactors and innovative nuclear reactor designs. This has been realized with very promising preliminary results whereas extension of the verification and validation effort is planned for the near future.

Regarding the development of ANET's inherent capability to analyze ADSs, which constituted another important task of the present thesis, FLUKA has been utilized as a high energy physics simulator in ANET so as neutron yields for spallation targets of various materials and dimensions can be predicted. A core configuration of the KUCA system in Japan was fully modelled and satisfactory results were obtained for the multiplication factor fulfilling thus the requirements of an advanced stochastic neutronics code with scope of application conventional as well as innovative nuclear fission reactors.

8 FUTURE WORK AND PERSPECTIVES

ANET's further development comprises:

a) the consideration of the (n, 2n) and (n, 3n) reactions,

b) the incorporation of the treatment for the less capturing nuclides so as to take into account their neutron capture reaction rates,

c) the implementation in the code of the option to reduce some of the initial time-steps in comparison to the selected larger time-steps in order to minimize the introduced error,

d) the study of the effect of the chosen time-step length,

e) the study of the Xe oscillations during reactor operation

f) parallelization of the code and utilization of a new method that results into faster MC simulations proposed by Dr A. Mylonakis in his thesis which was realized in NCSR "Demokritos"

g) and the extensive benchmarking of ANET's ability to perform burnup calculations along with simulations of ADSs.

In a second stage, ANET will incorporate achievements that have been obtained in the frame of another thesis work performed in the Computational Nuclear Technology Group of NCSR "Demokritos" and are related with

a) improved optimized neutronic / thermal hydraulic coupling,

b) inherent stochastic treatment of short time transients and

c) acceleration of the Monte Carlo calculations.

In the frame of the study of innovative reactor concepts, ANET will be further used to confirm or refute a remark that has been made when analyzing various possible ADS designs. Preliminary findings pointed to the conclusion that an ADS may be conceived that works following a closed cycle, producing fissile material that compensates for the fuel depletion. Finally, ANET could be utilized to perform short-time behaviour studies, such as Xe oscillations during reactor operation and accident scenarii as well as simulations of various nuclear systems like Th loaded cores and small modular reactors.

REFERENCES

Aarnio P.A. et al., Fluka user's guide. Technical Report TIS-RP-190, CERN, (1987), (2000).

Aufiero M., Cammi A., Fiorina C., Leppänen J., Luzzi L., Ricotti M., "An extended version of the Serpent-2 code to investigate fuel burn-up and core material evolution of the molten salt fast reactor", J. Nucl. Mat., Vol. 441, p. 473-486, (2013).

Bacha, F., Maillard, J., Vergnes, J., "Utilisation du code GEANT pour l'étude d'un réacteur de type hybride (Présentation et qualification du code) ", LPC-95-27. Collége de France, Laboratoire de Physique Corpusculaire, IN2P3-CNRS, (1995).

Barros G.P., Pereira C., Veloso M.A.F., Costa A.L., Reis P.A.L., "Neutron production evaluation from a ADS target utilizing the MCNPX 2.6.0 code", Brazizian Journal of Physics, 40(4), p. 414-418, (2010).

Bateman H., "Solution of a system of differential equations occurring in the theory of radio-active transformations", Math. Proc. Cambridge 15, p. 423-427, (1910).

Benchmark on the Three-dimensional VENUS-2 MOX Core Measurements, Final Report, NEA/NSC/DOC, ISBN 92-64-02160-4, (2004).

Bowman C.D. et al., Nucl. Instr. and Meth. A, p. 320-336, (1992).

Bowman S.M., DeHart M.D., and Petrie L.M., "Integrated KENO Monte Carlo Transport for 3-D Depletion with SCALE" Proc. of The Monte Carlo 2005 Topical Meeting, The Monte Carlo Method: Versatility Unbounded in a Dynamic Computing World, on CD-ROM, American Nuclear Society (2005).

Brun R., Hansroul M., Lassalle J.C., "GEANT3 User's Guide", CERN DD/EE/84- 1. Computing and Networks Division, CERN (1994).

Bungau C., Barlow R., Bungau A., Cywinski R., "Neutron Spallation Studies for an Accelerator Driven Subcritical Reactor", Proc. of 23rd Particle Accelerator Conference PAC09, Vancouver, BC, (2009).

Briesmeister J.F., "MCNP-A general Monte Carlo N-Particle Transport Code System", Version 4C. LA-13709-M, Los Alamos National Laboratory (2000).

Cabellos O., García-Herranz N., Diez de la Obra C.J., Alvarez-Cascos R., Sanz J., Ogando F., Sauvan P. “Propagation of Nuclear Data Uncertainties in Transmutation Calculations Using ACAB Code”, Int. Conf. on Nuclear Data for Science and Technology, (2010).

Cash J.R., Karp A.H., “ACM Transactions on Mathematical Software”, 16, p. 201-222, (1990).

Catsaros N., Gaveau, B., Jaekel, M.-T., Maillard, J., Maurel, G., Savva, P., Silva, J., Varvayanni, M., Zisis, Th., “Criticality qualification of a new Monte Carlo code for reactor core analysis”, Ann. Nucl. Energy 36, p. 1689–1693, (2009).

Catsaros N., Gaveau B. , Jaekel M.-T., Maillard J., Maurel G., Savva P., Silva J., Varvayanni M., "Building a Dynamic Code to Simulate New Reactor Concepts", Nuclear Eng. & Design, 246, p. 41-48, (2012).

Catsaros N., Gaveau B. , Jaekel M.-T., Jejcic A., Maillard J., Maurel G., Savva P., Silva J., Varvayanni M., Xenofontos T., "Investigating the Breeding Capabilities of Hybrid Soliton Reactors". Nucl. Eng. & Design, 261, p. 251-259, (2013).

Cetnar J., “A method of transmutation trajectories analysis in accelerator driven system”, Proceedings of the IAEA Technical Committee Meeting on Feasibility and Motivation for Hybrid Concepts for Nuclear Energy Generation and Transmutation, IAEA TC-903.3, p 419-428, (1999).

Cetnar J., Gudowski W., Wallenius J., “User Manual for Monte Carlo Continuous Energy Burnup (MCB) Code – Version 1C”, NEA-1643/01, (2002).

Cetnar J., “General Solution of Bateman Equations for Nuclear Transmutations”, Ann. Nucl. Energy 33, p. 640-645, (2006).

Croff A.G., “A User’s Manual for the ORIGEN2 Computer Code”, ORNL/TM-7175, (1980).

Croff A.G., ORIGEN-2, “A Versatile Computer Code for Calculating the Nuclide Compositions and Characteristics of Nuclear Materials”, Nuclear Technology. 62,p 335-352, (1983).

Dat, H.T., “Mise au point de la bibliothèque physique et développement du système PEPABAC (PROGICIEL FAKIR) à l’aide des codes PEPIN et APOLLO 1” ; Thèse du doctorat CEA Saclay, Note CEA-N-2815, (1996).

David J.-C., Varignon C., Borne F., Boudard A., Brochard F., Crespin S., Duchazeaubeneix J.C., Durand D., Durand J.M., Fréhaut J., Hannappe F., Lebrun C., Lecolley J.F., Ledoux X., Lefèbvres F., Legrain R., Leray S., Louvel M., Martinez E., Ménard S., Milleret G., Patin Y., Petitbon E., Plouin F., Schapira J.P., Stuggé L., Terrien Y., Thun , J. Volant C., Whittal D.M., “Spallation Neutron Production on Thick Target at SATURNE,” Proc. of the Workshop on Nuclear Data for the Transmutation of Nuclear Waste, GSI- Darmstadt, Germany, ISBN 3-00-012276-1, edited by A. Kelic and K.-H. Schmidt, (2003).

DeHart M. D., Brady M. C., Parks C. V., “OECD/NEA, Burnup Credit Calcunational Criticality Benchmark Phase I-B Results”, NEA/NSC/DOC(96)-06, ORNL-6901, (1996).

DICE: International Handbook of Evaluated Criticality Safety Benchmark Experiments”, NEA, OECD, NEA/NSC/DOC (95), Edition (2001).

Duderstadt J., Hamilton L., “Nuclear Reactor Analysis”, John Wiley & Sons, (1976).

El Bakkari B., El Bardouni T., Merroun O., El Younoussi C., Boulaich Y., Boukhal H., Chakir E., “Validation of a new continuous Monte Carlo burnup code using a mox fuel assembly”, Nuclear Engineering and Design, 239, p. 1828-1838, (2009).

Experiments for Nuclear-Chicago Student Training Reactor, Nuclear Chicago Corporation, (1959).

Euratom
http://ec.europa.eu/research/energy/euratom/index_en.cfm?pg=fission&section=generation

Feghhi S.A.H., Gholamzadeh Z., “a MCNP simulation Study of Neutronic Calculations of spallation targets”, Nuclear Technology & Radiation Protection, Vol. 28, No. 2, p. 128-136, (2013).

Ferrari A., Sala P.R., “A New Model for Hadronic Interactions at Intermediate Energies for the FLUKA Code”, Int. Conf. on Monte-Carlo Simulation in High-Energy and Nuclear Physics, Florida, USA (1993).

Fernandes A.C., Santos J.P., Marques J.G., Kling A., Ramos A.R., Barradas N.P., " Validation of the Monte Carlo model supporting core conversion of the Portuguese Research Reactor (RPI) for neutron fluence rate determinations", Annals of Nuclear Energy, 37, p. 1139-1145, (2010).

Gomin E.A., Maiorov L.V., “The MCU Monte Carlo Code for 3D Depletion Calculation”, Proc. of International Conference on Mathematics and Computations, Reactor Physics, and Environmental Analyses in Nuclear Applications, 2, p. 997-1006, (1999).

Gomit J.M, Cousinou P., Diop C., Fernandez de Grado G., Gantenbein F., J.P. Grouiller, A. Marc, D. Mijuin, H. Toubon, “CRISTAL V1: Criticality package for burn up credit calculations”, Proc. of the 7th International conference on nuclear safety safety- Challenges in the pursuit of global nuclear criticality safety (ICNC2003), Report JAERI-CONF--2003-019-PT2, (2003).

Hanan N.A., Olson A. P., Pond R. B., Matos J. E., “A Monte Carlo burnup code linking MCNP and REBUS”, ANL-TD-CP-97492, also Proc. of the 21st RERTR Meeting, (1998).

Isotalo A., “Computational Methods for Burnup Calculations with Monte Carlo Neutronics”, PhD Thesis, (2013).

Kadi Y., Carminati F., “Simulation of Accelerator-Driven Systems”, Workshop on Hybrid Nuclear Systems for Energy Production, Utilisation of Actinides & Transmutation of Long-Lived Radioactive Waste, European Organization for Nuclear Research: CERN, (2001).

Krása A., Křížek F., Wagner V., Kugler A., Henzl V., Henzlová D., Majerle M., Adamb J., Čaloun P., Chultem D., Kalinnikov V. G., Krivopustov M. I., Solnyshkin A. A., Stegailov V. I., Tsoupko-Sitnikov V. M., Tumendelger T. “Neutron Production in Spallation Reactions of 0.9- and 1.5-GeV Protons on a Thick Lead Target – Comparison of Experimental Data and MCNPX Simulations” AIP Conf. Proc., 769, p. 1555, (2005).

Křížek F., Wagner V., Krivopustov M.I.†, Adam J. †, Čaloun P.†, Henzl V., Henzlová D., Krása A., Kugler A., Majerle M., Stegailov† V.I., Tsoupko-Sitnikov† V.M., "The study of spallation reactions, neutron production and transport in a thick lead target and a uranium blanket during 1.5 GeV proton irradiation", Czechoslovak Journal of Physics, 56, Issue 3, p 243-252, (2006).

Lamarsh J. R., Baratta A. J., Introduction to Nuclear Engineering, Prentice Hall, New Jersey, (2001).

Leppänen J., "Development of a New Monte Carlo Rreactor Physics Code", VTT Publication 640, (2009).

Leprince A., David J.-C., Ene D. and Leray S., "Reliability and use of INCL4.6-Abla07 spallation model in the frame of European Spallation Source target design", Progress in Nuclear Science and Technology, 4, p. 491-495, (2014).

Lewis E.E, Miller W.F., "Computational Methods of Neutron Transport". American Nuclear Society, p. 14-16, (1993).

Louis H., Amin E., Aziz M., Bashter I., "Studies on Production of Neutrons in the Spallation Reactions Using the Monte Carlo Code MCNPX", Nuclear Science and Engineering, Vol. 170 (1), p. 61-65, (2012).

Majerle M., "Monte Carlo methods in spallation experiments", Report for the PhD State Exam, Department of Physics, Faculty of Nuclear Sciences and Physical Engineering, Czech Technical University in Prague, (2008).

Mantha V., Mohanty A. K., Satyamurthy P., "Thermal hydraulic studies of spallation target for one-way coupled indian accelerator driven systems with low energy proton beam", Pramana Journal of Physics, 68(2), p. 355-363, (2007).

Matos J.E., Stevens, J.G., Feldman, E.E., Stillman, J.A., Dunn, F.E., Kalimullah, K., Marques, J.G., Barradas, N.P., Ramos, A.R., Kling, A., Core conversion analyses for the Portuguese Research Reactor. In: Proceedings of 28th International Meeting on Reduced Enrichment for Research and Test Reactors, (2006).

Matos J.E., Argonne National Laboratory, Private Communication, (2005).

Meloni P., Bandini G., Polidori M., “T/H and transient analyses to confirm EFIT preliminary design”, Journal of Nuclear Materials, 376(3), p. 405-408, (2008).

MCNPX User’s Manual, Version 2.4.0, LANL report LA-CP-02-408, Los Alamos (2002).

Mole C., Van Loan C., “Nineteen Dubious Ways to Compute the Exponential of a Matrix, Twenty-five Years Later”, SIAM Rev. 45, pp 3-49, (2003).

Na B.-C., Messaoudi, N., “Benchmark on the Three-dimensional VENUS-2 MOX”. (2003).

Nelson, T., Eddy, B.G., Foreign Research Reactor Uranium Supply Program: The Y-12 National Security Complex Process. In: Transactions of the Research Reactor Fuel Management Meeting RRFM-2010, Marrakech, European Nuclear Society, Brussels, ISBN 978-92-95064-10-2, (2010).

Nuclear Regulatory Commission, Safety Evaluation Report related to the Evaluation of Low-Enriched Uranium Silicide-Aluminium Dispersion Fuel for use in Non-Power Reactors, NRC, Washington, (1988).

OECD/NEA: https://www.oecd-nea.org/dbforms/data/eva/evatapes/jeff_31/JEFF312/

Oden M., Krása A., Majerle M., Svoboda O., Wagner V. “Monte-Carlo Simulations: FLUKA vs. MCNPX” AIP Conf. Proc., 958, p. 219, (2007).

Parks C. V., “Overview of ORIGEN2 and ORIGEN-S: Capabilities and limitations”, p. 57-63 Proc. of the 3rd International Conference on High-Level Radioactive Waste Management, Vol.1, (1992).

Petit O., Hugot F.X., Lee Y.K, Jouanne C., Mazzolo A., “TRIPOLI -4 User Guide. Report” CEA-R-6169. Code available from OECD/NEA Data Bank, (2008).

Piénkowski L.P., Gawlikowicz W., Hilscher D., “FLUKA simulation for NESSI experiments”, EURISOL-05-25-2006-0014, (2006).

Prael R. E., Liechtenstein H., “User Guide to LCS:The LAHET Code System” Los Alamos National Laboratory informal report LA-UR-89-3014 (1989).

Pusa M., Leppänen J., “Computing the Matrix Exponential in Burnup Calculations”, Nucl. Sci. Eng. 164, p 140-150, (2010).

Pusa M., Leppänen J., “Efficient Implementation of CRAM method for Solving Burnup Equations”, PHYSOR 2012, on CD-ROM ISBN 978-0-89448-085-9, (2012).

Pyeon C.H. et al., “Experimental Benchmarks of Neutronics on Solid Pb-Bi in Accelerator-Driven System with 100 MeV Protons at Kyoto University Critical Assembly”, (2017).

Ren G., W. Li, Y. Li, M. Zeng, “Simulation for Radiation Field caused by beam loss of C-ADS INJECTOR II”, p. 489-491, Proc. of International Beam Instrumentation Conference, Oxford’s University, Vol. 1, (2013).

Romano P. K., Forget B., “The OpenMC Monte Carlo particle transport code”, Nucl. Technol., 51, p. 274-81, (2013).

Rose D.J., Tarjan R.E., “Algorithmic Aspects of Vertex Elimination on Directed Graph”s, SIAM J. Comput. 5, p. 266-283, (1976).

Rosenthal M.W., “An Account of Oak Ridge National Laboratory’s Thirteen Nuclear Reactors”, ORNL/TM-2009/181, Rev. 1, ORNL, Oak Ridge, 45–46. (2010).

Rubbia C. et al., Report CERN=AT=95‑44 (ET), (1995).

Samson M., Grouiller J. P, Pavageau J., Marimbeau P., “Cesar: a simplified evolution code for reprocessing applications”, Proc. of the 5th International Conference on recycling, conditioning and disposal (RECOD 98), Nice (France), (1998).

Sasa T., Tsujimoto K., Takizuka T., Takano H., “Code development for the design study of the OMEGA Program accelerator-driven transmutation systems”, Nuclear Instruments and Methods in Physics Research. Section A v. 463(3), p. 495-504, (2001).

Savva P., M.Varvayanni, A.C. Fernandes, J.G. Marques, N. Catsaros, "Comparing Neutronics Codes Performance in Analyzing a Fresh-fuelled Research Reactor Core", Annals of Nuclear Energy, Vol. 63, p. 731-741, (2014).

She D. et al., “Development of Burnup Methods and Capabilities in Monte Carlo Code RMC”, Annals of Nuclear Energy, Vol. 51, p. 289-294, (2013).

Sumner T. and Goluoglu S., "Verification of KENO V.A and KENO-VI Using Analytical Benchmarks", Proc. of the 8th International Conference on Nuclear Criticality Safety (ICNC 2007), Vol. 1, p. 361-363, (2007).

Toppel B. J., "A User's Guide for the REBUS -3 Fuel-Cycle-Analysis Capability," ANL-83-2, Argonne National Laboratory (1983).

Vijaya A.D., Kumar A., “The neutron spectrum of Am-Be neutron sources”, Nucl. Instrum. Methods, III p. 435-440 (1973).

Wang K. et al., “RMC - A Monte Carlo Code for Reactor Core Analysis”, Annals of Nuclear Energy, Vol. 82, p. 121-129, (2015).

Zhang Y. L., Zhang X. C., Qi J., Wu Z., Yang L., “Study on the Parameters of the ADS Spallation Target” Journal of Physics: Conference Series 420, 012064, (2013).

Zheng M., Tian W., Wei H., Zhang D., Wu Y., Qiu S., Su G., “Development of a MCNP–ORIGEN burn-up calculation code system and its accuracy assessment”, Annals of Nuclear Energy, Vol. 63, p. 491-498, (2014).

Zhong Z., Gohar Y., Talamo A., “MCNPX and MCB Coupled Methodology for the Burnup Calculation of the KIPT Accelerator Driven Subcritical System”, Proc. of “International Conference on Mathematics, Computational Methods & Reactor Physics (M&C 2009), Saratoga Springs, on CD-ROM, American Nuclear Society, LaGrange Park, IL, (2009).

SUMMARY IN GREEK

Η ανάγκη λεπτομερούς προσομοίωσης ενός πυρηνικού αντιδραστήρα, ειδικά στις περιπτώσεις διατάξεων με περίπλοκη γεωμετρία και σύσταση καυσίμου, επέβαλε την ολοένα και αυξανόμενη χρήση των νετρονικών κωδίκων Monte Carlo. Εκτός αυτού, απαιτούνται επιπλέον εγγενείς δυνατότητες στους στοχαστικούς κώδικες που αφορούν κυρίως σε προσομοιώσεις της χρονικής μεταβολής της ισοτοπικής σύστασης του καυσίμου σε συνδυασμό με την ενσωμάτωση της θερμοϋδραυλικής ανάδρασης. Επιπροσθέτως, ο σχεδιασμός καινοτόμων σχεδίων πυρηνικών αντιδραστήρων, όπως των Αντιδραστήρων Οδηγούμενων από Επιταχυντή (ΑΟΕ), δημιούργησε πρόσθετες απαιτήσεις στις δυνατότητες των κωδίκων προσομοίωσης. Πιο συγκεκριμένα, ο συνδυασμός επιταχυντή και πυρηνικού αντιδραστήρα στους ΑΟΕ, απαιτεί την προσομοίωση αμφότερων των υποσυστημάτων για την ολοκληρωμένη ανάλυση του συστήματος. Επομένως, ανακύπτει η ανάγκη για εξελιγμένα εργαλεία προσομοίωσης τα οποία θα είναι ικανά να καλύψουν το ευρύ ενεργειακό φάσμα των νετρονίων που παρατηρείται στα προαναφερθέντα συστήματα.

Οι πιο ευρέως διαδεδομένοι στοχαστικοί νετρονικοί κώδικες είναι ο MCNP, ο KENO και ο TRIPOLI. Ουσιαστικά αυτοί οι κώδικες πραγματοποιούν στατικούς υπολογισμούς ενώ έχουν τη δυνατότητα εκτέλεσης χρονοεξαρτώμενων υπολογισμών, μέσω της σύζευξής τους με εξωτερικά υποπρογράμματα που επιλύουν τη θεωρία διάχυσης νετρονίων. Η εκτίμηση της εξάντλησης καυσίμου απο τον MCNP ή τον KENO πραγματοποιείται παραδοσιακά μέσω της σύζευξης με τους κώδικες ORIGEN, REBUS και MCB. Οι δυναμικοί υπολογισμοί με τον TRIPOLI λαμβάνουν χώρα μέσω της ενσωμάτωσης του στο σύστημα κωδίκων CRISTAL V1 που περιέχει μεταξύ άλλων τον κώδικα CESAR, ο οποίος εκτελεί υπολογισμούς εξάντλησης καυσίμου. Εκτός από τους προαναφερθέντες στοχαστικούς νετρονικούς κώδικες, άλλοι γνωστοί Monte Carlo νετρονικοί κώδικες είναι ο OpenMC, ο MCU και ο Serpent, με τον τελευταίο να διαθέτει επίσης τη δυνατότητα υπολογισμού της εξάντλησης καυσίμου.

Όσον αφορά στην ανάλυση των ΑΟΕ, η συνήθης διαδικασία περιλαμβάνει το διαχωρισμό του θρυμματιζόμενου στόχου από την υποκρίσιμη καρδιά του αντιδραστήρα μέσω της χρήσης δύο κωδίκων, ενός κώδικα Φυσικής Υψηλών Ενεργειών (ΦΥΕ) για τον επιταχυντή (π.χ. FLUKA ή MCNPX) και ενός νετρονικού

κώδικα για το τμήμα της καρδιάς του αντιδραστήρα. Τα παραδείγματα προσπαθειών ανάλυσης των ΑΟΕ χρησιμοποιώντας έναν ενιαίο κώδικα είναι πολύ λίγα.

Στην εργασία αυτή παρουσιάζονται τα κύρια χαρακτηριστικά και οι δυνατότητες του νέου στοχαστικού νετρονικού κώδικα ANET (Advanced Neutronics with Evolution and Thermal hydraulic feedback) ο οποίος αναπτύχθηκε σε συνεργασία του Εθνικού Κέντρου Έρευνας Φυσικών Επιστημών "Δημόκριτος" (ΕΚΕΦΕ-Δ, Ελλάδα) με το ινστιτούτο Institut de Développement et des Ressources en Informatique Scientifique / Centre National de la Recherche Scientifique (IDRIS/ CNRS, Γαλλία) και το πανεπιστήμιο Université de Paris VI Pierre et Marie Curie (UPMC, Γαλλία) με σκοπό να ικανοποιήσει τις απαιτήσεις που περιγράφονται ανωτέρω. Ο ANET έχει ως βάση τον κώδικα ΦΥΕ ανοικτού λογισμικού GEANT3.21 και προορίζεται για να πραγματοποιήσει αναλύσεις τόσο συμβατικών πυρηνικών αντιδραστήρων όσο και ΑΟΕ. Ο ANET έχει δημιουργηθεί με τις εγγενείς δυνατότητες

α) να πραγματοποιεί υπολογισμούς εξάντλησης καυσίμου

β) να προσομοιώνει τη διαδικασία θρυμματισμού στην περίπτωση του ΑΟΕ

και έχει σχεδιασθεί να λαμβάνει υπ'όψιν θερμοϋδραυλική ανάδραση. Η βάση του ANET στηρίχθηκε σε μια τροποποίηση του κώδικα GEANT3.21 προκειμένου να καταστεί δυνατή η παρακολούθηση των νετρονίων με ενέργεια μικρότερη από 20 MeV, δηλαδή των νετρονίων που παράγονται στους πυρηνικούς αντιδραστήρες. Οι πρώιμοι υπολογισμοί κατέδειξαν την ικανότητα του ANET να προσομοιώνει τις αντιδράσεις νετρονίων (ελαστική κρούση, απορρόφηση και σχάση). Σε αυτούς, η κρισιμότητα εξαγόταν εμμέσως από το πηλίκο του αριθμού των παραγόμενων νετρονίων από δύο διαδοχικές γενιές σχάσεων ενώ για την διαδικασία θρυμματισμού υιοθετήθηκε η υπόθεση μιας σταθερής και προκαθορισμένης παραγωγής νετρονίων. Στη συνέχεια, η ανάπτυξη της δομής και των δυνατοτήτων του ANET βελτιωνόταν συνεχώς.

Η τρέχουσα έκδοση του ANET χρησιμοποιεί τους τρεις συνήθεις εκτιμητές Monte Carlo για τον υπολογισμό του συντελεστή πολλαπλασιασμού k_{eff}, δηλαδή τους εκτιμητές collision, absorption και tracklength. Για τον υπολογισμό της νετρονικής ροής και του ρυθμού αντιδράσεων με νετρόνια, οι εκτιμητές collision και tracklength ενσωματώθηκαν στον ANET ακολουθώντας την Monte Carlo προσέγγιση. Όσον

αφορά στους δυναμικούς υπολογισμούς, π.χ. εξάντληση καυσίμου, επιλέχθηκε μια προσέγγιση καθαρώς στοχαστική (να σημειωθεί οτι η συνήθης διαδικασία είναι η σύζευξη ενός στοχαστικού νετρονικού κώδικα με έναν αιτιοκρατικό κώδικα για τους υπολογισμούς εξάντλησης καυσίμου). Η προσέγγιση αυτή χωρίζεται σε δύο στάδια, δηλαδή α) υπολογισμός της κατανομής πυκνότητας νετρονίων και β) εκτίμηση των μεταβολών στις συγκεντρώσεις των διαφόρων νουκλιδίων, υποθέτοντας ότι αυτές οι παράμετροι μπορούν να υπολογιστούν διαδοχικά και κυκλικά με εναλλαγή των δύο σταδίων υπολογισμού (νετρονικοί / μεταβολή της σύστασης) και χρησιμοποιώντας κάθε φορά τα αποτελέσματα που ελήφθησαν στο προηγούμενο χρονικό βήμα. Σε αυτήν τη διαδικασία, η χρονικά σταθερή ροή νετρονίων (και συνεπώς οι ρυθμοί αντίδρασης) για δεδομένη ισοτοπική σύσταση υπολογίζονται στο πρώτο βήμα ενώ οι μεταβολές της ισοτοπικής σύστασης υπολογίζονται στο δεύτερο βήμα υποθέτοντας σταθερό ρυθμό αντιδράσεων για όλο το θεωρούμενο χρονικό διάστημα. Η μεθοδολογία αυτή χρησιμοποιείται στον ANET με τη διαφορά ότι οι ρυθμοί αντίδρασης υπολογίζονται και χρησιμοποιούνται απευθείας. Στην τρέχουσα έκδοση περιλαμβάνονται περίπου 150 νουκλίδια που παρακολουθούνται για τις αντιδράσεις μεταστοιχείωσης και για τις ραδιενεργές διασπάσεις. Για την ανάλυση AOE και συσκεκριμένα την προσομοίωση της αντίδρασης θρυμματισμού, το υποπρόγραμμα INCL/ABLA έχει ενσωματωθεί στον ANET. Η ικανότητα του ANET να προσομοιώνει συμβατικούς πυρηνικούς αντιδραστήρες έχει καταδειχθεί χρησιμοποιώντας πειραματικά δεδομένα καθώς και αποτελέσματα προσομοιώσεων επαλήθευσης με τη χρήση καθιερωμένων στοχαστικών νετρονικών κωδίκων.

Για την επαλήθευση και την επικύρωση των δυνατοτήτων του ANET χρησιμοποιήθηκαν δεδομένα από διάφορες διατάξεις και διεθνείς πρότυπες αναλύσεις προβλημάτων (benchmarks). Με αυτόν τον τρόπο :

- Πραγματοποιήθηκαν από τον ANET υπολογισμοί κρισιμότητας και ροής νετρονίων στον αντιδραστήρα της Λισαβόνας (RPI) μετά την μετατροπή του για χρήση καυσίμου χαμηλού εμπλουτισμού σε U235
- Οι υπολογισμοί κρισιμότητας και ρυθμών αντιδράσεων νετρονίων που πραγματοποιήθηκαν από διεθνώς αναγνωρισμένους κώδικες στα πλαίσια της άσκησης της OECD/NEA για την ανάλυση του αντιδραστήρα VENUS-2 MOX αναπαράχθησαν από τον ANET

- Η υποκρίσιμη διάταξη του Αριστοτελείου Πανεπιστημίου της Θεσσαλονίκης αναλύθηκε από τον ANET
- Η δυνατότητα προσομοίωσης χρονοεξαρτώμενων φαινομένων από τον ANET επιβεβαιώθηκε χρησιμοποιώντας δεδομένα από το διεθνές benchmark της OECD/NEA "Burnup Credit Calculational Criticality Benchmark Phase I-B"
- Ο υπολογισμός κρισιμότητας στην περίπτωση ΑΟΕ πραγματοποιήθηκε με τη χρήση δεδομένων από τον αντιδραστήρα KUCA (Kyoto University Critical Assembly) που βρίσκεται στο Πανεπιστήμιο του Κυότο (Ιαπωνία).

Εν κατακλείδι, τα αποτελέσματα που προέκυψαν από συγκρίσεις με πειραματικές μετρήσεις ή προσομοιώσεις που πραγματοποιήθηκαν χρησιμοποιώντας άλλους στοχαστικούς ή ντετερμινιστικούς νετρονικούς κώδικες, δείχνουν ότι ο ANET έχει τη δυνατότητα να υπολογίζει σωστά σημαντικές παραμέτρους κρίσιμων ή υποκρίσιμων συστημάτων. Επιπλέον, η προκαταρκτική εφαρμογή του ANET σε προβλήματα υπολογισμού εξάντλησης καυσίμου παρέχει ενθαρρυντικά αποτελέσματα, εάν ληφθούν υπ' όψιν οι αβεβαιότητες της τάξης 20% και άνω που παραδοσιακά αναμένονται σε υπολογισμούς εκτίμησης της σύστασης καυσίμου. Στην πραγματικότητα, εκτός από τις αβεβαιότητες που εισάγονται από τους αλγορίθμους που εφαρμόζονται στους κώδικες υπολογισμού, μια μη αμελητέα πηγή αβεβαιότητας είναι αυτή των διαφορετικών πυρηνικών δεδομένων (χρόνος ημιζωής στις ραδιενεργές διασπάσεις, απόδοση-yield των διαφόρων αντιδράσεων ως ακόμη και οι τιμές των ενεργών διατομών αντιδράσεων). Τέλος, τα αποτελέσματα που ελήφθησαν στην περίπτωση του KUCA αποδεικνύουν οτι ο ANET είναι σε θέση να αναλύσει επιτυχώς έναν ΑΟΕ πληρώντας τις προϋποθέσεις ενός εξελιγμένου στοχαστικού νετρονικού κώδικα με πεδίο εφαρμογής τους συμβατικούς αλλά και καινοτόμους πυρηνικούς αντιδραστήρες σχάσης.

SUMMARY IN FRENCH

La nécessité de simulations précises d'un réacteur nucléaire et spécialement dans des cas de cœurs et de configurations de combustible complexes, a imposé un usage accru de Codes Neutroniques Stochastiques (CNS). De plus, une demande a émergé pour des CNS à capacité inhérente d'estimation en continu de la variation de la composition isotopique du cœur ainsi qu'à couplage thermo-hydraulique optimisé. Des capacités supplémentaires sont exigées de ces codes en vue de leur utilisation pour l'étude de nouveaux concepts de réacteur comme les Réacteurs Conduits par Accélérateur (RCA). Plus précisément, le réacteur hybride comprenant un réacteur nucléaire conventionnel et un accélérateur, nécessite l'analyse des deux composantes (réacteur – accélérateur) par un outil capable de couvrir le spectre énergétique neutronique extrêmement étendu qui caractérise ce système hybride.

Les CNS les plus répandus sont MCNP, KENO et TRIPOLI. Essentiellement, ces codes effectuent des calculs statiques. Ils ont la possibilité d'exécuter des calculs d'évolution une fois couplés à des modules externes utilisant la théorie de diffusion neutronique. Ainsi, la consommation du combustible est traditionnellement calculée par MCNP ou KENO en couplage avec ORIGEN, REBUS et MCB. Pour TRIPOLI il a été reporté que les calculs d'évolution s'effectuent avec le code intégré au système de codes CRISTAL V1 qui contient – entre autres – le module CESAR capable de calculer la consommation du combustible. A part les CNS susmentionnés, autres codes neutroniques Monte Carlo bien connus sont OpenMC, MCU et Serpent, le dernier ayant aussi des capacités de calcul d'évolution du combustible.

Pour ce qui concerne l'analyse des RCA, la procédure usuelle consiste à séparer la cible de spallation du cœur sous-critique en utilisant deux codes, un premier de Physique des Hautes Energies (PHE) pour l'accélérateur (par exemple FLUKA ou MCNPX) et un code neutronique pour la partie cœur du réacteur. Des exemples de tentative d'analyse de RCA en utilisant un seul code sont très peu nombreux.

Ce travail présente les principales caractéristiques et capacités du nouveau CNS ANET (Advanced Neutronics with Evolution and Thermal hydraulic feedback) développé en collaboration du NCSR Demokritos (Grèce) avec CNRS/IDRIS et UPMC (France) et couvrant autant que possible les exigences exposées ci-dessus. ANET est basé sur la version ouverte du code PHE GEANT3.21 et est destiné à

effectuer des analyses de cœurs de réacteurs conventionnels de génération II et III ainsi que des RCA. ANET est construit avec la capacité inhérente

a) d'effectuer des calculs d'évolution du combustible

b) de simuler le processus de spallation dans le cas des RCA

et est dessiné pour tenir compte de la thermo-hydraulique du système. La base d'ANET est une modification de GEANT3.21 pour rendre possible le suivi de neutrons d'énergie inférieure à 20 MeV, c.à.d. de neutrons qui sont présents dans le cœur des réacteurs nucléaires. Des calculs préliminaires ont démontré la capacité d'ANET de simuler les réactions neutroniques (collision élastique, capture, fission). La criticité du cœur découlait de la division du nombre de neutrons de deux générations consécutives de fissions alors que l'hypothèse d'une production neutronique fixe et prédéfinie avait été retenue pour la spallation. Par la suite, le développement de la structure et des capacités d'ANET a été continuellement amélioré.

La version actuelle d'ANET utilise les trois estimateurs standard Monte Carlo pour le calcul du facteur de multiplication neutronique effectif (keff), soit l'estimateur de collision, celui d'absorption et celui de longueur de trace. Pour ce qui est du calcul du débit de fluence neutronique et des taux de réaction, les estimateurs de collision et de longueur de trace sont implémentés dans ANET suivant la procédure standard Monte Carlo. Pour ce qui concerne les calculs d'évolution (par exemple la consommation du combustible), une approche purement stochastique est implémentée dans ANET (à noter que la procédure usuelle consiste à coupler le code neutronique stochastique avec un code déterministe qui calcule la consommation du combustible). Ceci s'articule en deux temps, c.à.d. (a) calcul de la distribution de la densité neutronique et (b) estimation des changements des concentrations des différents nuclides, faisant l'hypothèse que ces paramètres peuvent être calculés séquentiellement et d'une manière cyclique en alternant les deux pas de calcul (neutronique / changement de composition) et en utilisant chaque fois les résultats obtenus au pas de temps précèdent. Dans cette procédure, le flux neutronique constant (et donc les taux de réaction) pour une composition isotopique donnée, sont calculés pendant le premier pas de temps alors que les changements de composition isotopique sont calculés pendant le second pas de temps en supposant des taux de réaction

constants. Cette procédure est utilisée dans ANET à la différence que les taux de réaction sont calculés et utilisés directement. Dans la version actuelle, quelques 150 nuclides sont inclus et peuvent être traités pour les réactions de transmutation et pour la décroissance radioactive. Pour les besoins d'analyse des RCA, le module INCL/ABLA a été incorporé dans ANET de façon à ce que le processus de spallation soit simulé par le code. La capacité d'ANET de simuler des configurations classiques a été démontrée en utilisant des résultats de mesures et des simulations de vérification effectuées en utilisant d'autres codes bien établis, ainsi qu'il est montré par la suite.

Des données provenant de plusieurs installations et des analyses de problèmes-type internationaux ont été utilisés pour vérifier et valider les capacités d'ANET. C'est ainsi que :

- Des mesures de réactivité et de flux neutronique au réacteur de Lisbonne (RPI) ont été utilisées après que le réacteur a été converti pour utiliser uniquement du combustible à bas enrichissement
- Des calculs de taux de réaction effectués par plusieurs codes internationaux dans le cadre de l'exercice organisé par l'OCDE/AEN sur l'analyse du cœur VENUS-2 MOX ont été reproduits par ANET
- L'assemblage sous-critique de l'Université de Thessaloniki a été analysé par ANET
- La capacité d'ANET de simuler des phénomènes dépendant du temps a été vérifiée en utilisant les données de l'exercice international organisé par l'OCDE/AEN « Burnup Credit Calculational Criticality Benchmark Phase I-B »
- La capacité d'ANET de simuler correctement le facteur de multiplication neutronique effectif dans le cas d'un RCA a été vérifiée en utilisant des données de mesures effectuées sur le KUCA (Kyoto University Critical Assembly)

Pour conclure, les résultats obtenus lors des comparaisons avec des mesures ou avec des simulations effectuées en utilisant d'autres codes neutroniques stochastiques ou déterministes, montrent qu'ANET possède la capacité de calculer correctement d'importants paramètres de systèmes critiques ou sous-critiques. Par ailleurs,

l'application préliminaire d'ANET à des problèmes dépendant du temps fournit des résultats encourageants. ANET produit des estimations de consommation de combustible raisonnables, compte tenu du fait que des incertitudes dans ce domaine sont souvent de l'ordre de 20% ou plus. En effet, à part les incertitudes introduites par les algorithmes implémentés dans les codes de calcul, une source non négligeable d'incertitudes est celle des différentes données nucléaires (demi-vie de décroissance radioactive, rendements des différentes réactions et même les valeurs des sections efficaces). Finalement, les performances du code dans le cas de KUCA montrent qu'ANET peut analyser des RCA de façon satisfaisante.

LIST OF PUBLICATIONS

1. N. Catsaros, B. Gaveau, M.-T. Jaekel, A. Jejcic, J. Maillard, G. Maurel, P. Savva, J. Silva, M. Varvayanni, T. Xenofontos, "*Investigating the breeding capabilities of Hybrid Soliton Reactors*", 20th Int. Conf. "Nuclear Energy for a New Europe", Bovec, Slovenia, September 5-7, (2011).

2. N. Catsaros, B. Gaveau, M.-T. Jaekel, A. Jejcic, J. Maillard, G. Maurel, P. Savva, J. Silva, M. Varvayanni, T. Xenofontos, "*Modeling and simulating a breeder hybrid soliton reactor*", 21st Int. Conf. "Nuclear Energy for a New Europe", Ljubljana, Slovenia, September 5-7, (2012).

3. N. Catsaros, B. Gaveau, M.-T. Jaekel, A. Jejcic, Maillard J. Maillard, G. Maurel, P. Savva, J. Silva, M. Varvayanni, T. Xenofontos, "*Investigating the Breeding Capabilities of Hybrid Soliton Reactors*". Nucl. Eng. & Design, 261, p. 251-259, (2013).

4. T. Xenofontos, G.-K. Delipei, P. Savva, M. Varvayanni, N. Catsaros, J. Maillard, J. Silva, "*Fluence Rate Benchmarking of the Stochastic Neutronic Code ANET* ", 24th Int. Conf. "Nuclear Energy for a New Europe", Portoroz, Slovenia, (2014).

5. T. Xenofontos, P. Savva, M. Varvayanni, N. Chrysanthopoulou, N. Catsaros, J. Maillard, J. Silva, G.-K. Delipei, A. Clouvas, "*Criticality Benchmarking of the Stochastic Neutronic Code ANET*", Int. Conf. "PHYSOR", Kyoto Japan, Sept. 28 - Oct. 3, (2014).

6. T. Xenofontos, G.-K. Delipei, P. Savva, M. Varvayanni, J. Maillard, J. Silva, N. Catsaros, "*ANET reaction rates validation based on the Venus-2 MOX core benchmark analysis*", 25th Int. Conf. Nuclear Energy for New Europe '15, Portoroz, Slovenia, September 14-17, (2015).

7. T. Xenofontos, A.G. Mylonakis, P. Savva, M. Varvayanni, N. Catsaros, "*The ANET code: from High Energy Physics to Stochastic Dynamic Neutronics with Thermal Hydraulic Feedback*", Proc. of European Research Reactor Conference, Berlin, Germany, March 13-17, (2016).

8. T. Xenofontos, G.-K. Delipei, P. Savva, M. Varvayanni, J. Maillard, J. Silva, N. Catsaros, "*Testing the new stochastic neutronic code ANET in simulating safety important parameters*", Nucl. Eng. & Design, 103, p. 85-96, (2017).

APPENDIX I

FISSION POWER NUCLEAR REACTOR DESIGNS[3]

As Power Reactors are characterized the nuclear reactors that produce great thermal power, i.e. up to 4000 MW_{th} and are mainly used for the generation of electricity (over 16% of the world's electricity is produced from nuclear energy). Versions of nuclear power reactors with lower thermal power are used for the propulsion of ships, aircrafts, rockets and satellites while direct use of the produced heat in the reactor is made for the heating of cities and various industrial processes.

Nuclear reactor technology has been under continuous development since the first commercial exploitation of civil nuclear power in the 1950s. This technological development is presented as a number of broad categories, or 'Generations', each representing a significant technical advance, either in terms of performance, cost and safety, compared with the previous generation. At present, three generations of nuclear power systems, i.e. Generations I, II and III are in operation worldwide. Nuclear reactors of Generation III+ are believed to be within the current state-of-the-art, hence fundamental research on nuclear reactors is focused on nuclear alternatives - commonly called Generation IV or other innovative designs such as Accelerator Driven Systems (ADS) - that still require considerable effort. An analysis of the basic features of all four generations is given hereafter. In each case, the reactors are divided in two main categories, i.e. thermal and fast breeder reactors. Furthermore, reactors are separated in categories with regards to the moderator or the coolant used in each design.

GENERATION I

Generation I refers to the prototype and power reactors that launched civil nuclear power. This generation consists of early prototype reactors from the 1950s and 1960s, such as gas-cooled reactors, i.e. Calder Hall-1 (1956-2003, UK) and G1, G2 and G3 (Fr), light-water reactors, i.e. Shippingport (1957-1982, Pensylvania USA), Dresden-1 (1960-1978, Illinois USA) as far as thermal reactors are concerned and Fermi-I (1963-1972, Michigan USA) as a fast breeder reactor *(Lamarsh and Baratta, 2001)*.

[3] The information presented below corresponds to reactor designs up to March 2014.

Thermal Reactors

Two main designs are included in this category, i.e. the Gas-Cooled Reactors and the Light-Water Reactors. Both are analysed below.

Gas-cooled Reactors

In the USA during the World War II, natural uranium graphite-moderated reactors were developed in order to convert ^{238}U to ^{239}Pu for military purposes and through the years following the war, this type of reactor formed the basis for the nuclear weapons programs of many nations. Subsequently, natural uranium fuelled reactors became the starting point for the nuclear power industry, especially in nations which lacked the facilities for the enrichment of uranium fuel, such as the UK and France *(Lamarsh and Baratta, 2001)*.

The predecessors of gas-cooled reactors were the reactors for the production of plutonium, which in the USA had a once-through, open cycle and water as coolant whereas in the UK a once through air-cooling system was utilized. However, a closed-cycle gas-cooling system was adopted early on by both France and the UK. The reactor types - which are quite similar - developed in these countries were MAGNOX and UNGG respectively. In these reactors, natural uranium is used as fuel, graphite as moderator and CO_2 as the coolant gas. CO_2 was chosen since it demonstrates quite good properties of heat transfer and has a low neutron capture cross section. It is a relatively chemically inert gas and below 540 °C is chemically stable and does not react with either the moderator or fuel *(Lamarsh and Baratta, 2001)*, *(Leonidou, 2000)*. Both MAGNOX and UNGG reactors exhibit serious disadvantages which can be summarized below *(Leonidou, 2000)*:

- At high temperatures, both the cladding and the fuel react with the atmospheric air and CO_2.
- Due to the significant neutron transport scattering length in graphite (19 cm), large reactor dimensions and hence high construction cost is required.
- Metallurgical constraints put a limit to relatively low temperatures of operation.

Light Water Reactors (LWR)

The most widely used reactor design for producing electric power is the thermal reactor which is moderated, reflected and cooled by ordinary light water, usually fuelled with UO_2. Light water has three significant properties which establish specific characteristics for the reactors *(Antonopoulos, 2005)*:

- Light water is an excellent moderator, for the thermalization of fast neutrons of the fission, so a relatively small distance inside the water is required. Hence, a core of relatively small volume can be designed and built.
- The high neutron capture cross section of H_2O imposes the use of enriched instead of natural uranium. The enrichment of uranium was originally feasible in the USA and USSR and the cost was extremely high. Subsequently, the ratio H_2O and UO_2 should be small so as to minimize the neutron absorptions in water. In LWR, water serves as moderator and coolant simultaneously, since a separate coolant system is not practically achievable in terms of space.
- Ordinary water can be easily converted from the liquid to the gaseous phase, which imposes specific requirements and limitations to the design of the reactor and raises important safety issues.

Three main designs of LWR were constructed worldwide, the Pressurized Water Reactor (PWR) which was initially developed in the USA and the USSR for the propulsion of ships and naval vessels, the Boiling Water Reactors (BWR) that were proven to be feasible by the famous BORAX experiments carried out in the early 1950s and the predecessor of RBMK form Russia.

Fast Breeder Reactors

Before the end of World War II scientists had discovered the fundamental principles that underlie the concept of fast breeder reactors, and the potential impact of breeder reactors on future energy supplies was immediately recognized. The first experimental breeder reactor had Plutonium as fuel, was cooled by Mercury, operated at a power level of 25 kW and first went critical in 1946 in Los Alamos, New Mexico. The world's first nuclear-energy electricity was produced a few years later, in 1951 in EBR-I, which was a Liquid-Metal Cooled Fast Breeder Reactor (LMFBR) *(Lamarsh and Baratta, 2001)*.

The LMFBR operates on the uranium-plutonium fuel cycle, the fuel is a mixture of PuO_2 and UO_2, the coolant that has been chosen worldwide for the LMFBR is liquid sodium.

GENERATION II

Generation II nuclear power plants began operation in the late 1960s. These reactors are of commercial use and had been designed to be economical and reliable with a typical operational lifetime of 40 years. This class of reactors comprises of Advanced Gas-cooled Reactors (AGR), High-Temperature Gas-Cooled Reactors (HTGR), Pressurized Water Reactos (PWR), Boiling Water Reactors (BWR), CANada Deuterium Uranium reactors (CANDU), Steam Generating Heavy Water Reactors (SGHWR) and Fugen, Reactor Bolshoy Moshchnosty Kanalny (RBMK), Vodo-Vodyanoi Energetichesky Reactors (VVER) and fast breeder reactors.

Thermal Reactors

In Generation II thermal reactors, in addition to the existing three main categories of thermal reactors, a new type of reactors has been introduced, namely the Heavy-Water moderated and cooled Reactors (HWR).

Gas-cooled Reactors

Two types of reactors are graphite moderated and gas-cooled, i.e. the AGR and the HTGR developed in the United Kingdom and the United States respectively. AGR is the evolution of the MAGNOX reactor and the main goal for its development was to fully exploit the high temperature potentials of the graphite-CO_2 combination. The overall efficiency of such a power plant is about 40%, comparable to the most efficient fossil fuel plant available today. Reactors of this type are operating only in the United Kingdom and their contribution to the network is ~ 8.400 MW_e. The type of the experimental High-Temperature Gas-cooled Reactor was developed by a consortium of European countries and operated at the Winfrith Research Centre in England, while further spectacular steps in gas-cooled reactor technology were made by the General Atomic Company in USA. This is a graphite moderated, helium-cooled, thermal reactor. Helium as a coolant exhibits certain excellent properties, since it is far more inert than CO_2, so it does not react with neither the graphite nor the

fuel, and does not absorb neutrons, therefore it does not become radioactive *(Lamarsh and Baratta, 2001), (Leonidou, 2000).*

Heavy Water Reactors (HWR)

The heavy-water reactor programmes were started in many countries, i.e. France, Germany, Italy, Japan, Sweden, Switzerland, the United Kingdom, the United States of America, the former USSR and in Canada *(Lamarsh and Baratta, 2001), (Antonopoulos, 2005), (IAEA, Heavy Water Reactors, 2002), (Leonidou, 2000), (Fugen)*. Different streams were followed by each country during the evolution of the heavy water reactor concept: pressure tube heavy water cooled, pressure vessel heavy water cooled, pressure tube light water cooled, pressure tube gas cooled and a pressure tube organic cooled design. Nevertheless, only the heavy-water moderated and cooled version developed in Canada proceeded to the stage of commercial implementation, became one of the three competitive reactor types internationally and has been exported in many countries.

Heavy water has two significant properties which are of high importance in nuclear technology:

- low absorption cross section of deuterium for thermal neutrons. Therefore the use of natural uranium as fuel is feasible. As a result, neither the construction of costly uranium enrichment plants nor the dependence on nations which can provide enriched uranium for the fuel is required. Moreover, apart from the fuel and the coolant, pressure tubes can be utilized within the reactor core due to the achieved neutron economy.
- significantly lower neutron transport scattering length L_s in comparison to light water. Hence, the volume of the moderator is considerably bigger relatively to that of a LWR, allowing for the installation of extra components in the reactor core. In addition, if the fuel tubes were immersed in a D_2O-filled pressure vessel, it would have quite large dimensions. As a consequence, all the HWR designs utilize the pressure tube concept, i.e. the fuel is contained in a pressure tube in which the coolant flows *(Lamarsh and Baratta, 2001), (Leonidou, 2000).*

The main representatives of HWR are the CANada Deuterium Uranium (CANDU) design with the unique characteristic of being refuelled online, while in

operation, the Steam Generating Heavy Water Reactor (SGHWR) which is quite similar with the CANDU design and was first constructed in the United Kingdom and finally the Fugen Advanced Test Reactor (ATR) from Japan.

Light Water Graphite Reactors

This category of power nuclear reactors consists of only one design, the Russian Reaktor Bolshoy Moshchnosty Kanalny *(Lamarsh and Baratta, 2001)*, *(RBMK)*. The combination of graphite moderator and pressurised water coolant is found in no other power reactors in the world and this type of reactor was involved in the Chernobyl accident in 1986.

Vodo-Vodyanoi Energetichesky Reactor (VVER)

The VVER reactors is a series of pressurized water reactor designs originally developed in the Soviet Union and were put in operation in the 1970s, by OKB Gildopress which is a subsidiary of the state atomic energy corporation, Rosatom. The basic design of a VVER reactor resembles a Western PWR *(Lamarsh and Baratta, 2001)*.

GENERATION III

A reactor of Generation III is a development of any of the Generation II nuclear reactor designs that incorporate evolutionary improvements in terms of fuel technology, superior thermal efficiency, passive safety systems, and standardized design for reduced maintenance and capital cost. In addition, many of the third-generation reactors are larger in comparison to their predecessors, while most of them are designed for load following. The first third-generation reactors are in operation in Japan while others are under construction or ready to be ordered. The demands of such a cause impose increasingly international collaborations although the certification of designs -based on safety requirements- is yet on a national basis. Reactors of Generation III *(Advanced Nuclear Power Reactors)* exhibit the following features:

- a standardised design for each type to expedite licensing, reduce capital cost and reduce construction time,
- a simpler and more rugged design, making them easier to operate and less vulnerable to operational upsets,

- higher availability and longer operating life - typically 60 years,
- further reduced possibility of core melt accidents,
- substantial grace period, so that following shutdown the plant requires no active intervention for (typically) 72 hours,
- resistance to serious damage that would allow radiological release from an aircraft impact,
- higher burn-up to use fuel more fully and efficiently and reduce the amount of waste,
- greater use of burnable absorbers ("poisons") to extend fuel life.

Thermal Reactors

Light Water Reactors (LWR)

Advanced designs of reactors have been proposed for both Pressurized and Boiling Water Reactors while many of them have received certification from many of the leading countries in nuclear technology, such as France, United Kingdom, Japan and United States of America. In this review, only the designs that have already received Design Certification or an interim design acceptance confirmation along with interim statements on design acceptability have been issued, will be discussed.

i. Pressurized Water Reactors

As far as PWRs are concerned, the main advanced designs that have been proposed are the following:

AP600

The Westinghouse Advanced Passive PWR AP-600 is a 600 MW_e pressurized water reactor (PWR) with advanced passive safety systems and extensive plant simplifications to enhance the construction, operation, and maintenance of the plant. The plant design utilizes proven technology which builds on approximately 40 years of operating PWR experience *(Advanced Passive Pressurized Water Reactor, IAEA, 2011).*

ACPR-1000$^+$

ACPR1000$^+$ is a 1,150 MW_e advanced nuclear power reactor developed by China Guangdong Nuclear Power Holding Co. (CGNPC). Its main performances meet the technical standards of the third generation technology and the multiple requirements of users in China and abroad *(ACPR).*

VVER-1000/V392

Gildopress late model VVER-1000/V392 of net power output is 999.5 MW_e, is the evolution of the Soviet-type pressurized light water reactor series VVER-440 with enhanced safety. Units of VVER-1000 are being built in India and China while another one will be built in Belene, Bulgaria (*VVER-1000).*

VBER-300

The VBER-300 reactor plant (RP) is a medium-size power source for ground-based nuclear power plants and nuclear cogeneration plants, as well as for floating nuclear power plants (FNPPs) and desalination complexes and is a result of the evolution of modular marine propulsion reactors. The design is being developed using the experience of VVER-type reactors operation. The priority was given to ensuring reliability and safety of the reactor core and entire reactor plant and achieving high economic indicators of the fuel cycle. Possible applications are electricity generation, cogeneration of electricity and heat for district heating, seawater desalination *(VBER-300, IAEA, 2011), (Official Site VBER-300*).

ii. Boiling Water Reactors

The main Generation III designs of BWRs are mentioned below.

Advanced Boiling Water Reactors (ABWR)

The ABWR is the world's first – and only – Generation III reactor that is in operation today, with over 15 years safe and successful operating experience in the first unit. The development of the ABWR started in 1978 as an international co-operation between five BWR vendors: General Electric of the USA, Hitachi and Toshiba of Japan, and European BWR vendors. An advanced engineering team, that comprised personnel from all five companies, developed a conceptual design of an improved BWR derived from a General Electric one, with nominal 1,300MW_e power.

Four ABWR plants are in commercial operation in Japan while two other are under construction in Japan and in Taiwan. Four more are planned in Japan and another two in the USA. The various companies quote several versions of this design with net electrical power ranging from 600 MW_e to 1,600 MW_e and a design life of 60 years *(Hitachi ABWR, 2007).*

Heavy Water Reactors (HWR)

Enhanced CANDU-6 (EC6)

The Enhanced CANDU-6 (EC6) is a Generation III, 700 MW_e class heavy-water moderated and cooled pressure tube reactor designed by Candu Energy Inc.. While retaining the basic features of the CANDU 6 design, the EC6 reactor incorporates innovative features and state-of- the-art technologies that enhance safety, operation and performance. In June 2013, the EC6 completed its third and final pre-licensing review by the Canadian Nuclear Safety Commission (CNSC) *(Enhanced CANDU 6, 2012).*

Advanced Heavy Water Reactor (AHWR)

The Advanced Heavy Water Reactor is a 300 MW_e design being developed in India as the third stage in its plan to utilize thorium to fuel its overall nuclear power program, since Indian resources of thorium are larger than those of uranium. It is designed and developed to achieve large-scale use of thorium for the generation of commercial nuclear power. This reactor will produce most of its power from thorium, with no external input of ^{233}U, in the equilibrium cycle. The reactor incorporates a number of passive safety features and is associated with a fuel cycle having reduced environmental impact *(Advanced Heavy Water Reactor, 2013).*

GENERATION III+

Generation III+ reactor designs are an evolutionary development of Generation III reactors, offering significant improvements in safety over the latter, while increased net electrical power output is also realised. International collaborations have been formed in order to meet the high-level challenges, in economic and scientific terms, of building reactors of this generation.

Light Water Reactors (LWR)

Generation III+ designs of both PWRs and BWRs have been proposed, based on earlier designs with increased power output and safety standards in compliance with EU and NRC standards.

i. Pressurized Water Reactors

EPR™

The European Pressurized Water Reactor (EPR™) of approximately 1,600 MW_e net electrical production capacity is an evolution to Generation III+ based on the proven technologies of the Konvoi (Siemens) and N4 (AREVA) reactors *(AREVA, EPRTM Reactor), (IAEA, 2004)*. The EPR™ is the designation for a development effort by Nuclear Power International and its parent companies, Framatome and Siemens, whereas the nuclear part of both companies have merged in the meantime into a joint company called Framatome ANP (*A*dvanced *N*uclear *P*ower) as an entity in the Areva group. The project was performed in cooperation with Electricité de France and German Utilities. It is the first generation III+ reactor to be deployed on an international scale, being built in three different countries, i.e. in Finland (Olkiluoto), in France (Flamanville) and in China (2 units in Taishan), and is currently undergoing certification in the United States and the United Kingdom**.**

The reactor pressure vessel (RPV) is designed for a lifetime of 60 years, not exceeding a total neutron fluence of 10^{19} n/cm^2. EPR™ reactor's high thermal efficiency ~37%, is achieved by the incorporation of an innovative design for the steam generators. It is optimised to meet the higher safety requirements of the new generation of nuclear power plants. The design approach integrates past experience to guarantee safety objectives through full diversity and redundancy of proven technologies so as to avoid common cause failure and overcome single failures. Last but not least, an optimized combination of active and passive systems leverages complementary solutions to provide comprehensive safety barriers while adoption of a double concrete containment design was also decided.

ATMEA1™

ATMEA™ is the joint venture created in July 2007 between AREVA NP (AREVA) and Mitsubishi Heavy Industries, Ltd (MHI). The purpose of the Joint

Venture is to design, market and sell worldwide, a 1,100 MW_e class evolutionary PWR that encompasses innovative and proven nuclear technologies from AREVA and MHI, including top-level safety systems, high-thermal efficiency, and a flexible 12- to 24-month operational cycle, leading to less waste and minimized impact to the environment. The primary system design, loop configuration, and main components are similar to those of currently operating PWRs, thus forming a proven foundation for the design *(AREVA & MHI ATMEA, 2011), (IAEA, ATMEA, 2011).*

Advanced Pressurized Reactor 1400 (APR1400)

The Advanced Power Reactor 1,400 MW_e (APR1400) is a standard evolutionary advanced light water reactor (ALWR) in the Republic of Korea developed in 2002 and the first, Shin-Kori-3 & 4, is being constructed. The design is based on the experience that has been accumulated through the development, construction, and operation of OPR1000, the Optimum Power Reactor 1,000MW_e, the first standard pressurized water reactor (PWR) plant in Korea. APR1400 also utilizes state-of-the-art proven technology and incorporates a number of advanced design features to meet the utility's needs for enhanced economic goals and to address the new licensing safety issues and requirements for an improved plant safety *(APR1400, IAEA, 2011).*

Advanced Pressurized Water Reactor (APWR)

The Advanced PWR (APWR) has been developed, as a nuclear power plant for future use in Japan, as a joint international cooperative development project by seven companies comprising the five PWR electric power companies (Hokkaido, Kansai, Shikoku, Kyushu Electric Power Company, and Japan Atomic Power Company) and Mitsubishi Heavy Industries (MHI) and Westinghouse. The standard APWR is going through the licensing process in Japan and two are being constructed at the Tsuruga plant.

The APWR is in the largest capacity class of LWRs in Japan, i.e. 1,538 MW_e gross and 4,451 MW_t, it is a 4-loop design and it has adopted high performance steam generators and low pressure turbines. Various improvements have been incorporated in the reactor core so that operation with long fuel cycles is possible using low enriched fuel in order to reduce uranium requirements, and to provide increased

flexibility for various application such as the use of plutonium fuel with 1/3 or more MOX cores and high burn-up fuels *(IAEA, Technical Document, 2004)*.

AP1000

The Westinghouse Advanced Passive PWR AP1000 is a 1,117 MW_e PWR based closely on the AP600 design. The AP1000 maintains the AP600 design configuration, use of proven components and licensing basis by limiting the changes to the AP600 design to as few as possible. The AP1000 design includes advanced passive safety systems and extensive plant simplifications to enhance the safety, construction, operation, and maintenance of the plant. The AP1000 is designed to meet U.S. NRC deterministic safety criteria and probabilistic risk criteria with large margins. Safety analysis has been completed and documented in the Design Control Document (DCD) and Probabilistic Risk Analysis (PRA). A AP1000 unit is being built in China and the Vogtle site is being prepared for initials units in USA *(IAEA, Technical Document, 2004)*.

ii. Boiling Water Reactors

Economic and Simplified Boiling Water Reactors (ESBWR)

GE Hitachi Nuclear Energy's Economic Simplified Boiling Water Reactor (ESBWR) is an advanced 1520 MW_e power plant design, based on the earlier 670 MW_e Simplified Boiling Water Reactor (SBWR) and the more recent ABWR *(Hitachi ESBWR Plant, 2011)*. The design certification application for the ESBWR was submitted to the U.S. Nuclear Regulatory Commission in 2005 and is nearing completion of its technical review. The Safety Evaluation Report was issued in March 2011.

Heavy Water Reactors (HWR)

Advanced CANDU Reactors (ACR)

The Advanced CANDU Reactor®-1000 (ACR-1000®) design is Atomic Energy of Canada Limited's (AECL®) evolutionary, Gen III+, 1,200 MW_e class pressure tube reactor *(ACR1000, IAEA, 2011)*. The designer's objectives have been to meet the industry and public expectations for safe, reliable, environmentally friendly, low-cost nuclear power generation. It has been designed to be licensable

internationally by ensuring its compliance with Canadian nuclear regulations and the fundamental safety objectives of the IAEA's safety standards.

The ACR-1000 design retains many essential features of the CANDU plant design, including horizontal fuel channel core, a low temperature heavy-water moderator, a water filled reactor vault, two independent safety shutdown systems, a highly automated control system, on-power fuelling and a reactor building that is accessible for on-power maintenance and testing. Nevertheless, the following key differences from the traditional CANDU design are incorporated into the design of the ACR-1000:

- the use of LEU fuel contained in CANFLEX-ACR® fuel bundles,
- the use of light water instead of heavy water as the reactor coolant,
- lower moderator volume to fuel ratio.

GENERATION IV

The development of GEN IV technologies is coordinated by Generation IV International Forum (GIF), an international organization founded in 2001. Generation IV nuclear power aim to become, in many countries, an important source of base load power in the middle - long term (2030-2050). Nowadays there are many designs of these nuclear power plants are under study but various only few of them will be deployed. The most dominant designs are: a) Very High Temperature Reactors (VHTRs), b) Sodium Fast Reactors (SFRs), c) Super-Critical Water Cooled Reactors, d) Gas Cooled Fast Reactors, e) Lead Cooled Fast Reactors and f) Molten Salt Reactors.

REFERENCES

J. R. Lamarsh, A. J. Baratta, Introduction to Nuclear Engineering, Prentice Hall, New Jersey, (2001).

M. Antonopoulos-Ntomis, Introduction to Nuclear Technology, Ziti, Thessaloniki, (2005).

D. Leonidou, Introduction to Nuclear Technology, NTUA Publications, Athens, (2000).

Breeder Reactor: http://www.inl.gov/research/experimental-breeder-reactor-1/

Euratom http://ec.europa.eu/research/energy/euratom/index_en.cfm?pg=fission&section=generation

S.E. Jensen, E. Nonbol, Description of the Magnox Type Gas Cooled Reactor (MAGNOX), Rise National Laboratory, Roskllde, Denmark, (1999).

IAEA, Heavy Water Reactors: Status and Projected Development, Technical Report Series no. 407, Vienna, (2002).

Fugen http://133.188.30.70/04/fugen/compilation/pamphlet/English/P6.html

RBMKhttp://www.world-nuclear.org/info/Nuclear-Fuel-Cycle/Power-Reactors/Appendices/RBMK-Reactors/#.UgUPvJynGjY

Nikolay Tikhonov, WWER-1000 Reactor Simulator, Milano, (2011).

Advanced Nuclear Power Reactors http://www.world-nuclear.org/info/Nuclear-Fuel-Cycle/Power-Reactors/Advanced-Nuclear-Power-Reactors/#.UgoqCJynGjY

IAEA, Advanced Passive Pressurized Water Reactor, Status Report no. 75, (2011).

ACPR http://www.cgnpc.com.cn/n1500/n1529/n1534/index.html

IAEA, VVER-1000 (V-466B), Status Report no. 93, (2011).

IAEA, VBER-300, Status Report no. 66, (2011).

Official Site VBER-300 http://www.okbm.nnov.ru/english/regional

Hitachi, The Hitachi ABWR plant general description, (2007).

Candu Energy Inc., Enhanced CANDU 6, Technical Summary, Ontario, (2012).

Bhabha Atomic Research Centre, Advanced Heavy Water Reactor, Overview, Mumbai, (2013).

AREVA, EPR™ Reactor, Presentation, Paris.

IAEA, Status of Advanced Light Water Reactor Designs, Technical Document no. 1391, (2004).

IAEA, ATMEA1™, Status Report no. 99, (2011).

AREVA&MHI, The AREVA & MHI ATMEA1™ Reactor: a mid-sized Generation III+ PWR, Presentation, Vienna, (2011).

IAEA, Advanced Power Reactor 1,400 MW_e (APR1400), Status Report no. 83, (2011).

Hitachi Nuclear Energy, The Hitachi ESBWR Plant General Description, General Description Book, (2011).

IAEA, Advanced CANDU Reactor 1000 (ACR1000), Status Report no. 69, (2011).

APPENDIX II

ACCELERATOR DRIVEN SYSTEMS (ADS)

Introduction

The long-term hazard of radioactive wastes arising from nuclear energy production is a matter of continued discussion and public concern in many countries. By the use of partitioning and transmutation (P&T) of the actinides and some of the long-lived fission products, the radiotoxicity of the high-level waste (HLW) and, possibly, the safety requirements for its geologic disposal can be reduced compared with the current once-through fuel cycle. To make the technologically complex enterprise worthwhile, a reduction in the HLW radiotoxicity by a factor of at least one hundred is desirable. This requires very effective reactor and fuel cycle strategies, including fast reactors (FRs) and/or accelerator-driven, subcritical systems *(OECD-NEA Report, 2002).*

Accelerator Driven Systems (ADSs) first conceived and analyzed in 1990s *(Bowman et al., 1992; Rubbia et al., 1995; Bacha et al., 1995), (Catsaros et al., 2013)* have recently been receiving increased attention due to their potential to improve the flexibility and safety characteristics of transmutation systems. In ADSs fissions are stimulated by a neutron source, which is obtained by spallation of target nuclei, producing a high number of neutrons under proton collisions. This reactor is designed to safely transmute the waste into stable elements or those whose radioactivity is relatively short lived, while producing useful power. Although nuclear reactors' safety is a large subject considering several initiating events, ADS is considered inherently safe because it remains sub-critical throughout its life and the nuclear reaction ceases when the outside source stops feeding neutrons. ADSs have not yet been integrated into future nuclear reactors, mainly due to concerns about the window separating the protons from the spallation target, which is expected to be exposed to stress under extreme conditions.

Production of fissile material during nuclear reactors operation provides a motivation for exploiting the potential energy content existing in the spent fuel, making thus breeding capabilities of a nuclear reactor to be of high interest. In more recent decades renewed interest has been expressed for breeders since, compared to conventional light-water reactors they would consume less natural uranium (less than 3%) and generate less waste for equal amounts of energy produced by converting

non-fissile isotopes of uranium into nuclear fuel (Pyroprocessing Technologies; Supply of Uranium). Commonly used Light Water Reactors have a conversion ratio (average number of fissile atoms created per fission event) of approximately 0.6 while Pressurized Heavy Water Reactors (PHWRs) fueled by natural uranium have a conversion ratio of 0.8 *(Kadak, 2012)*. PWRs can recycle self-generated plutonium for reuse as reactor fuel, but their breeding capabilities appear rather limited *(Stacey, 2001)*. Reactors optimized for fuel breeding (customarily referred to as true breeders) are designed to have a conversion ratio higher than one, while "breakeven" occurs when the conversion ratio becomes equal to 1 and the reactor produces exactly as much fissile material as it uses. It is mentioned that breeding and closed fuel cycles are usually achieved based on sodium-cooled fast reactors, since in conventional PWRs neutron parasitic absorption and leak prevent breeding *(Bussac and Reuss, 1985)*, while breeder reactors may face sodium/air or sodium/water interaction problems, since sodium ignites spontaneously in air and reacts explosively with water.

The ADS Concept

The concept of accelerator-driven systems (frequently called hybrid systems) combines a particle accelerator with a sub-critical reactor core (see *Figure II.1*). Most proposals assume proton accelerators, delivering continuous-wave beams with an energy around 1 GeV. The accelerator is either a linear accelerator (linac) or a circular accelerator (cyclotron). High-power accelerators have been under continuous development, and the construction of machines with the required specifications, i.e. electrical efficiencies in the vicinity of 50% and beam powers up to 10 MW for cyclotrons and up to 100 MW for linacs, now appears to be feasible.

The protons are injected onto a spallation target to produce source neutrons for driving the subcritical core. The target is made of heavy metal in solid or liquid state. Spallation reactions in the target emit a few tens of neutrons per incident proton, which are introduced into the sub-critical core to induce further nuclear reactions. Except for the sub-critical state, the core is very similar to that of a critical reactor. It can be designed to operate either with a thermal or fast neutron spectrum.

The energy conversion part of an accelerator-driven nuclear power system is similar to that of a normal power plant. However, in the accelerator-driven system, the electrical energy which is recycled to the accelerator reduces the net electrical

efficiency of the system. For an ADS with a neutron multiplication factor of 0.95, the reduction amounts to about 12%. This means that the accelerator driven system produces about 14% more high-level waste and rejects about 20% more heat to the atmosphere than a normal power plant with the same net electrical output.

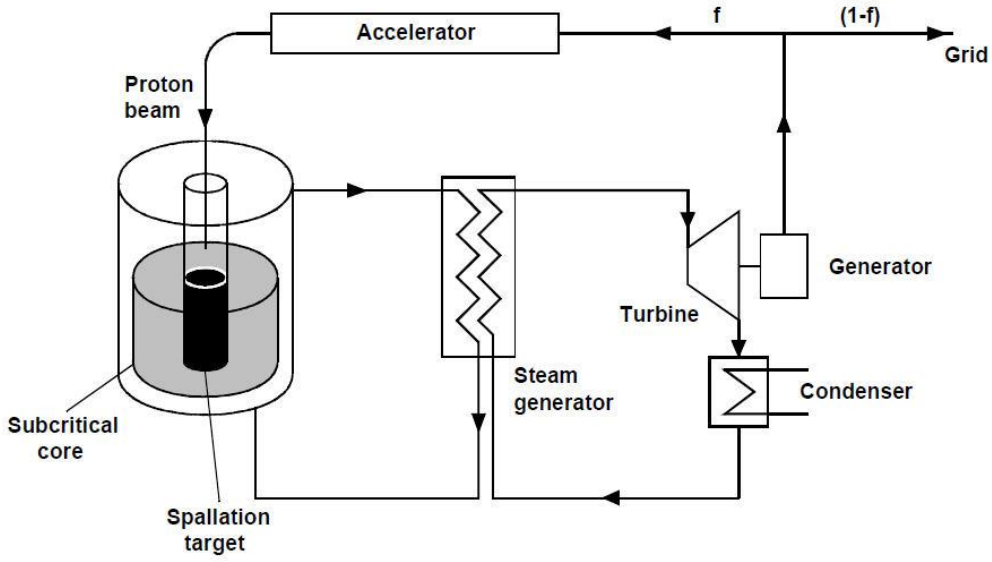

Figure II.1*:* Concept of an accelerator-driven system.

The principal advantages and disadvantages of accelerator-driven systems as compared with the corresponding critical reactor systems are summarized in *Table II.1*. The comparison applies not only to transmutation applications but also to other applications such as the breeding of fissile material (electro-breeding), the development of the thorium-233U fuel cycle, and the development of ultra-safe energy producers. For instance, the potential for improving the neutron economy, which is related to the neutron abundance of the spallation process, is more relevant for breeding than for transmutation applications.

In the context of transmutation, the principal non safety-related advantage of the ADS is the increased core design and fuel management flexibility resulting from the removal of the criticality condition. However, this advantage has to be weighted against several technical and operational disadvantages. For example, the benefit from lengthening the reactor cycle has to be balanced against the investment in the more powerful accelerator required for coping with the lower end-of-cycle neutron multiplication factor.

Important design and material problems arise from the installation of a target in the centre of a reactor: the interfacing of an accelerator with a reactor rises containment questions, and the target and surrounding structure materials are subjected to complex degradation phenomena due to combined thermo-mechanical loads, high-energy particle irradiation and, in contact with liquid heavy metals, corrosion effects which are much more severe than those encountered in normal reactors. This applies particularly to the beam window which may, therefore, require frequent replacement.

High-power accelerators will have to be improved with respect to the beam losses which cause radiation damage and activation in the accelerator components and the frequency of beam trips. In an ADS, beam trips cause similar temperature and mechanical stress transients as fast control rod insertions (scrams) in critical reactors. Current accelerators feature beam trip frequencies which lie orders of magnitude above the current criteria for such transients.

Regarding safety aspects, the prominent feature of the ADS is its reduced potential for reactivity induced accidents. This is particularly relevant for actinide burners which suffer from a general degradation of the safety parameters of the core. From the viewpoint of transmutation, a general conclusion from *Table II.1* is that an ADS has interesting design and safety advantages, but that these must be weighted against non-trivial technical and operational disadvantages which will also have economic consequences *(OECD-NEA Report, 2002)*.

Discussion on the Basic ADS Components

Only a few Accelerator Driven Subcritical reactors have been designed to some degree of details. These are, essentially, those described by *(Rubbia et al., 1995)* by *(Bowman, 1998)* and by *(Furukawa, 1982)*. However, significant and growing efforts are going on in the USA, Japan, Western Europe and Russia. These efforts aim at exploring the rather large space of possible ADSR concepts and designs. Choices have to be made concerning:

1. The type of neutron spectrum: fast or thermal.
2. The type of fuel: solid (metallic, oxides, nitrides, carbides, etc.) or liquid (fluorides, chlorides).
3. The type of spallation target: lead, lead-bismuth, tungsten, molten salt, etc.

4. The nature of the cooling agent: gas, molten metal, molten salt.

5. The accelerator system: cyclotrons or LINACs.

The difficulty to find an optimum design can be illustrated by a short discussion of each of these parts (*Nifenecker* et al., 2001).

Table II.1: Comparison of accelerator-driven sub-critical and critical reactor systems.

	Advantages of accelerator-driven systems	**Disadvantages of accelerator-driven systems**
Design and operation	♦ The possibility to operate a reactor core at a *neutron multiplication factor below 1* opens opportunities for new reactor concepts, including concepts which are otherwise ruled out by an insufficient neutron economy ♦ In particular, this allows transmuters to be designed as pure Trans-Uranium (TRU) or Minor Actinides (MA) burners and hence the fraction of specialized transmuters in the reactor park to be minimized ♦ The proportionality of the reactor power to the accelerator current greatly simplifies the reactor control	*Accelerator:* Very high reliability required to protect structures from thermal shocks ♦ *Beam window and target* subjected to unusual stress, corrosion and irradiation conditions ♦ *Sub-critical core:* Increased power peaking effects due to external neutron source ♦ Compromises between neutron multiplication factor and accelerator power required ♦ Increased overall complexity of the plant ♦ Reduction in net plant electrical efficiency due to power consumption of accelerator
Safety	♦ The reactivity margin to prompt criticality can be increased by an extra margin which does *not depend on the delayed neutrons* ♦ This enables the safe operation of cores with degraded characteristics as they are typical e.g. for pure MA burners ♦ *Excess reactivity can be eliminated*, allowing the design of cores with a reduced potential for reactivity-induced accidents	♦ New types of reactivity and source transients have to be dealt with (external neutron source can vary rapidly and reactivity feedbacks in TRU- and MA-dominated cores are weak)

a) The Neutron Spectrum

Thermal neutron reaction cross-sections are, generally, much higher than those for fast neutrons. This gives the potential of higher incineration rates with thermal spectra, as stressed by Bowman *(Bowman, 1998)*. However, this is only true for fissile mixtures, like plutonium, but not in the case of non-thermally fissile ones like Minor Actinides (*Nifenecker* et al., 2001). In this case fast neutron spectra allow easier incineration due to their larger fission cross-sections.

The protactinium effect, which limits the achievable values of k_∞, is less severe for fast spectra. In general, reactor control is easier with fast spectra especially for the thorium based cycle. For solid fuels the variations of k_∞ are less severe for fast than for thermal spectra due to smaller capture cross-sections of fission products. However, the inventory of ^{233}U is much larger in fast reactors (about 7 times), with the associated larger breeding times and inventory radiotoxicity.

b) The Fuel

Solid fuels, especially oxides, have the advantage to be very well known and documented. A large experience with their reprocessing is available, mostly with wet processes, but also with pyro-chemistry. Due to progressive poisoning by fission products, the neutronics of solid fuels are not optimized. On the other hand, liquid fuels like molten salts allow a continuous monitoring and optimization of the neutronics. However, in spite of the very successful Molten Salt Reactor Experiment *(Bettis and Robertson, 1970)* at Oak Ridge, the reliability and safety of the on-line processing of the salt for large reactors has to be demonstrated. Similarly, although the MSRE has shown that hastalloy-n had good properties against corrosion by the salt, this has to be verified also for the very high irradiation doses expected with ADSRs. Fluorides are less corrosive than chlorides and appear to be the choice fuel. Their small atomic weight slows down neutrons and may be incompatible with fast spectra. However, a recent study concludes to the feasibility of a fast reactor with fluoride fuel (*Nifenecker* et al., 2001).

The modern tendency to consider metallic fuels as the most promising when associated to pyrochemistry reprocessing involves a fluorization step. It would, then, be tempting to stop the process at this stage and use molten fluoride fuels.

Notwithstanding these technological challenges, molten salt fuels appear as very promising option for a new generation of nuclear reactors, either critical or subcritical.

c) The Spallation Target

Due to their higher neutron yields only heavy targets are considered practical. Lead *(Rubbia et al., 1995*, or more often, lead-bismuth *(ANL-99/16, 1999)*, are proposed as liquid targets. Lead has a rather high fusion temperature of 327ºC and it might be difficult and costly to keep it in a fused state at all times. Lead-bismuth has a fusion temperature of only 123.5°C, bismuth leads to ample production of the very radiotoxic and volatile ^{210}Po. It is also produced, but at a very much lower rate, by lead. However, since it is possible for the lead-bismuth target to work at much lower temperature than pure lead the evaporation rates of ^{210}Po can be similar in both cases. Both lead and lead-bismuth corrode metals, the more so at higher temperatures. In this respect the lower working temperature of lead-bismuth is a further advantage.
Tungsten has been chosen as a solid target in several projects *(Van Tuyle et al., 1993, Takizuka et al., 1989; Mizumoto et al., 1992)*. Very high energy depositions by the proton beam have to be disposed off. This is done with molten metal coolants, either sodium, lead or lead-bismuth. Sodium leads to the well-known safety problems related to the high chemical reactivity of sodium. Lead and lead-bismuth lead to the same solidification and corrosion problems as in the case of all liquid targets. Furthermore, the possibility of embrittlement of tungsten has to be considered.

Finally, building upon the Soviet experience with lead-bismuth cooling of the reactors of nuclear submarines, lead-bismuth spallation targets seem to be especially attractive.

d) The Cooling Agent

Gas cooling

Some recent designs of ADSs *(Ridikas and Mittig, 1998)* are inspired by High Temperature Gas Reactors. Such HTGR have some very appealing features:

- The high temperatures allow very high thermodynamical efficiencies with the possible implementation of combined cycles.

- For not too big reactors, radiation cooling is able to prevent fusion of the very refractory fuel (uranium or thorium carbides).
- Very high burn-ups of the rugged fuel could be obtained.

However, some limitations do exist: possible difficulties for a reliable fuel fabrication, difficulties for reprocessing the refractory and chemically inert fuel, low power densities due to the small thermal capacity of the gas, significant probability for a loss of coolant accident.

Present experience of HTGR fuels is with carbides. The large quantity of carbon in the reactor leads, naturally, to thermal reactors and would limit the possibility of HTGR for minor actinides incineration. For that matter Framatome (the French reactor building company) is studying a new type of fuel based on Nickel alloys which might allow fast neutron spectra. However, it is not clear that such new fuels would allow one to reach as high temperatures as carbides would.

Lead Cooling

The Energy Amplifier proposed by Rubbia et al. makes an extensive use of molten lead both as spallation target and as cooling agent. The beam tube as well as the fuel elements lie in a swimming pool of 10 000 tons of molten lead. The design offers many advantages like convective cooling, passive safety and apparent simplicity. The simple design may help in keeping the lead molten and controlling the corrosion, although this remains a difficult challenge. One of the most delicate points of the design is the long beam tube which might be difficult to position and change. Furthermore, due to the high irradiation damages by the proton beam, this tube will have to be changed rather frequently. Finally, long-lived radiotoxic spallation products of lead like ^{194}Hg would be diffused in the whole 10 000 tons of lead and might cause serious decommissioning problems.

Lead–bismuth Cooling

Because of the high melting temperature of lead it has been proposed to use eutectic lead-bismuth as coolant *(ANL-99/16, 1999)*. However, due to the high working temperature of the coolant necessary to obtain a good thermodynamical efficiency, the ^{210}Po evaporation may become a severe problem. The cost of bismuth is much higher than that of lead, and it is not clear that the bismuth reserves will be abundant enough to provide a large pool of reactors with the required quantities.

Molten Salt Cooling

Molten salt fuels are used simultaneously as coolant, with the possible problems of contamination of the secondary coolant loop. Even with solid fuels molten salts might be considered as an interesting option for cooling, provided corrosion can be managed. One of the advantages of molten salts over molten metals is that they are transparent to visible light, and thus allow visual inspections.

e) The Accelerator

For acceleration either cyclotrons *(Rubbia et al., 1995)* or LINACs *(Furukawa, 1982; Bowman et al., 1992; ANL-99/16, 1999)* are considered. Record intensities of more than 1 mA have been obtained for both types of accelerators at PSI for a cyclotron, and at Los Alamos Meson Physics Facility **(**LAMPF) for a LINAC. Cyclotrons are more compact and thus require less space and are more economical. Due to the continuous nature of the beam structure and the compactness of the cyclotron center, it appears that the space charges and HF loadings obtained at PSI are already close to the limits. It seems difficult for cyclotrons to provide beam intensities larger than 5-10 mA. In the LINAC case, mA beam intensities have been obtained at LAMPF with 1% duty cycle. Space charge and instantaneous HF power are no limitations for reaching much higher beam intensities. Intensities in the 100 mA range are considered to be feasible. Since intensities between 5 and 10 mA are required for most ADSs projects, LINACs are usually preferred. However, if k_s (source multiplication factor) values larger than 0.99 together with $k_{eff} < 0.98$ could be demonstrated, cyclotrons might become a good possibility again.

REFERENCES

A Roadmap for developing ATW Technology. ANL-99/16, (1999).

Accelerator-driven Systems (ADS) and Fast Reactors (FR) in Advanced Nuclear Fuel Cycles, OECD-NEA Report, (2002).

Bacha, F., Maillard, J., Vergnes, J., " Utilisation du code GEANT pour l'étude d'un réacteur de type hybride (Présentation et qualification du code)". LPC-95-27. Collége de France, Laboratoire de Physique Corpusculaire, IN2P3-CNRS, (1995).

Bettis E.S., Robertson R.C., Nucl. Appl. Technol. 8, p. 190, (1970).

Bowman C.D. et al., Nucl. Instr. and Meth. A 320, p. 336, (1992).

Bussac, J., Reuss, P., " Traité de neutronique ", Hermann, Paris, (1985).

Catsaros N., Gaveau B. , Jaekel M.-T., Jejcic A., Maillard J., Maurel G., Savva P., Silva J., Varvayanni M., Xenofontos T., "Investigating the Breeding Capabilities of Hybrid Soliton Reactors". Nucl. Eng. & Design, 261, p. 251-259, (2013).

Furukawa K. et al., "The combined system of accelerator molten salt breeder (AMSB) and molten salt converter reactor (MSCR)", Japan‑US Seminar on Thorium Fuel Reactors, (1982).

Kadak, Prof. Andrew C. "Lecture 4, Fuel Depletion & Related Effects", Operational Reactor Safety 22.091/22.903, Hemisphere, as referenced by MIT. p. Table 6–1, "Average Conversion or Breeding Ratios for Reference Reactor Systems". http://www.learningace.com/doc/3103775/a22b70ccd4d6c2b95d5cc687c2e09c06/mit22 091s08 lec04 (retrieved 24.12.12).

Mizumoto M. et al., "High intensity proton accelerator for nuclear waste transmutation", 16th International Linear Accelerator Conference LINAC-92, Ottawa, (1992).

Nifenecker H., David S, Loiseaux J.M., Meplan O., "Basics of accelerator driven subcritical reactors", Nuclear Instruments and Methods in Physics Research A 463, p. 428‑467, (2001).

Ridikas D., Mittig W., Nucl. Instr. and Meth. A 418, p. 449, (1998).

Rubbia C. et al., Report CERN=AT=95‑44 (ET), (1995).

Stacey, W.M., "Nuclear Reactor Physics", John Wiley & Sons Inc., New York, (2001).

Takizuka T. et al., “A study of Incineration Target System”, Proceedings of the Fifth International Conference on Emerging Nuclear Systems, Karlsruhe, (1989).

Van Tuyle G.J. et al., Nucl. Technol. 101, p. 1, (1993).

APPENDIX III

Table 1: Chart of nuclides with Z = 35 up to Z = 40. Microscopic cross-sections for thermal neutron capture are indicated as well as half-lives of radioactive decay.

Table 2: Chart of nuclides with Z = 41 up to Z = 46. Microscopic cross-sections for thermal neutron capture are indicated as well as half-lives of radioactive decay.

Table 3: Chart of nuclides with Z = 47 up to Z = 49. Microscopic cross-sections for thermal neutron capture are indicated as well as half-lives of radioactive decay.

Table 4: Chart of nuclides with Z = 52 up to Z = 57. Microscopic cross-sections for thermal neutron capture are indicated as well as half-lives of radioactive decay.

Table 5: Chart of nuclides with Z = 58 up to Z = 63. Microscopic cross-sections for thermal neutron capture are indicated as well as half-lives of radioactive decay.

Table 6: Chart of nuclides with Z = 62 up to Z = 64. Microscopic cross-sections for thermal neutron capture are indicated as well as half-lives of radioactive decay.

Table 7: Chart of nuclides with Z = 90 up to Z = 96. Microscopic cross-sections for thermal neutron capture are indicated as well as half-lives of radioactive decay.

Z \ A	85		86		87		88		89		90		91		92		93		94		95		96		97
35	^{85}Br **1.304%**	Direct Fission Product (DFP) Cumulative Yield																							
	β⁻ ↓ **$T_{1/2}$ = 2.9m**																								
36	^{85}Kr																								
	β⁻ ↓ $T_{1/2}$ = 10.8y																								
37	^{85}Rb	σ_γ=0.48b →	^{86}Rb	σ_γ=1.56b →	^{87}Rb	σ_γ=0.12b →	^{88}Rb	σ_γ=1.00b →	^{89}Rb																
	stable		β⁻ ↓ $T_{1/2}$ = 18.6d		~ stable		**β⁻ ↓** **$T_{1/2}$ = 17.8m**		**β⁻ ↓** **$T_{1/2}$ = 15.2m**																
38			^{86}Sr	σ_γ=1.04b →	^{87}Sr	σ_γ=16.00b →	^{88}Sr	σ_γ=0.006b →	^{89}Sr	σ_γ=0.42b →	^{90}Sr **5.730%**														
			stable		stable		stable		β⁻ ↓ $T_{1/2}$ = 50.5d		β⁻ ↓ $T_{1/2}$ = 28.9y														
39									^{89}Y	σ_γ=1.28b →	^{90}Y*	σ_γ=3.30b →	^{91}Y	σ_γ=1.40b →	^{92}Y										
									stable		β⁻ ↓ $T_{1/2}$ = 64.0h		β⁻ ↓ $T_{1/2}$ = 58.5d		**β⁻ ↓** **$T_{1/2}$ = 3.5h**		DFP- 26th in Poison Table % of Poisoning								
40											^{90}Zr	σ_γ=0.01b →	^{91}Zr	σ_γ=0.83b →	^{92}Zr	σ_γ=0.23b →	**26P 0.63%** ^{93}Zr	σ_γ=2.24b →	^{94}Zr	σ_γ=0.05b →	^{95}Zr **6.502%**	σ_γ=1.20b →	^{96}Zr	0.02b →	^{97}Zr
											stable		stable		stable		~ stable		stable		β⁻ ↓ $T_{1/2}$ = 64.0d		~ stable		β⁻ ↓ $T_{1/2}$ = 16.7h

Table 1: Chart of nuclides with Z = 35 up to Z = 40. Microscopic cross-sections for thermal neutron capture are indicated as well as half-lives of radioactive decay.

● corresponds to direct fission products ● corresponds to direct fission products that are poisons ● indicates half-lives shorter than 1 day

Z \ A	95		96		97		98		99		100		101		102		103		104		105		106		107		108		109
41	^{95}Nb **6.498%**	σ_γ<7.0b →	^{96}Nb	σ_γ=1.0b →	^{97}Nb																								
	β⁻ ↓ $T_{1/2}$= 35.0d		β⁻ ↓ $T_{1/2}$= 23.4h		β⁻ ↓ $T_{1/2}$= 72.1m																								
42	**17P 1.94%** ^{95}Mo	σ_γ=13.56b →	^{96}Mo	σ_γ=0.60b →	**33P 0.39%** ^{97}Mo	σ_γ=2.10b →	**37P 0.17%** ^{98}Mo	σ_γ=0.13b →	^{99}Mo **6.132%**	σ_γ=8.00b →	^{100}Mo																		
	stable		stable		stable		stable		β⁻ ↓ $T_{1/2}$= 66.0h		~ stable																		
43									**7P 4.53%** ^{99}Tc **6.132%**	σ_γ=22.80b →	^{100}Tc																		
									~ stable		β⁻ ↓ **$T_{1/2}$= 15.5s**																		
44											^{100}Ru	σ_γ=5.02b →	**18P 1.71%** ^{101}Ru	σ_γ=5.22b →	**43P 0.10%** ^{102}Ru	σ_γ=1.23b →	**23P 0.67%** ^{103}Ru **3.103%**	σ_γ=8.00b →	^{104}Ru	σ_γ=0.47b →	^{105}Ru	σ_γ=0.39b →	^{106}Ru						
											stable		stable		stable		β⁻ ↓ $T_{1/2}$= 39.2d		stable		β⁻ ↓ **$T_{1/2}$= 4.4h**		β⁻ ↓ $T_{1/2}$= 371.8d						
45																	**2P 9.34%** ^{103}Rh	σ_γ=144.91b →	^{104}Rh	σ_γ=39.87b →	**22P 0.81%** ^{105}Rh	σ_γ=1.58·10⁴b →	^{106}Rh	σ_γ=36.89b →	^{107}Rh	σ_γ=19.63b →	^{108}Rh		
																	stable		β⁻ ↓ **$T_{1/2}$= 42.3s**		β⁻ ↓ $T_{1/2}$= 35.4h		β⁻ ↓ **$T_{1/2}$= 30.1s**		β⁻ ↓ **$T_{1/2}$= 21.7m**				
46																			^{104}Pd	σ_γ=0.65b →	**20P 1.29%** ^{105}Pd	σ_γ=20.87b →	^{106}Pd	σ_γ=0.31b →	**28P 0.60%** ^{107}Pd	σ_γ=2.01b →	**27P 0.60%** ^{108}Pd	σ_γ=8.48b →	^{109}Pd
																			stable		stable		stable		~ stable		stable		β⁻ ↓ **$T_{1/2}$= 13.7h**

Table 2: Chart of nuclides with Z = 41 up to Z = 46. Microscopic cross-sections for thermal neutron capture are indicated as well as half-lives of radioactive decay.

Z \ A	109		110		111		112		113		114		115	
47	**15P 2.11%** ^{109}Ag	$\xrightarrow{\sigma_\gamma=9.11b}$	^{110}Ag											
	stable		$\beta^- \downarrow$ $T_{1/2}$ = **24.6s**											
48			^{110}Cd	$\xrightarrow{\sigma_\gamma=11.05b}$	^{111}Cd	$\xrightarrow{\sigma_\gamma=6.89b}$	^{112}Cd	$\xrightarrow{\sigma_\gamma=2.20b}$	**36P 0.22%** ^{113}Cd	$\xrightarrow{\sigma_\gamma=2.06b}$	^{114}Cd	$\xrightarrow{\sigma_\gamma=0.35b}$	^{115}Cd	
			stable		stable		stable		~ stable		~ stable		$\beta^- \downarrow$ $T_{1/2}$ = 53.5h	
49													^{115}In	
													~ stable	

Table 3: Chart of nuclides with Z = 47 up to Z = 49. Microscopic cross-sections for thermal neutron capture are indicated as well as half-lives of radioactive decay.

Z \ A	127		128		129		130		131		132		133		134		135		136		137		138		139		140		141
52											^{132}Te 4.276%						^{135}Te												
											β⁻ ↓ $T_{1/2}$= 3.2d						β⁻ ↓ $T_{1/2}$= 19.2s												
53	42P 0.11% ^{127}I	σ_γ=6.14b →	^{128}I	σ_γ=2.19b →	35P 0.25% ^{129}I	σ_γ=30.40b →	^{130}I	σ_γ=18.00b →	^{131}I 2.878%	σ_γ=80.00b →	^{132}I	σ_γ=11.33b →	^{133}I 6.590%	σ_γ=4.26b →	^{134}I	σ_γ=4.41b →	^{135}I 6.390%												
	stable		β⁻ ↓ $T_{1/2}$= 25.0m		~ stable		β⁻ ↓ $T_{1/2}$= 12.4h		β⁻ ↓ $T_{1/2}$= 8.0d		β⁻ ↓ $T_{1/2}$= 2.3h		β⁻ ↓ $T_{1/2}$= 20.8h	^{133m}I - IT $T_{1/2}$= 9s	β⁻ ↓ $T_{1/2}$= 52.5m		β⁻ ↓ $T_{1/2}$= 6.6h												
54			^{128}Xe	σ_γ=5.19b →	^{129}Xe	σ_γ=2.10b →	^{130}Xe	σ_γ=4.78b →	4P 6.05% ^{131}Xe	σ_γ=90.00b →	^{132}Xe	σ_γ=0.45b →	^{133}Xe 6.600%	σ_γ=190.00b →	^{134}Xe	σ_γ=0.27b →	1P 15.41% ^{135}Xe 6.610%	σ_γ=2.65·10^{6}b →	^{136}Xe										
			stable		stable		stable		stable		stable		β⁻ ↓ $T_{1/2}$= 5.2d	^{133m}Xe -IT $T_{1/2}$= 2.2d	~ stable		β⁻ ↓ $T_{1/2}$= 9.1h		~ stable											
55													5P 5.77% ^{133}Cs	σ_γ=29.00b →	21P 1.02% ^{134}Cs	σ_γ=139.67b →	34P 0.38% ^{135}Cs	σ_γ=8.66b →	^{136}Cs	σ_γ=13.00b →	^{137}Cs 6.221%									
													stable		β⁻ ↓ $T_{1/2}$= 2.1y		~ stable		β⁻ ↓ $T_{1/2}$= 13.0d	^{136m}Cs -IT $T_{1/2}$= 17.5s	β⁻ ↓ $T_{1/2}$= 30.1y									
56															^{134}Ba	σ_γ=1.50b →	^{135}Ba	σ_γ=5.87b →	^{136}Ba	σ_γ=0.68b →	^{137}Ba	σ_γ=3.60b →	^{138}Ba	σ_γ=0.40b →	^{139}Ba	σ_γ=5.77b →	^{140}Ba 6.314%	σ_γ=1.57b →	^{141}Ba
															stable		stable		stable		stable		stable		β⁻ ↓ $T_{1/2}$= 83.1m		β⁻ ↓ $T_{1/2}$= 12.8d		β⁻ ↓ $T_{1/2}$= 18.3m
57																									31P 0.52% ^{139}La	σ_γ=9.04b →	^{140}La 6.315%	σ_γ=2.70b →	^{141}La
																									stable		β⁻ ↓ $T_{1/2}$= 1.7d		β⁻ ↓ $T_{1/2}$= 3.9h

Table 4: Chart of nuclides with Z = 52 up to Z = 57. Microscopic cross-sections for thermal neutron capture are indicated as well as half-lives of radioactive decay.

Z \ A	140		141		142		143		144		145		146		147		148		149		150		151	
58	^{140}Ce	σ_γ=0.58b →	**38P 0.16%** ^{141}Ce **5.860%**	σ_γ=29.00b →	^{142}Ce	σ_γ=0.96b →	^{143}Ce	σ_γ=6.00b →	^{144}Ce **5.474%**	σ_γ=1.00b →	^{145}Ce	σ_γ=1.06b →	^{146}Ce	σ_γ=5.33b →	^{147}Ce	σ_γ=1.19b →	^{148}Ce							
	stable		β⁻ ↓ $T_{1/2}$= 32.5d		~stable		β⁻ ↓ $T_{1/2}$= 33.0h		β⁻ ↓ $T_{1/2}$=284.9d		**β⁻ ↓ $T_{1/2}$= 3.0m**		**β⁻ ↓ $T_{1/2}$= 13.5m**		**β⁻ ↓ $T_{1/2}$= 56.4s**		**β⁻ ↓ $T_{1/2}$= 56.0s**							
59			**24P 0.66%** ^{141}Pr	σ_γ=11.5b →	^{142}Pr	σ_γ=20.0b →	^{143}Pr	σ_γ=89.86b →	^{144}Pr **5.474%**	σ_γ=2.70b →	^{145}Pr	σ_γ=1.74b →	^{146}Pr	σ_γ=33.30b →	^{147}Pr	σ_γ=18.66b →	^{148}Pr	σ_γ=34.45b →	^{149}Pr	σ_γ=2.41b →	^{150}Pr			
			stable		**β⁻ ↓ $T_{1/2}$= 19.2h**		β⁻ ↓ $T_{1/2}$= 13.6d		**β⁻ ↓ $T_{1/2}$= 17.3s**		**β⁻ ↓ $T_{1/2}$= 6.0h**		**β⁻ ↓ $T_{1/2}$= 24.2m**		**β⁻ ↓ $T_{1/2}$= 13.4m**		**β⁻ ↓ $T_{1/2}$= 2.3m**		**β⁻ ↓ $T_{1/2}$= 2.3m**		**β⁻ ↓ $T_{1/2}$= 6.2s**			
60					^{142}Nd	σ_γ=18.69b →	**3P 7.69%** ^{143}Nd	σ_γ=325.14b →	**39P 0.14%** ^{144}Nd **5.475%**	σ_γ=3.59b →	**12P 2.64%** ^{145}Nd	σ_γ=49.83b →	^{146}Nd	σ_γ=1.49b →	^{147}Nd **2.232%**	σ_γ=4.41b →	**40P 0.13%** ^{148}Nd	σ_γ=2.58b →	^{149}Nd	σ_γ=26.59b →	^{150}Nd	σ_γ=1.04b →	^{151}Nd	σ_γ=24.00b →
					stable		stable		~stable		stable		stable		β⁻ ↓ $T_{1/2}$= 11.0d		stable		**β⁻ ↓ $T_{1/2}$= 1.7h**		~stable		**β⁻ ↓ $T_{1/2}$= 12.4m**	
61															**9P 4.09%** ^{147}Pm **2.232%**	σ_γ=166b →	^{148}Pm	σ_γ=2000b →	^{149}Pm **1.053%**	σ_γ=1400b →	^{150}Pm	σ_γ=72.10b →	^{151}Pm	
															β⁻ ↓ $T_{1/2}$= 2.6y		β⁻ ↓ $T_{1/2}$= 5.4d		β⁻ ↓ $T_{1/2}$= 53.1h		**β⁻ ↓ $T_{1/2}$= 2.7h**		β⁻ ↓ $T_{1/2}$= 28.4h	
62															**24P 0.66%** ^{147}Sm	σ_γ=57.00b →	^{148}Sm	σ_γ=2.40b →	**6P 5.70%** ^{149}Sm	σ_γ=$4.01\cdot10^4$b →	**16P 1.96%** ^{150}Sm	σ_γ=100b →	**10P 3.81%** ^{151}Sm	σ_γ=$1.52\cdot10^4$b →
															~stable		~stable		stable		stable		β⁻ ↓ $T_{1/2}$= 90.0y	
63																							^{151}Eu	σ_γ=$9.2\cdot10^3$b →
																							~stable	

Table 5: Chart of nuclides with Z = 58 up to Z = 63. Microscopic cross-sections for thermal neutron capture are indicated as well as half-lives of radioactive decay.

Z \ A	152		153		154		155		156		157		158	
62	**8P 4.36%** ^{152}Sm	σ_γ=205.9b →	^{153}Sm	σ_γ=4.07b →	^{154}Sm	σ_γ=8.32b →	^{155}Sm	σ_γ=22.71b →	^{156}Sm	σ_γ=15.01b →	^{157}Sm	σ_γ=15.01b →	^{158}Sm	
	stable		β⁻ ↓ $T_{1/2}$= 46.3h		stable		**β⁻ ↓ $T_{1/2}$ =22.3m**		**β⁻ ↓ $T_{1/2}$ = 9.4h**		**β⁻ ↓ $T_{1/2}$ = 8.0m**		**β⁻ ↓ $T_{1/2}$ = 5.3m**	
63	^{152}Eu	σ_γ=1.28·10^{4}b →	**11P 3.29%** ^{153}Eu	σ_γ=312b →	**14P 2.26%** ^{154}Eu	σ_γ=1.35·10^{3}b →	**13P 2.47%** ^{155}Eu	σ_γ=3.76·10^{4}b →	**41P 0.12%** ^{156}Eu	σ_γ=100b →	^{157}Eu	σ_γ=1.11·10^{2}b →	^{158}Eu	
	β⁻ ↓ $T_{1/2}$= 13.5y		stable		β⁻ ↓ $T_{1/2}$= 8.6y		β⁻ ↓ $T_{1/2}$= 4.8y		β⁻ ↓ $T_{1/2}$= 15.2d		**β⁻ ↓ $T_{1/2}$ = 15.2h**		**β⁻ ↓ $T_{1/2}$ = 45.9m**	
64	^{152}Gd	σ_γ=7.35·10^{2}b →	^{153}Gd	σ_γ=2.25·10^{4}b →	^{154}Gd	σ_γ=85.19b →	^{155}Gd	σ_γ=6.10·10^{4}b →	^{156}Gd	σ_γ=1.79b →	**32P 0.46%** ^{157}Gd	σ_γ=2.54·10^{4}b →	^{158}Gd	
	~ stable		β⁻ ↓ $T_{1/2}$= 240.4d		stable		stable		stable		stable		stable	

Table 6: Chart of nuclides with Z = 62 up to Z = 64. Microscopic cross-sections for thermal neutron capture are indicated as well as half-lives of radioactive decay.

Z \ A	232		233		234		235		236		237		238		239		240		241		242		243		244		245
90	^{232}Th	σ_γ=2.7b →	^{233}Th	σ_γ=1450.0b →	^{234}Th	σ_γ=1.75b →	^{235}Th	σ_γ=5.3b →	^{236}Th	σ_γ=2.8b →	^{237}Th	σ_γ=4.8b →	^{238}Th	σ_γ=2.3b →	^{239}Th												
	stable		β⁻ ↓ $T_{1/2}$= 22.3m		β⁻ ↓ $T_{1/2}$= 24.1d		β⁻ ↓ $T_{1/2}$= 7.2m		β⁻ ↓ $T_{1/2}$= 37.3m		β⁻ ↓ $T_{1/2}$= 4.7m		β⁻ ↓ $T_{1/2}$= 9.4m														
91			^{233}Pa	σ_γ=541.5b →	^{234}Pa	σ_γ=9.4b →	^{235}Pa	σ_γ=8.0b →	^{236}Pa	σ_γ=8.5b →	^{237}Pa	σ_γ=7.8b →	^{238}Pa	σ_γ=7.4b →	^{239}Pa	σ_γ=6.7b →	^{240}Pa										
			β⁻ ↓ $T_{1/2}$= 27.0d		β⁻ ↓ $T_{1/2}$= 6.7h		β⁻ ↓ $T_{1/2}$= 24.5m		β⁻ ↓ $T_{1/2}$= 9.1m		β⁻ ↓ $T_{1/2}$= 8.7m		β⁻ ↓ $T_{1/2}$= 2.3m		β⁻ ↓ $T_{1/2}$= 1.8h												
92			^{233}U	σ_γ= 45.3b →	^{234}U	σ_γ=99.8b →	^{235}U	σ_γ=100.0b →	^{236}U	σ_γ=5.3b →	^{237}U	σ_γ=452.4b →	^{238}U	σ_γ=2.8b →	^{239}U	σ_γ=10.9b →	^{240}U	→	^{241}U								
					~stable				~stable		β⁻ ↓ $T_{1/2}$= 6.8d				β⁻ ↓ $T_{1/2}$= 23.5m		β⁻ ↓ $T_{1/2}$= 14.1h		β⁻ ↓ $T_{1/2}$= 16.8m								
93											^{237}Np	σ_γ=172.0b →	^{238}Np	σ_γ=202.8b →	^{239}Np	σ_γ=37.0b →	^{240}Np	σ_γ=9.1b →	^{241}Np								
											~stable		β⁻ ↓ $T_{1/2}$= 2.1d		β⁻ ↓ $T_{1/2}$= 2.4d		β⁻ ↓ $T_{1/2}$= 61.9m		β⁻ ↓ $T_{1/2}$= 13.9m								
94													^{238}Pu	σ_γ=540.3b →	^{239}Pu	σ_γ=271.4b →	^{240}Pu	σ_γ=285.9b →	^{241}Pu	σ_γ= 361.5b →	^{242}Pu	σ_γ=18.8b →	^{243}Pu	σ_γ=88.1b →	^{244}Pu		
												α ↙ ^{234}U $T_{1/2}$= 87.7y			~stable	α ↙ ^{236}U $T_{1/2}$= 6564y	~stable		β⁻ ↓ $T_{1/2}$=14.3y		~stable		β⁻ ↓ $T_{1/2}$=5.0h				
95																			^{241}Am	σ_γ=647.0 b →	^{242}Am	σ_γ=218.8 b →	^{243}Am	σ_γ=76.7 b →	^{244}Am	σ_γ=600.0 b →	
																		α ↙ ^{237}Np $T_{1/2}$= 432.3y			β⁻ ↓ $T_{1/2}$=16.0h		~stable		β⁻ ↓ $T_{1/2}$=10.0h		
96																					^{242}Cm	σ_γ=15.9b →	^{243}Cm	σ_γ=130.2b →	^{244}Cm		

● corresponds to direct fissile nuclides

Table 7: Chart of nuclides with Z = 90 up to Z = 96. Microscopic cross-sections for thermal neutron capture are indicated as well as half-lives of radioactive decay.